Annual Report
Jahresbericht

2022

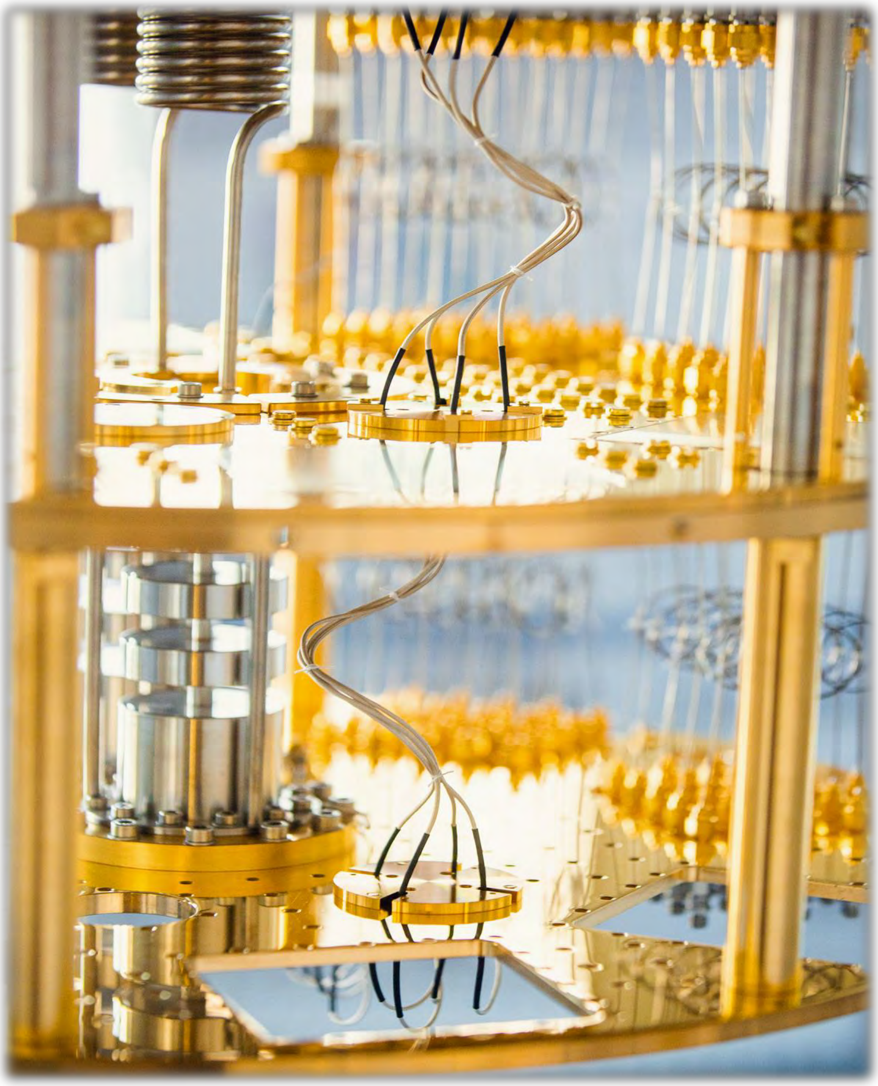

Walther–Meißner–Institut
für Tieftemperaturforschung

Bayerische Akademie der Wissenschaften

BAYERISCHE
AKADEMIE
DER
WISSENSCHAFTEN

Cover photo: interior view of a dry dilution refrigerator

Contact:

Prof. Dr. Rudolf Gross and **Prof. Dr. Stefan Filipp**
Walther–Meißner–Institut für Tieftemperaturforschung
Bayerische Akademie der Wissenschaften
and
Lehrstuhl für Technische Physik – E23
Technische Universität München

Address:

Walther–Meißner–Str. 8	e–mail:	Rudolf.Gross@wmi.badw.de
D - 85748 Garching	e–mail:	Stefan.Filipp@wmi.badw.de
GERMANY	www:	https://www.wmi.badw.de

Secretary's Office and Administration:

Emel Dönertas	Phone:	+49 – (0)89 289 14202
	Fax:	+49 – (0)89 289 14206
	e–mail:	Emel.Doenertas@wmi.badw.de
		Sekretariat@wmi.badw.de
Andrea Person	Phone:	+49 – (0)89 289 14205
	Fax:	+49 – (0)89 289 14206
	e–mail:	Andrea.Person@wmi.badw.de
		Verwaltung@wmi.badw.de

Walther-Meißner-Institut
DER BAYERISCHEN AKADEMIE DER WISSENSCHAFTEN

Preface

Dear colleagues, friends, partners, and alumni of the Walther-Meißner-Institute (WMI),

in the year 2022 we could carry on the success story of the previous year. It was not only characterised by filling the new projects in quantum science and technology with life, but also by further strengthening the WMI's research focus with new basic science projects. Moreover, we could win Prof. Dr. Peter Rabl as a new Scientific Director. When starting in February 2023 as a Professor in Theoretical Physics at the TU Munich he will ideally complement the existing activities at the WMI with his research on quantum systems. The annual report 2022 highlights important scientific results, technology developments and infrastructural measures that have been taken to make the WMI ready for the highly competitive environment in quantum technologies. It includes relevant statistical data on our scientific progress, public engagement events, projects and collaborations as well as on teaching and training activities to showcase the excellent national and international standing of the WMI.

It is only with the motivation and commitment of all WMI members that we can be successful in our research and reach the ambitious goals that we have set for the next few years. I want to thank the entire WMI team for their engagement: the technical staff for their excellent support, the administration for dealing with the huge workload accompanying the increased number of projects, and all researches who not only do an excellent job in science but also take care of existing and new WMI infrastructure as the basis for continued high-level research. I would also like to thank out collaboration partners and all our sponsors for their continued support. As in previous, we strongly appreciate and acknowledge the continued support of the Bavarian Ministry for Science and Arts, the German Research Foundation (DFG), the Federal Ministry of Education and Research (BMBF), and the European Union (EU).

The year 2022 started with the formal establishment of the Munich Quantum Valley (MQV) e.V. as a registered society in January with the WMI as one of the initiators and key players. While our main effort is to investigate and develop quantum processors based on superconducting qubits the WMI could also strengthen its basic research focus: It participates in two MQV lighthouse projects, which both start in January 2023 and run for three years. In the project *Networked Quantum Systems (NeQuS)*, WMI will investigate new approaches to the networking of quantum systems and in the project *Integrated Spin Systems for Quantum Sensors (IQSense)* integrated quantum sensors will be developed and investigated. Moreover, the WMI has received further support from the BMBF to upgrade the infrastructure for the fabrication and integration of superconducting quantum circuits with deposition and etching tools as well as tools for 3D integration. At the European level the WMI has been successful in acquiring a European grant on the exploration of non-classical states of mechanical motion *(SuperMeQ)*. It is is a key partner in the QuantERA project *Shortcuts to Adiabaticity for Quantum Computation and Simulation (STAQS)*, which started in 2022 to explore efficient control of quantum systems. Finally, the WMI plays a key role in the second phase of the European Flagship project OpenSuperQPlus, which provides a roadmap towards large scale quantum processors based on superconducting qubits. As part of this project, which involves most of the key players in Europe, the WMI forms a hub with focus on novel types of quantum devices.

The WMI not only play an important scientific role in these projects, it also significantly contributes to the technology transfer from basic quantum science to quantum products that are developed by the partnering research organizations and industrial players. In numerous meetings with our project partners we provide the expertise in quantum concepts, we help shaping a clear understanding of the challenges and we manage the – sometimes exaggerated – expectations in future quantum applications. In this context, we were also very actively engaging in public outreach activities with our participation in panel discussions, talks at public events as well as visits and lab tours at the WMI, to communicate clearly the prospects but also the many challenges on the way towards useful quantum technologies.

Wit the received funding we can continue investing in our technological infrastructure. In 2022 the new UHV MBE/PLD deposition cluster and the new helium liquefaction system has been successfully installed and put into operation. Three more dilution cryostats have been installed. Our new scanning electron microscope is up and running as an indispensable inspection tool. Moreover, we have installed a wafer-saw that allows us to develop reproducible wafer-scale fabrication methods and a five-axis CNC lathe, which enhances the capabilities and the throughput of our machine shop. While we still notice the influence of the covid-19 pandemic mostly in the delivery of new infrastructure, fortunately its effect on our research and our daily life has almost diminished over the year. Still, the planned new reactive ion-etching system has been significantly delayed because of the world-wide disruptions in the supply chains. Needless to say that these massive upgrades in the infrastructure in 2022 and the planned further installations put a very high extra workload on the involved team members and I want to thank all the supporting team members for their engagement!

Despite the considerable amount of time required to set up the many new project we could still keep a high level of research output with numerous high level publications. Examples are the observation of the nonreciprocal magnon Hanle effect, the investigation of multi-qubit operations on superconducting qubit chains and the mechanical frequency control in inductively coupled electromechanical systems. The high impact of our research work is documented by about 2500 citations of WMI publications in 2022 (ISI Web of Science).

A central focus of the WMI is the training and education of the next generation of scientists and professionals. It is key to our success to attract the best talents at the different career levels. Therefore, we are very happy that 3 bachelor, 12 master and 6 Ph.D. students completed their theses in 2022, while 17 master, 29 Ph.D. students and 2 habilitation candidates are ongoing. Because of the third-party funding acquired in 2021 and 2022 the number team members has significantly increased. It has become a challenge to provide sufficient space for the team. As part of the MQV project we are, thus planning to install a temporary office container building. Because of numerous bureaucratic hurdles this could, however, not be completed yet and is expected to be completed 2023. Another challenge regards the hiring of technical and senior scientific staff. While the WMI benefits from the great visibility of the Munich area in the quantum and the technology sector in general, a particular drawback for the Munich area is its very high living expenses combined with the uncompetitive salary scale in the public sector compared to industry. As a consequence, finding qualified researchers, technicians and engineers becomes increasingly difficult, not to say impossible.

I am, however, confident that with the strategic directions set in 2022 and before, the infrastructure upgrades and – most importantly – the expertise and skill-set brought in by the entire WMI team, the WMI will become an even stronger player in the field of quantum science and technology at the national and the international level in the next years to come.

I would, therefore, again like to thank the scientific, technical and administrative staff of WMI for its outstanding performance in 2022! I also would like to thank our Scientific Advisory Board for their trust and guidance and, last but not least, all our friends and sponsors for their interest and continuous support. I am looking forward to a successful continuation in 2023.

Garching, December 2022

Contents

The Walther–Meißner–Institute

General Information

The ***Walther-Meißner-Institute for Low Temperature Research (WMI)*** was originally operated by the Commission for Low Temperature Research of the ***Bavarian Academy of Sciences and Humanities (BAdW)***. Between 2013 and 2015, the Bavarian Academy of Sciences and Humanities with its more than 300 employees was reorganized. With the passing of the new statutes in October 2015, the 36 Commissions (Research Groups) of the Academy — they were originally set up in order to carry out long-term projects, which are too ambitious for the lifetime or capacity of any single researcher, or which require the collaboration of specialists in various disciplines — were abolished. The research program of BAdW is now implemented in Academy Institutes (such as the Walther-Meißner-Institute, the Leibniz Supercomputing Center or the Bavarian Research Institute for Digital Transformation) and Academy Projects. The Academy Institutes and Projects are managed by the Institute and Project Committees and supervised by the Institute and Project Advisory Boards, respectively. In this way a clear separation between the managing bodies of the institutes/projects (responsible for the implementation of the research programs) and the corresponding supervisory bodies (responsible for the quality control) was established. To this end, also the Commission for Low Temperature Research was dissolved and replaced by the WMI Committee and the WMI Advisory Board in 2015.

The historical roots of WMI go back to ***Walther Meißner***. He founded the Commission for Low Temperature Research in 1946 when he was president of BAdW (1946 – 1950). The first research activities then were started in 1946 in the Herrsching barracks. After the retirement of Walther Meißner in 1952, Heinz Maier-Leibnitz, who followed Walther Meißner on the Chair for Technical Physics of the Technical University of Munich (TUM), became the new head of the Commission for Low Temperature Research. In 1967, the commission moved to the Garching research campus after the construction of the new *«Zentralinstitut für Tieftemperaturforschung»* (ZTTF) was completed (director: Prof. Heinz Maier-Leibnitz, technical director: Prof. Franz Xaver Eder). Until 1972, the theory group of the Institute Laue Langevin was hosted at the ZTTF with prominent members such as Peter Fulde. In 1980, Prof. Dr. Klaus Andres became the new director of the ZTTF again associated with the Chair for Technical Physics (E23) at TUM. In 1982, the ZTTF was renamed into Walther-Meißner-Institute for Low Temperature Research (WMI) on the occasion of the 100. anniversary of Walther Meißner's birth.

In 2000, Prof. Dr. Rudolf Gross followed Klaus Andreas on the Chair for Technical Physics (E23) at TUM and as the new director of WMI. He significantly reoriented and extended the scientific focus of WMI by starting new activities in the field of quantum science and technology, as well in magnetism, spin dynamics and spin electronics. Even more importantly, he newly established the materials technology for superconducting and magnetic materials (both in form of thin films and single crystals) and a clean room facility, allowing for the fabrication of solid-state nanostructures. These measures had been very successful and allowed WMI to play a leading role in several coordinated research projects in the field of quantum science and technology [e.g. Collaborative Research Center 631 on Solid-State Quantum Information Processing (2003-2015), Cluster of Excellence ***Munich Center for Quantum Science and Technology*** (since 2019), EU Quantum Technology Flagship Project QMiCS (2018-2022)] as well as in nanosciences [e.g. Cluster of Excellence Nanosystems Initiative Munich (2006-2019)]. The WMI also played a leading role in initiating the ***Munich Quantum Valley*** in 2020 (see strategy paper ***«Munich Quantum Valley Initiative»***). To accommodate the new activities, starting from 2000 the so far unused basement of the WMI building was made available for technical infrastructure (airconditioning, particulate airfilters, pure water system etc. for clean room) and additional laboratory space. Fortunately, in 2008 WMI succeeded in getting extra money from the state government within the so-called *«Konjunkturpaket II»* to establish the new *«WMI Quantum Science Laboratory»* in the basement of the building, providing about 150 m^2 additional laboratory space particularly suited for low temperature facilities and ultra-sensitive studies on solid state quantum systems. The WMI Quantum Science Laboratory was fully operational early in 2011 and meanwhile hosts several mK systems and sophisticated experimental techniques for the study of solid state based quantum systems and circuits. In 2016, the Bavarian Ministry for Science and Arts granted more than 6 Mio. Euro for redevelopment measures regarding the technical infrastructure, safety requirements and energy efficiency. An important part of the building project implemented in 2017/18 was the reconstruction of the entrance area and the main staircase, providing now direct access to the new WMI Quantum Laboratories in the basement of the WMI building as well as additional communication areas and meeting rooms in the ground floor. Moreover, it included the replacement of all windows and doors, the upgrade of the technical infrastructure for cooling water, air conditioning, liquid nitrogen and helium storage, as well as the complete redevelopment of the mechanical workshop and various safety measures.

With the availability of additional laboratory space and the success of the WMI in Germany's Excellence Initiative (2006-2018), Excellence Strategy (starting from 2019), and other third-party funded research projects, the research activities, the number of staff and obviously the related administrative tasks at WMI were strongly growing. Therefore, Rudolf Gross proposed in 2017 to start the appointment procedure for his successor at an early stage to guarantee sufficient temporal overlap. Moreover, due to the strong increase of staff, research projects and administrative tasks he proposed to change the governance structure of WMI from a single director to a board of up to three directors headed by a managing director. This change of governance structure has been supported by the Scientific Advisory Board of WMI and the decision-making bodies of BAdW. Meanwhile, it is implemented in the new rules of order of WMI valid since 18th October 2019. Already in June 2020, Prof. Dr. Stefan Filipp started as the second scientific director of WMI with strong focus on superconducting quantum computing. He coordinates the activities on superconducting quantum computing within the ***Munich Quantum Valley*** and the BMBF projects ***German Quantum Computer based on Superconducting Qubits (GeQCoS)*** and ***Munich Quantum Valley Quantum Computer Demonstrators - Superconducting Qubits (MUNIQC-SC)***.

As already mentioned, it is a long tradition that WMI hosts the Chair for Technical Physics (E 23) of TUM with the director of the WMI being a full professor at the Faculty of Physics of TUM. However, in general WMI has established tight links to research groups of both Munich universities, joining technological and human resources in the fields of experimental and theoretical solid-state and condensed matter physics, low temperature techniques, materials science as well as thin film and nanotechnology. Noteworthy, the WMI supplies liquid helium to more than 25 research groups at both Munich universities and provides the technological basis for low temperature research.

Important Discoveries

The WMI looks back on a long history of successful research in low temperature physics. In the following we list some important discoveries as well as experimental and technical developments made at WMI:

- **1961: discovery of flux quantization in multiply connected superconductors**

  (R. Doll, M. Näbauer, *Experimental Proof of Magnetic Flux Quantization in a Superconducting Ring*, Phys. Rev. Lett. **7**, 51-52 (1961)).

- **1986: discovery of an anomalous temperature dependence of the penetration depth in UBe_{13}**

  (F. Gross, B.S. Chandrasekhar, D. Einzel, K. Andres, P.J. Hirschfeld, H.R. Ott, J. Beuers, Z. Fisk, J.L. Smith, *Anomalous Temperature Dependence of the Magnetic Field Penetration Depth in Superconducting UBe_{13}*, Z. Physik B - Condensed Matter **64**, 175-188 (1986)).

- **1992: discovery the intrinsic Josephson effect**

  (R. Kleiner, F. Steinmeyer, G. Kunkel, and P. Müller, *Intrinsic Josephson Effects in $Bi_2Sr_2CaCu_2O_8$ Single Crystals*, Phys. Rev. Lett. **68**, 2394-2397 (1992)).

- **2002: development of dilution refrigerators with pulse tube refrigerator precooling**

  (K. Uhlig, *$^3He/^4He$ Dilution Refrigerator with Pulse Tube Precooling*, Cryogenics **42**, 73-77 (2002)).

- **2010: first demonstration of ultrastrong light-matter interaction**

  (T. Niemczyk, F. Deppe, H. Huebl, E. P. Menzel, F. Hocke, M. J. Schwarz, J. J. Garcia-Ripoll, D. Zueco, T. Hümmer, E. Solano, A. Marx, R. Gross, *Circuit Quantum Electrodynamics in the Ultrastrong-Coupling Regime*, Nature Physics **6**, 772-776 (2010)).

- **2010: development of dual path method for state tomography of propagating quantum microwaves**

  (E.P. Menzel, M. Mariantoni, F. Deppe, M.A. Araque Caballero, A. Baust, T. Niemczyk, E. Hoffmann, A. Marx, E. Solano, R. Gross, *Dual-Path State Reconstruction Scheme for Propagating Quantum Microwaves and Detector Noise Tomography* , Phys. Rev. Lett. **105**, 100401 (2010)).

- **2012: first realization of path entanglement of propagating quantum microwaves**

  (E. P. Menzel, R. Di Candia, F. Deppe, P. Eder, L. Zhong, M. Ihmig, M. Haeberlein, A. Baust, E. Hoffmann, D. Ballester, K. Inomata, T. Yamamoto, Y. Nakamura, E. Solano, A. Marx, R. Gross, *Path Entanglement of Continuous-Variable Quantum Microwaves*, Phys. Rev. Lett. **109**, 250502 (2012)).

- **2013: discovery of the spin Hall magnetoresistance** (jointly with partners at Tohoku University and TU Delft)

  (H. Nakayama, M. Althammer, Y.-T. Chen, K. Uchida, Y. Kajiwara, D. Kikuchi, T. Ohtani, S. Geprägs, M. Opel, S. Takahashi, R. Gross, G. E. W. Bauer, S. T. B. Goennenwein, E. Saitoh, *Spin Hall Magnetoresistance Induced by a Non-Equilibrium Proximity Effect*, Phys. Rev. Lett. **110**, 206601 (2013)).

- **2013: first demonstration of strong magnon-photon coupling**

  (H. Huebl, Ch. Zollitsch, J. Lotze, F. Hocke, M. Greifenstein, A. Marx, R. Gross, S.T.B. Goennenwein, *High Cooperativity in Coupled Microwave Resonator Ferrimagnetic Insulator Hybrids*, Phys. Rev. Lett. **111**, 127003 (2013)).

- **2017: first experimental observation of the spin Nernst effect**

  (S. Meyer, Yan-Ting Chen, S. Wimmer, M. Althammer, S. Geprägs, H. Huebl, D. Ködderitzsch, H. Ebert, G.E.W. Bauer, R. Gross, S.T.B. Goennenwein, *Observation of the spin Nernst effect*, Nature Materials **16**, 977-981 (2017)).

- **2019: first demonstration of remote state preparation in the microwave regime**

  (S. Pogorzalek, K. G. Fedorov, M. Xu, A. Parra-Rodriguez, M. Sanz, M. Fischer, E. Xie, K. Inomata, Y. Nakamura, E. Solano, A. Marx, F. Deppe, R. Gross, *Secure Quantum Remote State Preparation of Squeezed Microwave States*, Nature Communications **10**, 2604 (2019)).

- **2021: first demonstration of quantum teleportation in the microwave regime**
  (K. G. Fedorov, M. Renger, S. Pogorzalek, R. Di Candia, Q. Chen, Y. Nojiri, K. Inomata, Y. Nakamura, M. Partanen, A. Marx, R. Gross, F. Deppe, *Experimental quantum teleportation of propagating microwaves*, Science Advances 7, eabk0891 (2021)).

Present Research Activities

The research activities of the Walther-Meißner-Institute are focused on low temperature condensed matter and quantum physics (see reports below). The research program is devoted to both **fundamental** and **applied research** and also addresses **materials science, thin film and nanotechnology** aspects. With respect to **basic research** the main focus of the WMI is on

- quantum phenomena and quantum coherence in solid state systems,
- superconductivity and superfluidity,
- magnetism, including spin transport, spin dynamics, spin mechanics and spin caloritronics,
- circuit quantum electrodynamics and circuit electro-nanomechanics,
- ordering and emergent phenomena in correlated quantum matter,
- and the general properties of metallic systems at low and very low temperatures.

The WMI also conducts **applied research** in the fields of

- superconducting quantum circuits for quantum computing,
- solid-state quantum information processing and quantum communication systems,
- superconducting and spin-based devices,
- multi-functional and multiferroic materials,
- and the development of low and ultra-low temperature systems and techniques.

With respect to **materials science, thin film and nanotechnology** the research program is focused on

- the synthesis of superconducting and magnetic materials,
- the single crystal growth of oxide materials,
- the thin film technology of complex superconducting and magnetic heterostructures, including multi-functional and multi-ferroic material systems,
- and the fabrication of superconducting, magnetic and hybrid nanostructures.

The WMI also develops and operates systems and techniques for low and ultra–low temperature experiments. A successful development have been dry mK-systems that can be operated without liquid helium by using a pulse-tube refrigerator for precooling. In the early 2000s, these systems have been successfully commercialized by the company VeriCold Technologies GmbH at Ismaning, Germany, which was taken over by Oxford Instruments in 2007. Currently, in a collaboration with Oxford Instruments such dry dilution refrigerators are used to establish a so-called cryolink, allowing for quantum communication in the microwave regime between two superconducting quantum processors over an about 10 m distance. WMI also operates a helium liquifier with an annual capacity of above 180.000 liters and supplies both Munich universities with liquid helium. To optimize the transfer of liquid helium into transport containers, WMI has developed a pumping system for liquid helium which has been commercialized in collaboration with a company.

To a large extent the research activities of WMI are integrated into national and international research projects such as Clusters of Excellence, Collaborative Research Centers, Research Units, or BMBF and EU projects. The individual research groups of WMI offer a wide range of attractive research opportunities for bachelor and master students, Ph.D. students and postdoctoral fellows.

Experimental Facilities and Resources

The WMI is equipped with state of the art facilities for the preparation and characterization of superconducting and magnetic materials as well as for various low and ultra–low temperature experiments. The main experimental and technological resources of WMI are listed in the following.

Materials Preparation and Fabrication of Nanostructures

- UHV-cluster cluster deposition system of DCA Instruments Oy consisting of the following parts: (i) UHV-pulsed-laser deposition system for complex oxide materials, (ii) UHV-molecular beam epitaxy system for topological insulators and metals, (iii) UHV sputter deposition system for superconducting metals. All subsystems are connected via a UHV buffer line with transfer system.
- Plassys MEB550 S4-I UHV electron beam evaporation and sputtering system for qubit fabrication
- molecular beam epitaxy (MBE) system for metals
- UHV cluster tool (Bestec GmbH) consisting of two magnetron sputter deposition systems for superconducting and magnetic heterostructures, respectively, and a load lock
- UHV magnetron sputtering system (Mantis Deposition GmbH) for large-area deposition of superconducting thin films and heterostructures
- Oxford Instruments Plasmalab 80 Plus reactive ion etching (RIE) system with ICP plasma source
- ion beam etching (IBE) system equipped with a LN_2 cooled sample holder
- automated critical point dryer Leica EM CPD 300
- polishing machine for substrate preparation
- DISCO DAD 3221 automatic dicing saw wafer sizes up to 150 mm
- ultrasonic bonding machine
- 50 m^2 class 1000 clean room facility
- maskless lithography UV Direct Laser Writer, PicoMaster 200 UV of the company 4PICO, The Netherlands
- 100 kV nB5 Electron Beam Lithography System by NanoBeam Limited, UK, with 6 inch laser stage
- optical lithography (Süss maskaligner MJB 3 and projection lithography)
- four-mirror image furnace for crystal growth

Characterization

- 2–circle x–ray diffractometer (Bruker D8 Advance, sample temperature up to 1 600°C)
- high resolution 4–circle x–ray diffractometer with Göbel mirror and Ge monochromator (Bruker D8 Discover)
- JEOL JSM-IT800 Schottky field emission Scanning Electron Microscope with EDX analysis
- UHV room temperature AFM/STM system
- tip-enhanced Raman spectroscopy (TERS) system
- SQUID magnetometer (Quantum Design, 1.5 to 700 K, up to 7 T)
- several high field magnet systems (up to 17 T Tesla) with variable temperature inserts
- 7 T split coil magnet systems with optical access and variable temperature insert
- 3D vector magnet (2/2/6 Tesla) with variable temperature inserts
- experimental set–ups for the measurement of noise including low noise SQUID amplifiers and signal analyzers

- high-frequency network analyzers (up to 40 GHz) and various microwave components (sources, mixers, circulators, attenuators) for the determination of high frequency parameters
- ultra-sensitive microwave receiver for state tomography of quantum microwaves (dual path method with FPGA signal processing)
- high-frequency cryogenic probing station (up to 20 GHz, $T > 4\,\mathrm{K}$)
- magnetooptical Kerr effect (MOKE) system
- broadband ferromagnetic resonance (FMR) system

Low temperature systems and techniques

- several ^{3}He/^{4}He dilution refrigerator inserts for temperatures down to 10 mK
- WMI cryogen-free mK-cooler based on a dilution refrigerator with pulse-tube precooling and equipped with a large number of microwave lines and cold electronics (e.g. amplifiers, circulators, attenuators, directional couplers) for ultra-sensitive experiments on solid state quantum systems
- Oxfod Instruments cryogen-free dilution refrigerator (model VDR 400-10) with a base temperature of about 10 mK equipped with a 3D vector magnet (1/1/6 Tesla)
- Oxfod Instruments cryogen-free dilution refrigerator (model TRITON-15-300) with a base temperature of about 10 mK equipped with a standard bucket tailset
- Oxford Instruments cryogenic link with supporting structure and superconducting microwave link
- Bluefors cryogen-free dilution refrigerator system (model BF-XLD 1000) with a base temperature below 10 mK and, in particular, with large cooling power (about 1 mW at 100 mK) and sample space
- Bluefors cryogen-free dilution refrigerator system (model XLD1000sl) equipped with 122 input lines and eight output lines including high-frequency lines which allow to measure up to 40 GHz
- Bluefors cryogen-free dilution refrigerator system (model BF-LD 400) with a base temperature below 10 mK for quantum microwave experiments
- Bluefors cryogen-free dilution refrigerator system (model BF-LD 400) with a base temperature below 10 mK for qubit testing
- Bluefors cryogen-free dilution refrigerator system (model BF-LD 400) with rapid sample loading option (bottom loader)
- "wet" dilution refrigerators based on liquid helium precooling and equipped with a large number of microwave lines and cold electronics (e.g. amplifiers, circulators, attenuators, beam splitters) for time-domain microwave experiments on solid state quantum systems
- experimental set–ups for the measurement of specific heat, magnetization, thermal expansion as well as electrical and thermal transport properties as a function of temperature, magnetic field and pressure

Peter Rabl Joins WMI as a New Scientific Director

R. Gross, S. Filipp [1]

On June 10, 2022, the Bavarian Ministry of Science and Arts announced support for new professorships in quantum science and technology (see press release). The universities of Augsburg, Würzburg, Erlangen-Nuremberg and both Munich universities Munich, as well as the technical universities of applied sciences in Regensburg and Nuremberg, received in total around 20 Mio. € for new professorships to further strengthen their profiles in quantum sciences and quantum technologies. The program is part of the ***High-Tech Agenda Bavaria*** in the framework of the ***Munich Quantum Valley e.V.*** (MQV).

Rudolf Gross of WMI successfully applied for a new professorship in Applied Quantum Theory, which is assigned to TUM and jointly appointed by TUM and BAdW. The professorship is funded with about 1.5 Mio. € by the High-Tech Agenda Bavaria for the next 4-year period and subsequently jointly financed by TUM and BAdW. The professorship could be filled in record time with ***Prof. Peter Rabl***. He accepted the offer of TUM/BAdW in December 2022 and will start in Munich already beginning of 2023.

Peter Rabl previously was an Full Professor at the Technical University of Vienna and head of the Atominstitut (ATI), where he was leading the research group on Theoretical Quantum Optics and Quantum Information. He also is member of the ***Erwin Schrödinger Center for Quantum Science & Technology (ESQ)*** of the ***Austrian Academy of Sciences (ÖAW)***. Peter Rabl is one of the pioneers in the emerging field of hybrid quantum devices. His group is working on various theoretical problems related to nano-mechanical quantum systems, defect centers and superconducting circuits, where the interest ranges from fundamental test of quantum mechanics, to the realization of practical quantum technologies and the implementation of many-body systems with engineered couplings and dissipation.

The appointment of Peter Rabl as Scientific Director at WMI is related to the ongoing change in the government structure of the Walther-Meißner-Institute. In 2017, BAdW decided to change the governance structure from a single director to a board of up to three scientific directors headed by a managing director. This new governance structure has been put in practice with the new rules of order of WMI valid since 18th October 2019. With the present scientific directors Rudolf Gross (since July 2000) and Stefan Filipp (since June 2020) and the newly appointed scientific director Peter Rabl, the new governance structure is now fully implemented.

The Walther-Meißner-Institute is particularly happy to host a theory group again and thereby to continue a long tradition. Until 1972, the theory group of the Institute Laue Langevin was hosted by WMI with prominent members such as Peter Fulde. Later on, Dietrich Einzel was working on the theory of superconductors and superfluids for more than three decades (1984-2015). After his retirement, the appointment of a theoretician has been postponed several

[1]Supported by the Bavarian Ministry of Science and Arts by the "Programm zur Stärkung der interdisziplinären Lehr- und Forschungskapazitäten auf dem Gebiet der Quantenwissenschaften und Quantentechnologien" within the Munich Quantum Valley e.V.

times due to coordination with ongoing appointments in the Physics Department of TUM and the appointment of a new scientific director in experimental physics at WMI. All the more, we are very happy about the appointment of Peter Rabl. He is an internationally renowned scientists and without any doubt will establish a strong theory group at WMI. We expect significant synergy effects with the experimental groups at WMI by hosting a theory group in the same building.

The new theory group at WMI is also an important cornerstone of the ***Munich Quantum Valley e.V. (MQV)***. It particularly aims at strengthening the theory activities in the field of interdisciplinary quantum research and the control of complex quantum systems. The theory support is of crucial importance for the broad experimental activities of the MQV, aiming at the development of quantum computers, quantum sensors, and quantum communication systems.

Building Projects and Reconstruction Measures

Infrastructure has to Follow Demands of Research Projects

Rudolf Gross, Stefan Filipp, Achim Marx

Topics in fundamental and applied research and the related experimental methods and techniques are continuously changing. Evidently, this requires a permanent adjustment of the technical infrastructure to the needs of the ongoing and planned research projects. Therefore, also in 2022 there has been a significant number of reconstruction measures required for accommodating new equipment and technical infrastructure. Moreover, several laboratories and office space had to be renovated and reorganized.

The delivery of the new helium liquefier was announced for October 2021, but had to be postponed until March 2022 due to delays related both to the Covid-19 pandemic and considerable delays in the supply of system components. Fortunately, the installation of the coldbox of the liquefier in the main building as well as the installation of system components such as the helium compressor or the balloons for the recovery system in the annexe building could be completed in 2022 without major problems. This would not have been possible with the professional support of the WMI helium team. Meanwhile, the new liquefaction system is in operation and will guarantee the save and cost efficient supply of liquid helium to the more than 30 research groups at TUM, LMU and MPG for the next two decades.

After considerable delays, important new technical infrastructure and scientific instrumentation has been delivered and could be installed in 2022. In particular, the scanning electron microscope (JEOL JSM-IT800, see report on page 94), the new automatic dicing saw DISCO DAD 3221 (see report on page 91), and the new UHV PLD-MBE cluster deposition system of DCA Instruments Oy were going into operation. With a total cost of about 2 Mio. € the UHV PLD-MBE cluster deposition system is the largest investment of WMI besides the helium liquefaction system (about 2.5 Mio. €). It is designed for the fabrication of complex heterostructures and novel quantum materials. It replaced the more than 25 years old UHV Laser-MBE system, which delivered the materials basis for more than 150 publications. Without any doubt, also the new state-of-the-art UHV Laser-MBE system will play a key role for the materials oriented research at WMI. It considerable extends the capabilities of WMI in thin film growth of quantum materials (see report on page 25).

In 2022, the WMI also could acquire a new 5-axis-configuration machining centre (Hermle C 12 U) for the Mechanical Workshop. This machine centre replaces the aged 3-axis machining tool Deckel Maho FP-3-50, which was purchased in the early 1990s. The new machining centre arrived in time to handle the increasing demand on complex parts for both cryogenic experimental setups and components for ultra high vacuum apparatus. The increasing complexity of dedicated sample holders designed at WMI requires rapid prototyping. The new

Hermle C 12 U system has a compact footprint and is designed for machining cubic parts up to 100 kg in weight. The integrated pick-up tool magazine features 36 tool pockets. It allows for manufacturing complex components with challenging geometries. Three of the axes are in the tool, two axes are in the swivelling rotatory table. This setup of the machining centre enables complex milling processes and milling and turning simultaneously. A direct interface to standard CAD software guarantees rapid transfer of complex designs and initialization of the fabrication process. A Heidenhain TNC 640 control unit provides for free contour programming and functions for fast 3D work.

A further important investment in technical infrastructure in 2022 was the acquisition of a new ultrapure water treatment unit to fulfill the highest standards for all cleanroom processes and sample fabrication technologies. The new unit replaces the 20 year old water purification system, which no longer was working reliably and could not match the highest standard requirements. The new unit consists of a reverse osmosis system with directly connected electrodeionisation for final demineralisation of the permeate. The unit is fitted on a sturdy aluminum frame set up in the cleanroom technical facility room. The system is controlled and monitored using a PLC with a touch screen panel. The unit is capable of providing up to 80 l ultrapure water per hour.

Already in 2021, three new dry dilution refrigerators of the company Bluefors Oy arrived and two of them, a standard dry dilution refrigerator (Model BF-LD 400) and a so-called bottom loader (Model BF-LD 250/400) allowing for fast sample change, have already been installed in 2021. The third system (Model BF-XLD 400/1000) providing large cooling power and very large sample space was delivered late in 2021 and taken into operation in 2022. A further system (Model BF-LD 400) was acquired within the BMBF project QuaMToMe in 2022 and replaced an old wet dilution refrigerator in the basement of WMI. Another system (Model BF-LD 400) was acquired within the MQV project (consortium K1) to test alternative superconducting qubit devices (see report on page 92).

The most relevant measures implemented in 2022 have been

- the movement of the administration of the WMI to the new double room 107/108,
- the renovation of the new office (room 103) of the third scientific director, Peter Rabl, who will arrive early in 2023 (cf. page 13),
- the completion of the renovation of the WMI annexe building, where part of the new helium liquifier has been installed, including the replacement of the old helium gasometers as well as the electric power, ventilation and compressed air systems (see report on page 21),
- the completion of the installation of three further dry dilution refrigerators, including the required closed-cycle cooling systems and related technical infrastructure (cf. page 92),
- the renovation of the thin film laboratory and adjustment of the required technical infrastructure for the installation of the new UHV PLD-MBE deposition system for quantum materials (cf. page 25),
- the renovation of laboratory for the installation of the new scanning electron microscope (cf. page 94), and
- the installation of the new 5-axis milling machine in the mechanical workshop, including the required reinforcement of the weight-bearing capacity of the floor.

New Technical Infrastructure

New Helium Liquefier Installed at WMI

R. Gross, P. Binkert, J. Höß, A. Marx, J. Naundorf, H. Schwaiger [1]

In 2022, a new helium liquefier of Vorbuchner GmbH has been installed at the Walther-Meißner-Institute (WMI) and taken into operation. The 2.5 Mio. Euro investment secures the future supply of liquid helium not only for WMI but also for the two Munich universities. The purchase of the liquefier was funded by the ***Major Research Instrumentation Programme*** of the German Research Foundation (DFG). Within this funding programme (according to Art. 91b of the Basic Law), DFG is contributing 50% of the investment costs from a dedicated federal budget as defined in the federal-state agreement on research buildings and major research instrumentation at universities, and national high-performance computing, decided by the Joint Science Conference (GWK).

After several optimization and testing procedures, the final approval of the machine has been made and meanwhile it is in full operation. Due to a clever system concept the parallel operation of the old liquefier is possible in the transition phase, guaranteeing a continuous supply with LHe.

A Long Tradition in Helium Liquefaction

The WMI operates a helium liquefaction plant since more than 60 years and supplies the two Munich universities and some other Munich research institutions with liquid helium. After Kamerlingh Onnes at Leiden (1908) and Mc Lennan at Toronto (1923), Walther Meißner was the third one worldwide who succeeded in liquefying helium in 1925 at Berlin. After moving to Munich in 1934, he continuously contributed to the improvement of helium liquefiers in collaboration with Linde AG. Even today, the reliable supply of liquid helium and efficient recovery of helium gas are key factors for internationally leading research locations.

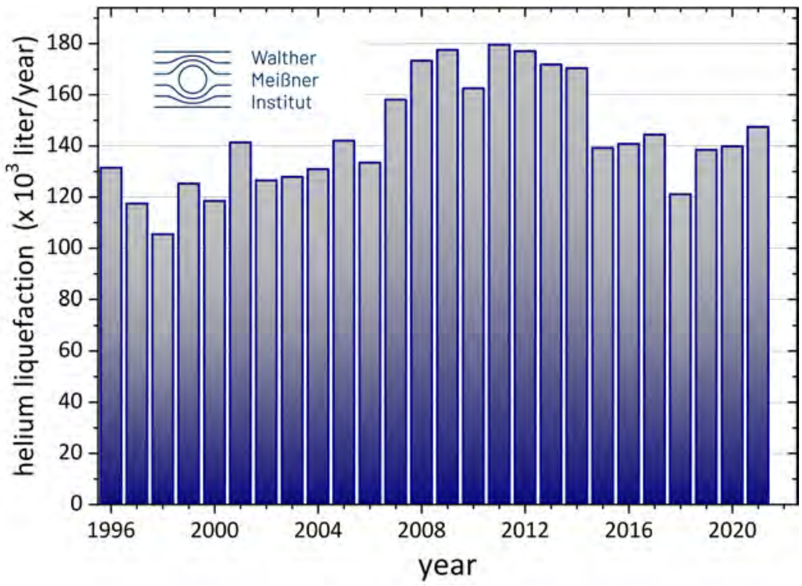

Figure 1: The annual amount of helium liquefied at WMI since 1996.

Over the last 30 years, WMI produced more than 140 000 liters of liquid helium per year on average (see Fig. 1) with a current market price of more than 2 Mio. Euro. The LHe consumption in the Munich area was changing over the past decades due to variations in research focus. For example, in the 1980s the LHe consumptions was strongly increasing after the discovery of the quantum Hall effect and the foundation of the Walter Schottky Institute at TUM. Presently, LHe consumption is decreasing again mainly due to the improvement of cooling techniques (e.g. dry dilution refrigerators, magnetic cooling) which do no longer need liquid helium.

[1] Supported by the German Research Foundation, Grant No. INST 95/1637-1 LAGG.

Year	Liquefier System
1967-1981	Linde helium liquefier, Linde AG, Germany
1982-2003	TCF 100 gas bearing turbine machine with ejector system, Sulzer AG, Switzerland
2004-2022	TCF 20 gas bearing turbine machine with ejector system, Linde Kryotechnik AG, Switzerland
since 2022	VL 100 gas bearing turbine machine with ejector system, Vorbuchner GmbH & Co. KG, Germany

Table 1: Commercial helium liquefiers operated at WMI.

History of Helium Liquefiers Operated at WMI. Already before the present WMI building was established on the Garching Research Campus in 1967, novel concepts of helium liquefiers have been developed at the Herrsching site. An example is the valve-less expansion machine developed by Doll and Eder. After WMI moved from Herrsching to Garching in 1967, several commercial helium liquefiers have been operated (cf. Tab. 1).

Submersible Pump for Liquid Helium. Since 1988, at WMI the liquid helium is transferred from the 5 000-liter liquid helium storage vessel into the transport containers delivered to the customers by a liquid helium transfer pump developed by Doll, Wiedemann and Berndt of WMI (patent Nos. DE3715216A1, EP0289980A3, US4948348, 1988). This approach considerably increased the efficiency of the helium liquefaction systems, as flash gas losses during the transfer of liquid helium between the storage vessel and the mobile transport containers are strongly reduced. At the same time, a liquefier with an ejector system is required to liquefy into an unpressurized liquefier tank. Details on the liquid helium transfer pump can be found here.

The Present Liquefaction Plant Based on a VL 100 Liquefier.

At present, the WMI helium liquefaction plant is based on the VL 100 helium liquefier from Vorbuchner GmbH. An overview of the whole liquefaction plant, including the liquefier as well as the recovery and storage system is shown in Fig. 2. The new VL 100 liquefier is a fully automated, processor-controlled helium liquefaction system with a screw compressor, gas-bearing expansion turbines and an integrated freezing-purifier for processing contaminated helium (He) as the main components.

Principle of Operation. For the cooling of the helium gas a Claude process is used. In this method the compressed gas is doing mechanical work at the expense of its kinetic energy and thereby cooling down. To liquefy the gas, this principle is combined with a Joule-Thomson expansion. In the compression step, a screw compressor compresses the purified helium gas from 1.05 to about 12.5 bar, constantly dissipating the resulting compression heat. Traces of oil in the circulating gas are removed by coalescer filters and a special oil absorber. In the expansion step, the cooling of the gas is achieved via two dynamic gas-bearing expansion turbines connected in series. In stationary operation, the final temperature after the second turbine is about 12 K. At temperatures below 8 K, part of the circulating gas is expanded to $\approx$ 1 bar by a Joule-Thomson valve (JT) and an ejector system. This produces partly liquid helium with a temperature of about 4.2 K. In the transfer line, the 4.2 K cold helium is transported from the cold box of the liquefier to the 5 000-liter liquid helium storage vessel.

Performance Data. The VL 100 liquefier system is optimized for helium liquefaction using LN_2 precooling. Despite the achievable liquefaction rate the energy consumed per liter of liquefied helium is of key importance as energy costs represent the key cost factor in helium liquefaction. Without (with) LN_2 precooling, a liquefaction rate of 26.2 (79.9) l/h at a power consumption of 3.29 (1.18) kW/liter LHe is achieved.

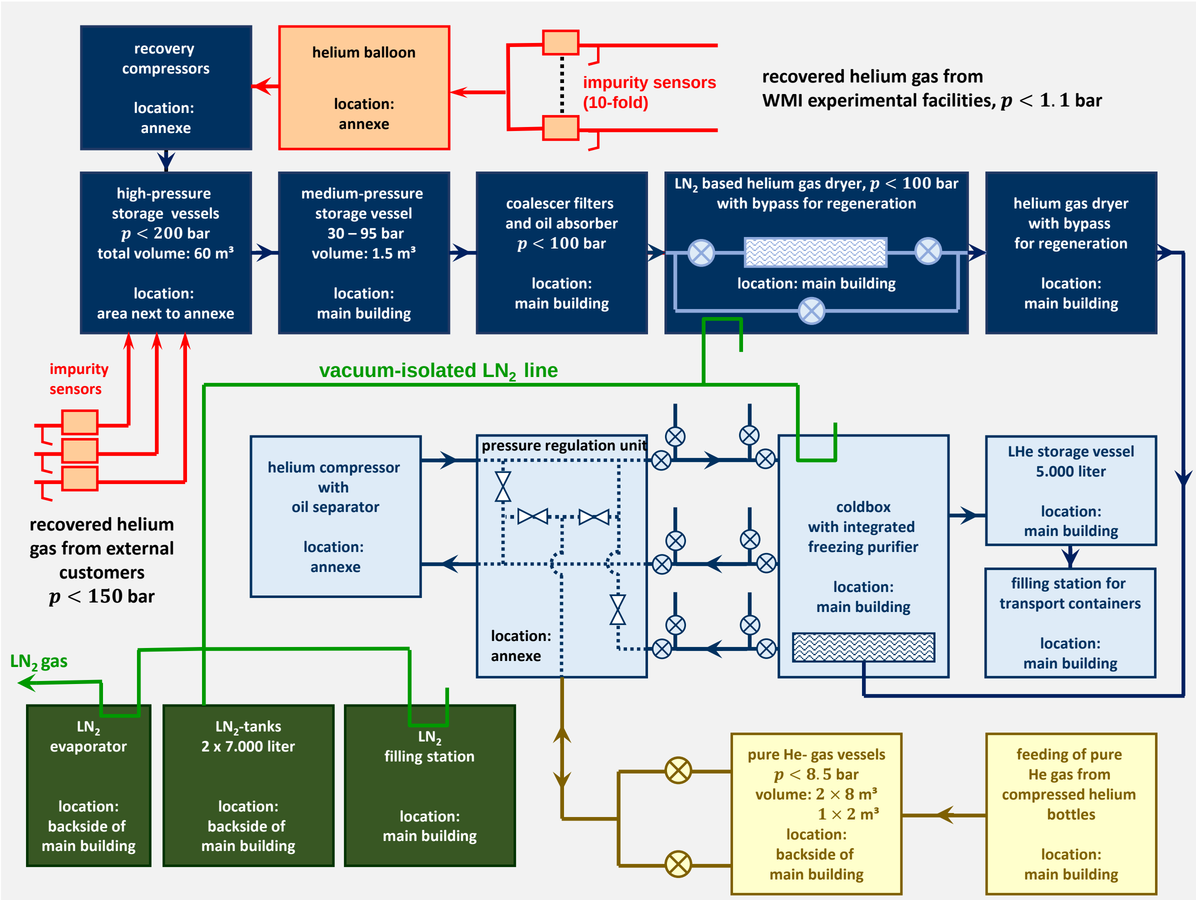

Figure 2: Overview of the WMI helium liquefaction plant consisting of the low-pressure recovery part (red), the high-pressure recovery and storage part (dark blue), the liquefier with the compressor, regulation unit, storage vessel and filling station (light blue), the LN_2 supply (green) and the high-pressure container for ultra-pure helium gas.

Heat Exchangers The cold helium gas generated in the expansion process is used together with the low-pressure flow from the turbines to precool the warm gas in a counterflow principle using aluminum plate fin heat exchangers.

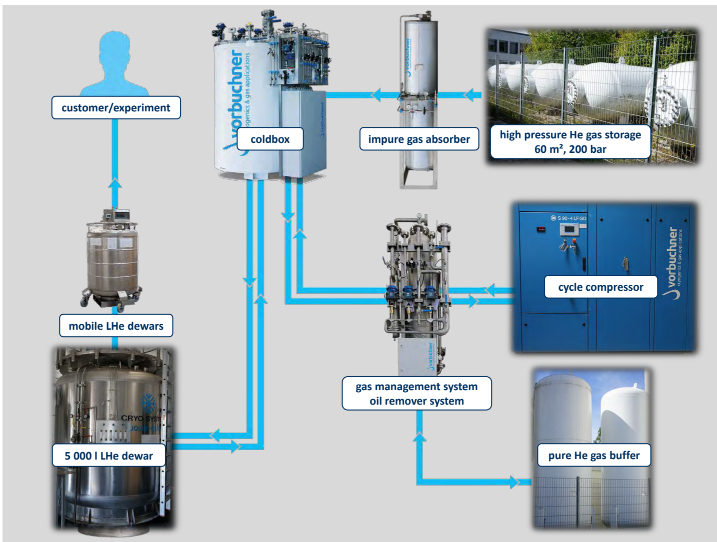

Figure 3: The main components of the present helium liquefaction systems operated at WMI.

Freezing purifier. Since air, moisture and other impurities in the recovered helium gas form frozen deposits during cooldown, they have to be removed efficiently. The VL 100 helium liquefier uses integrated cleaning lines inside the coldbox based on cold surfaces generated by the process gas. The contaminated helium gas can be cooled down to about 30 K in order to remove contaminations by freeze-out.

Helium Recovery System. Since helium gas, which has escaped to the ambient atmosphere, can no longer be recovered, WMI does not only operate a helium liquefier, but also a complex recovery system together with the Munich universities. The helium gas is recovered at the various experimental facilities/buildings of LMU, TUM and MPQ and fed back into the liquefaction process at WMI. On the Garching Research Campus, this is realized by underground tubes. Overall, a recovery rate of about 90% is achieved, providing safe helium supply and significant independence of the fluctuating helium market.

WMI itself also operates a helium recovery system with a recovery rate of about 95%. It consists of the following components: (i) Two 10 m^3 helium balloons equipped with a non-contact level measurement, (ii) compressors and high-pressure storage vessels. WMI operates 3 Sauer & Sohn helium compressors with a capacity ranging between 25 and 80 m^3/h. The helium gas is compressed into five high-pressure cylinders with a total storage volume of 62.5 m^3 and storage pressure of up to 200 bar.

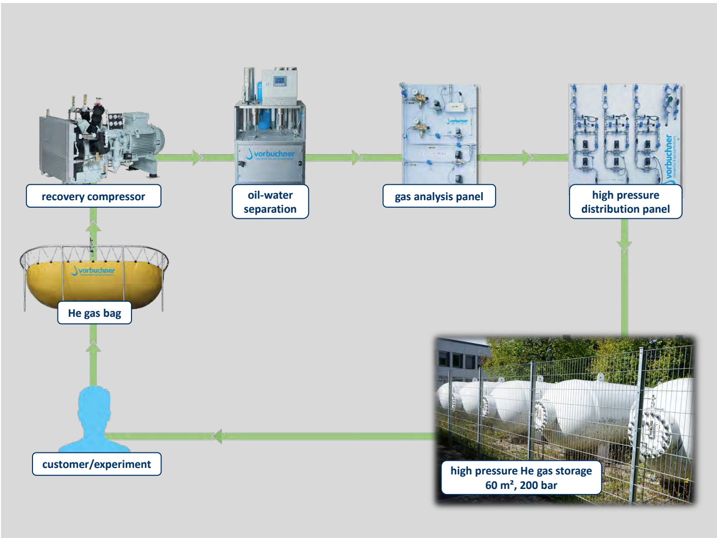

Figure 4: The present helium recocery system at WMI.

Impurity analysis. Contamination of the helium gas with air, oil and other impurities are reducing the efficiency of the liquefaction process. Therefore, the quality of the helium gas must be monitored continuously. In the worst case, contaminated gas can be fed into a quarantine bundle. To increase the uptime of the system, contaminations are quickly detected and reduced to a level preventing failures of the freezing purifier.

Gas purifying systems. Since air, moisture, oil vapor and other impurities in the recovered helium gas form frozen deposits during cool-down, they have to be removed efficiently. Therefore, the WMI helium liquefaction plant uses several systems for purifying the helium gas (oil-water separator, coalescer filters, LN_2 based gas dryer, freezing purifier).

Safety measures To avoid losses of helium gas both in the low and the high-pressure part of the recovery systems, all relevant pipes are equipped with gas meters. In this way, leaks can be detected immediately. In particular, the rotating compressors can also be continuously monitored.

New UHV-Cluster Deposition System for the Fabrication of Complex Heterostructures and Novel Quantum Materials

S. Geprägs, R. Gross [1]

High-quality thin film samples and complex heterostructures with well-defined interfaces are the key ingredient for several research fields in modern solid-state physics. They are of key relevance for most of the research projects at the Walther-Meißner-Institute in superconductivity, magnetism, spin electronics, and novel quantum materials. To replace a more than 20-year old UHV deposition cluster and to upgrade WMI thin film technology to today's requirements, WMI has purchased and installed a new state-of-the-art ultrahigh-vacuum (UHV) cluster deposition system. The system was funded in part by the German Research Foundation via the Cluster of Excellence "Munich Center for Quantum Science and Technology (MCQST)".

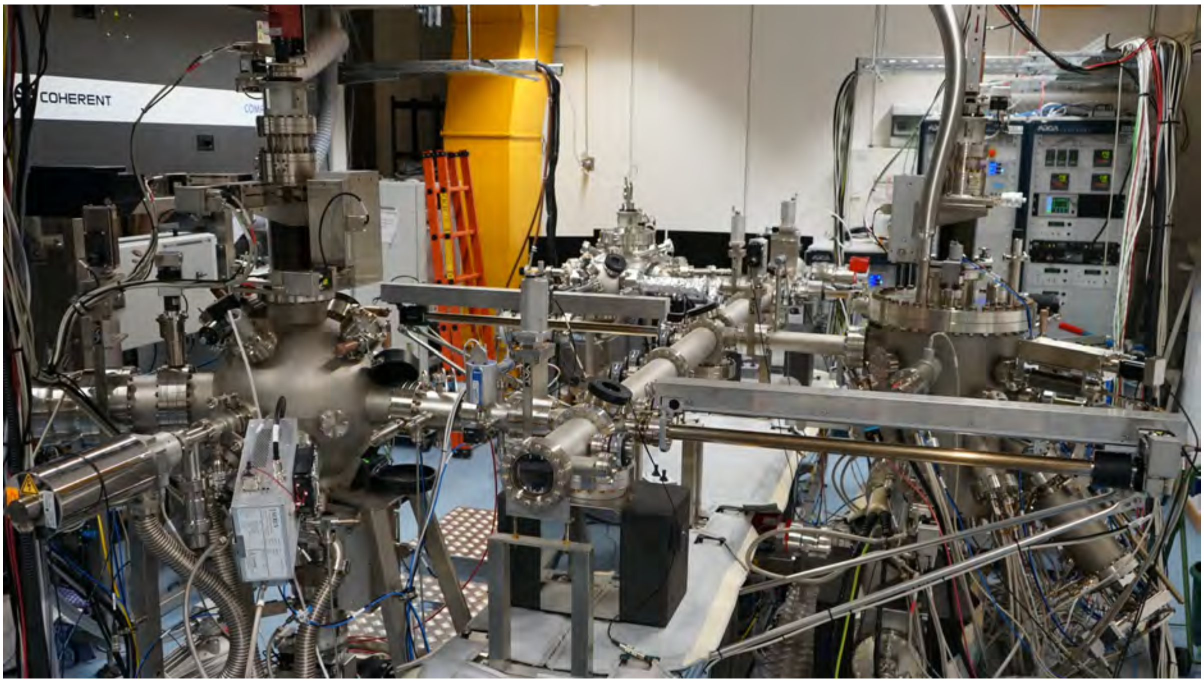

Figure 1: The new UHV-cluster deposition system after installation at WMI. Left part: New UHV-pulsed-laser deposition (UHV-PLD) system for the fabrication of complex oxide materials, middle part: buffer line with transfer system, right part: new UHV-molecular beam epitaxy (UHV-MBE) system for the deposition of topological insulators and metals, back-left: UHV-sputtering system for the fabrication of superconducting thin films.

The new UHV cluster deposition tool significantly extends the resources of the WMI in materials research, in particular with focus on (topological) quantum materials. The properties of the latter materials are uniquely defined by quantum mechanical effects which manifest themselves over a broad range of energy and length scales. These materials have become an emergent and strongly growing field of condensed matter physics, not only due to the possibility to study fascinating new physics but also due to the fact that these materials are promising for applications in the field of topological quantum computing. Prominent examples of quantum materials are unconventional (topological) superconductors, topological insulators, or Weyl semimetals. Moreover, intentionally designed heterostructures based on e.g. topological

[1]Supported by the German Research Foundation under Germany's Excellence Strategy "EXC-2111-390814868".

insulators and superconducting or magnetic materials provide a rich playground in materials design. The fabrication of such materials and heterostructures requires different physical vapour deposition techniques such as pulsed-laser-deposition (PLD), molecular-beam epitaxy (MBE), and sputtering in an ultra-high vacuum environment.

In 2020, after a Europe-wide tender a new UHV-cluster deposition system, which meets these requirements, could be ordered. Due to Covid-19 related delays the new system was delivered by the supplier DCA Instruments Oy only in October 2022. For the installation of the system, which was performed between October and December 2022, our previous, 25 year old cluster deposition system was removed except of the UHV sputter deposition chamber. This system was upgraded with a new sample manipulator enabling substrate heating during deposition and was connected to the new UHV-buffer line. Therefore, the new UHV-cluster deposition system consists of a UHV chamber laser (PLD) molecular beam epitaxy used for the fabrication of epitaxial, oxide materials (left side of Fig. 1), a UHV-MBE system for the deposition of metals and topological insulators (right side in Fig. 1), a sputter deposition chamber for the fabricating of superconducting materials (back left of Fig. 1), and a load-lock for inserting substrates and PLD-targets. These chambers are connected to a UHV-buffer line enabling transfer of samples between the various chambers without breaking UHV. Therefore, this system is particularly designed for the fabrication of heterostructures with clean and well-defined interfaces.

The key elements of the cluster deposition system are the UHV-PLD as well as the UHV-MBE chambers, which will be described in more detail in the following. A schematic drawing of the UHV-PLD system for the fabrication of epitaxial oxide thin films is shown in Fig. 2. The system is equipped with a substrate manipulator, enabling continuous rotation as well as x-, y-scanning to increase homogeneity and uniformity of the thin film material over a lateral size of $10 \times 10\,\mathrm{mm}^2$. Furthermore, a laser head placed on top of the sample manipulator together with a 140 W IR-heater allows for direct and local heating as well as rapid annealing of the substrate. The pressure during deposition of the gas mixture of up to four components (Ar, N_2, O_2, Ar/H_2) can be automatically controlled using an up- or down-stream regulation. Moreover, a differentially pumped RF-atom source for atomic oxygen allows the fabrication of oxide thin films within an highly oxidizing atmosphere also at high partial pressures. To measure and adjust the laser fluence at the target surface the energy of the UV-light of the excimer laser can be measured inside the chamber and automatically adjusted via a motorized attenuator. The PLD system is further equipped with a target carousel with five target carriers, enabling script controlled fabrication of heterostructres. Furthermore, the carousel exhibits some unique features such as an aperture for the laser plume, scanning of the target surface, and a cold plate protecting the targets from heat radiation. To in-situ monitor the growth process, a double-differentially pumped RHEED-system with an acceler-

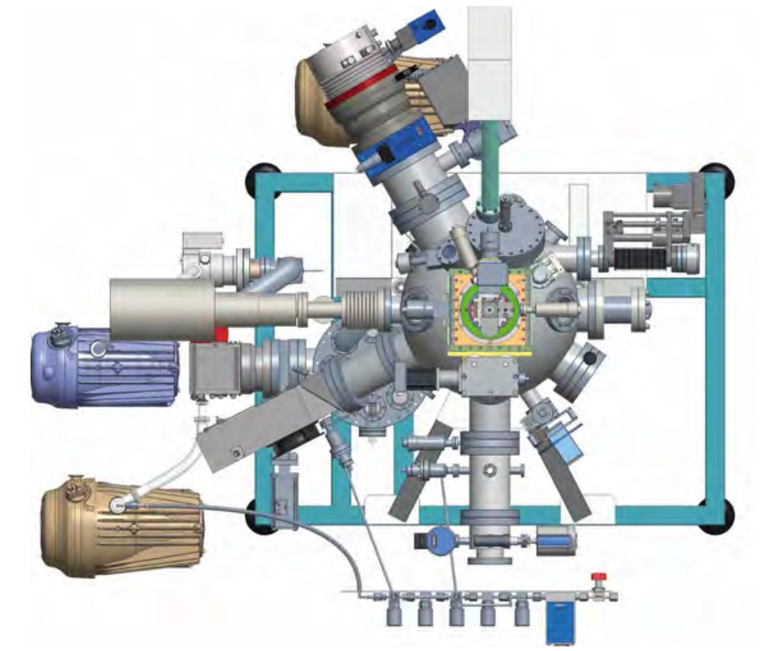

Figure 2: Technical drawing (top-view) of the new UHV-pulsed-laser deposition (UHV-PLD) system.

ating voltage of up to 30 kV is used. It is important to note that all assembled components are UHV-compatible ensuring a base pressure of the PLD-chamber of less than 5×10^{-10} mbar.

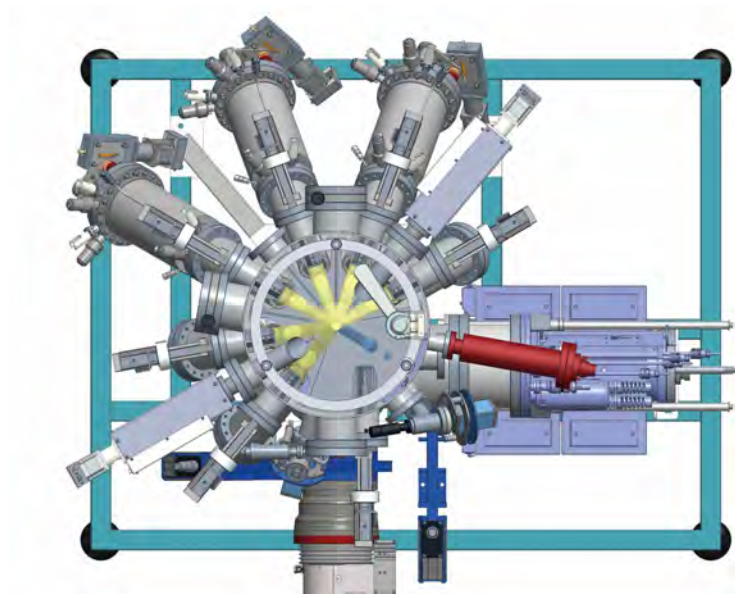

Figure 3: Illustration of the new UHV-molecular beam epitaxy (MBE) system.

The second key component of the new cluster deposition system is the UHV-MBE chamber for the fabrication of topological insulators and metals. As shown in Fig. 3 the system is equipped with three large thermal cracker cells with a crucible size of 500 cm^3 for high-vapour pressure materials such as Se, Sb or Te. The MBE system is further equipped with a low-temperature and two high-temperature cells for Bi and Fe as well as Co, respectively. Additionally, a 6-pocket electron beam evaporation (EVAP) source allows for the deposition of high-melting point materials such as Pt, Pd or W. To determine and control flux ratios and growth rates at the sample position, a beam flux monitor (BFM) as well as a quartz crystal monitor (QCM) is used. Furthermore, the MBE system is also equipped with a low-pressure RHEED system to monitor the growth process. Similar to the PLD-system, the substrate can be heated locally using a laser-head in combination with a IR-laser system. To ensure high purity of the deposited material, ultra-high vacuum within the chamber is required. To this end, the system is pumped by a turbo molecular pump as well as an ion pump combined with a titanium sublimation pump. After bake-out, a base pressure of less than 2×10^{-10} mbar is reached.

Except for the manual process of sample loading and sample transfer all parts of the PLD and MBE systems are fully automated by the supplied computers and software. In particular, all processes can be controlled by user-written scripts, which allows for fully automated deposition processes. This enables a high repeatability of the thin film fabrication.

The new UHV-cluster deposition system will be of key importance for the materials oriented research at the WMI. It will represent the foundation for further progress in the field of quantum materials and will be an important nucleus for future research projects.

Joint Research Projects

WMI Receives Funding for Two MQV Lighthouse Projects

R. Gross, K. Fedorov, S. Filipp, H. Huebl, A. Marx [1]

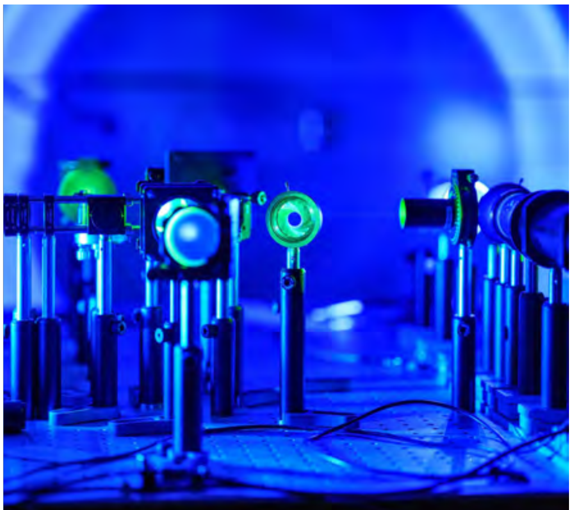

Bavaria funds Lighthouse Projects in quantum science

Basic research projects in quantum science and technology (QST) are essential to keep Bavaria's leading role in this field. Therefore, the Free State of Bavaria provides funding for five interdisciplinary "**Lighthouse Projects**" with a total budget of about 17 million euros as part of the ***Munich Quantum Valley e.V. (MQV)*** (see press release from 04 August 2022). The projects will start in January 20223 and obtain funding for a 3-year period.

The Lighthouse Projects involve the universities in Erlangen-Nuremberg, Munich, Passau, Regensburg and Würzburg. Moreover, the OTH Regensburg and the Deggendorf Institute of Technology were successful with their proposals. Among the non-university institutions, the Walter-Meißner-Institute of the Bavarian Academy of Sciences and Humanities, the Max-Planck Institute of Quantum Optics and the Fraunhofer Institute for Integrated Circuits contribute to the research projects.

Promotion of quantum sciences throughout Bavaria

Science Minister Markus Blume strongly supports the promotion of QST throughout Bavaria by the Lighthouse Projects: *«We want to provide targeted support for interdisciplinary and cross-university projects that can lay the foundations for ground-breaking innovations. Innovations that we can't even imagine today. And which will have a positive impact on us and on future generations. Thus, the future-oriented topic of quantum technologies demonstrates the great visionary quality of the Hightech Agenda of our Minister President Dr. Markus Söder. With Munich Quantum Valley as its epicenter, the Free State is an internationally recognized top location for quantum technologies.»*

The Lighthouse Projects are a particular measure within the ***High-Tech Agenda Bavaria***, aiming to support Bavaria's universities in bringing innovations into practical applications. Bavaria is investing around 300 Mio. € into quantum sciences and technologies. At the heart of this effort is the ***Munich Quantum Valley e.V.***, an alliance of the Bavarian Academy of Sciences and Humanities (BAdW), the Fraunhofer-Gesellschaft (FhG), the Friedrich-Alexander University Erlangen-Nuremberg (FAU), the German Aerospace Center (DLR), the Ludwig-Maximilians-Universität München (LMU), the Max Planck Society (MPG) and the Technical University of Munich (TUM).

[1] Supported by the Bavarian Ministry of Science and Arts within the "Förderprogramm Grundlagenorientierte Leuchtturmprojekte für Forschung, Entwicklung und Anwendungen im Bereich Quantenwissenschaften und Quantentechnologien" within the Munich Quantum Valley e.V.

WMI contributes to two ambitious Lighthouse Projects

The WMI is a key partner in two of the Lighthouse Projects. It contributes to the ambitious projects **Networked Quantum Systems (NeQuS)** and **Integrated Spin Systems for Quantum Sensors (IQ-Sense)**, aiming at the development of integrated quantum sensors for imaging applications in tissue analysis or the hardware for network nodes in hybrid quantum systems. Rudolf Gross was strongly pushing the idea of basic research oriented Lighthouse Projects in the application phase of MQV. He is sure that the Lighthouse Projects will boost Bavarian-wide collaborations and trigger many innovations.

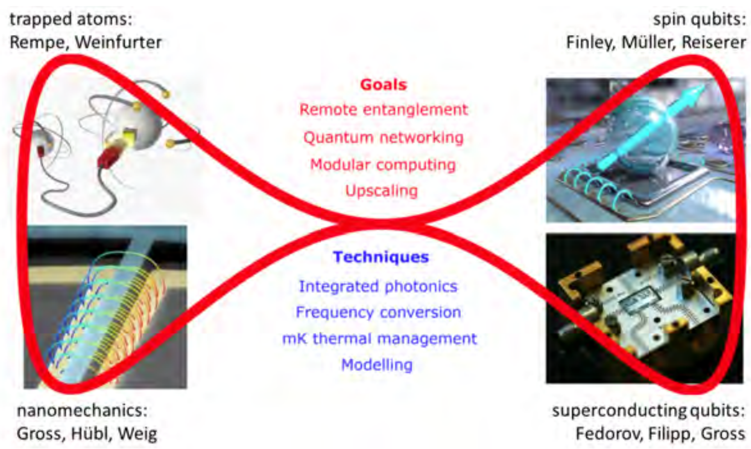

I. Networked Quantum Systems (NeQuS). In quantum technologies, presently no hardware platform fulfills all requirements for useful applications. Thus, hybrid systems that fortuitously combine the advantageous properties of different quantum systems, while circumventing their disadvantageous characteristics, are extremely powerful. The NeQuS project aims to establish such hybrid quantum systems, in which nodes located in different research institutes are linked together using quantum interfaces. The nodes will be based on different hardware platforms including all major systems investigated in quantum technology: superconducting circuits, trapped atoms, nanomechanical resonators, and spins in solids. The project aims at interfacing all of these platforms via quantum states of light propagating in room-temperature optical fibers.

The key challenge in this context is that the individual platforms operate at very different energy scales. While superconducting quantum circuits and nano-electro-mechanical systems use microwave photons with characteristic energies in the range of $10^{-6} - 10^{-5}$ eV, neutral atoms and spins in solids emit visible or infrared photons with an energy around 1 eV - each at a different frequency. To be able to connect these different systems, each of them will establish an interface to photons at telecommunication wavelength. Such photons in the minimal loss regime of optical fibers are ideal carriers of quantum information over many kilometers at ambient temperature, which will lay the ground to distribute entanglement between the different platforms in NeQuS.

Building on established photonic technologies and protocols for quantum state distribution, the central goals of NeQuS are:

- to implement hybrid quantum transducers that allow each platform to generate or receive photons at a telecommunication wavelength,
- to develop performant quantum interconnects between the different platforms,
- to establish entanglement between the individual systems,
- to build quantum network demonstrators and develop protocols for their up-scaling.

With these key capabilities, the envisioned hybrid systems will gain access to the full functionality and strengths of each of the involved hardware platforms.

Consortium:

- Walther-Meißer-Institute (BAdW/TUM): K. Fedorov, S. Filipp, R. Gross, H. Hübl
- Technical University of Munich (TUM): J. Finley, K. Müller, A. Reiserer, E. Weig
- Ludwig-Maximilians Universität (LMU): H. Weinfurter
- Max Planck Institute of Quantum Optics (MPQ): G. Rempe

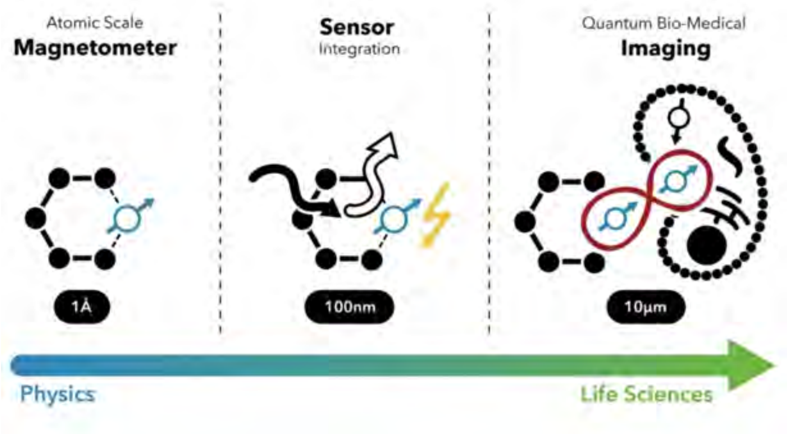

II. Integrated Spin Systems for Quantum Sensors (IQ-Sense). The precise measurement of physical quantities transcends all of the natural and engineering sciences, as well as life sciences and medicine. In the quest to achieve higher precision, and open the doors towards the development of radically new technologies, sensors are now reaching the quantum limit for which the "*sensing element*" is a discrete quantum system that interacts with its environment.

The central goal of the Lighthouse Project IQ-Sense is to synergistically link leading groups from natural science (physics, chemistry), engineering (electrical engineering, information sciences) with researchers working in life sciences and medicine. Thereby, IQSense will develop and demonstrate integrated quantum sensors for a range of application scenarios, including fast screening methods for biological matter. The project IQSense joins leading Bavarian groups working in materials science and quantum sensing technologies and brings them together with clinicians working on the development of cutting edge imaging and sensing technologies.

Consortium:

- Julius-Maximilians-Universität Würzburg (JMUW): V. Dyakonov, B. Hecht, K. Heinze, S. Höfling, M. Sauer
- Walther-Meißer-Institute (BAdW/TUM): R. Gross, H. Hübl
- Technical University of Munich (TUM): Ch. Back, M. Brandt, D. Bucher, J. Finley, F. Schilling, G. Westmeyer

More Information:

- Press release of the Bavarian State Ministry of Science and Arts
- Press release of the Munich Quantum Valey e.V.

Munich Quantum Valley – Quantum Computing with Superconducting Qubits

K. Liegener, H. Hübl, R. Gross, S. Filipp [1]

In January 2022, only one year after the declaration of intent by the Bavarian State Government, the Munich Quantum Valley e.V. was formally established as a registered society. The MQV consists of seven founding members: Max-Planck-Gesellschaft (MPG), Ludwig-Maximilians-University (LMU), Technical University of Munich (TUM), Bavarian Academy of Science (BaDW), Fraunhofer-Gesellschaft (FhG), Deutsche Luft- und Raumfahrtgesellschaft (DLR) and Friedrich-Alexander University (FAU). The WMI, as one of the initiators, has been a key player in shaping the directions and visions of this initiative. Its main objective is to build quantum computers based on different technology platforms, to make them accessible to users as well as to develop the required hardware and software technologies, bringing Germany on par with the worldwide leading countries in quantum technologies by the different consortia (see Figure 1). This powerful Bavarian initiative is accompanied by several programs of the Federal Ministries of Education and Research as well as of Economic Affairs and Energy.

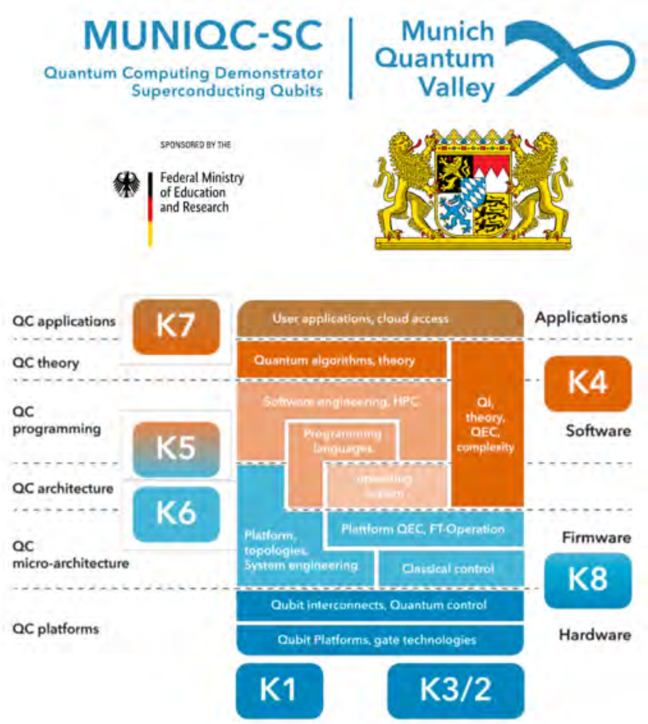

Figure 1: Consortium structure of the Munich Quantum Valley for building a full-stack quantum computer (bottom) along with the logo of the MQV project and the associated BMBF-funded MUNIQC-SC project.

Superconducting Qubit Quantum Computing (SQQC)

Apart from its involvement in the MQV fundamental science Lighthouse Projects and the Quantum Technology Park & Entrepreneurship (QTPE), the WMI is leading the MQV consortium K1 'Superconducting Qubit Quantum Computing (SQQC)' focussing on the development of superconducting qubit technology for enhanced quantum processors . It is partnering with the groups of M. Hartmann (FAU), M. Tornow, C. Jirauschek (TUM, Electrical Engineering) and A. Holleitner, J. Knolle (TUM, Physics) to build and improve the performance of superconducting qubit quantum processors by implementing alternative superconducting qubits going beyond the standard transmon-type qubits. WMI will provide a quantum computing system to execute quantum algorithms for quantum advantage and for benchmarking against the other platforms. A particular focus will be the improvement of materials and fabrication

[1] We acknowledge support by the Bavarian state government with funds the Munich Quantum Valley e.V. from the Hightech Agenda Bayern Plus and the support and funding received for the MUNIQC-SC initiative from the Federal Ministry of Education and Research (BMBF) under funding number 13N16188.

processes: Together with partner EMFT from consortium K6 and the TUM we will develop and test different qubit materials and fabrication methods (e.g. Tantalum, NbTiN) along with the respective fabrication optimizations and surface treatments or loss-less coatings to avoid re-oxidation and dissipation. Making use of the available expertise in quantum materials at the WMI we will further investigate non-reciprocal quantum materials for circulators and isolators used for the readout of the qubits.

Although the Corona pandemic has delayed the installation of relevant equipment, important progress has been witnessed in 2022. Most importantly, the quality of the fabrication process has drastically increased during the year, now reaching resonator quality factors of almost five million, which surpasses the original target of an important milestone at MQV. In cooperation with TUM, WMI is studying the environment of qubits to avoid in the future noise due to two-level-systems and is improving snail-based TWPAs. WMI fabricated already first fluxonium devices and is ready to perform a full characterization of the system in the beginning of 2023.

Munich Quantum Valley Quantumcomputer Demonstrators – Superconducting Qubits (MUNIQC-SC)

Complementary to the MQV SQQC efforts, S. Filipp (via his TU Munich affiliation) is coordinating the BMBF-funded project Munich Quantum Valley Quantum Computer demonstrators – Superconducting Qubits (MUNIQC-SC), which has started in January 2022. This initiative targets crucial challenges when scaling up quantum computers, with the goal to reach up to hundred superconducting qubits within the next five years. With a total budget of 44 Mio. €, a diverse team of research institutes and industry partners has teamed up to tackle that challenge: Friedrich-Alexander University (FAU), Fraunhofer-Gesellschaft (FhG), Infineon (IFX), Leibniz institute for innovative microelectronics (IHP), IQM Germany GmbH (IQM), Kiutra GmbH (KIU), Leibniz supercomputing centre (LRZ), Parity Quantum Computing GmbH (PQC), Qruise GmbH (QRU), TU Munich (TUM) and Zürich Instruments (ZI).

The key innovation directions are the development of a qubit fabrication technology that is suitable for industry, the scaling of a few-qubit devices to larger quantum registers, extended qubit control for high-fidelity operations towards error correction and the standardization and unification of routine operations. For those purposes, MUNIQC-SC includes research on microwave circuits, investigations of 3D-integration methods for superconducting circuits and the development of adapted compilers and prototyping applications for quantum computers. Eventually, it is aimed to make the quantum computing demonstrator available to a broad audience by the means of cloud access. Currently, the MUNIQC-SC project is still in its ramp-up phase. In addition to implementing a sufficient laboratory infrastructure, TUM/WMI and its partners are in the process of hiring qualified personnel to execute the envisioned tasks within this project. Of particular importance are the building up of the characterization infrastructure for rapid-turnaround testing of quantum processors and components and the setting up of a large-scale cryogenic system.

The EU Quantum Flagship Project QMiCS

F. Deppe, K. G. Fedorov, A. Marx, M. Renger, R. Gross [1]

The EU project ***Quantum microwave communication and sensing (QMiCS)*** was one the 20 projects funded by the European Union (EU) within the first call of the Quantum Flagship program (www.qt.eu). It was coordinated by the Walther-Meißner-Institute. Scientific project partners were Aalto University (AALTO, Finland), École Normale Superieure der Lyon (ENSL, France), Instituto de Telecomunicações (Portugal), Universidad del País Vasco / Euskal Herriko Unibertsitatea (UPV/EHU, Spain), and VTT (Finland). Active industry partners were Oxford Instruments Nanotechnology Ltd. (OINT, United Kingdom) and TTI Norte S.L. (Spain). The QMiCS project started in 2018 and was successfully completed in 2022. It provided major scientific and technical innovations in the field of continuous-variable quantum microwave communication and sensing. The three main goals – the realization of a 6.6 meter long quantum local area network (QLAN) cable connecting two dilution refrigerators at millikelvin temperatures, the implementation of a proof-of-principle quantum illumination experiment, and a the development of a roadmap towards real-life applications of quantum microwaves – could be achieved within the project period.

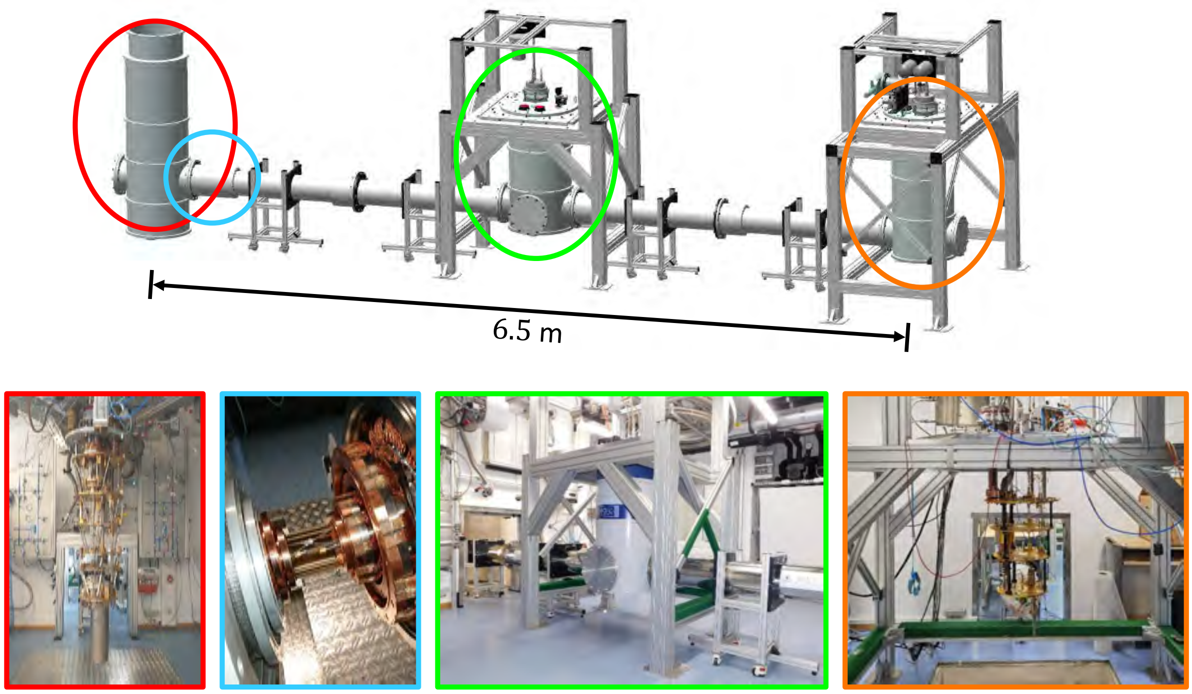

Figure 1: The WMI cryolink: Schematics (top) and images of sub-components (bottom) marked by different colors.

A major achievement of WMI in collaboration with the industry partner Oxford Instruments Nanotechnology Ltd. was the realization of a 6.6 meter long quantum local area network (QLAN) cable connecting two dilution refrigerators (see Fig. 1). This so-called cryolink is fully operable and has been used to demonstrate quantum teleportation of truly propagating microwave states between two distant dilution fridges for the first time, after intra-fridge quantum teleportation already has been demonstrated in 2021 [1]. Using two-mode squeezed

[1] We acknowledge support by the German Research Foundation via Germany's Excellence Strategy (EXC-2111-390814868) and the EU Flagship project QMiCS (Grant No. 820505).

states as entanglement resource, we have exceeded a no-cloning threshold for coherent states. Furthermore, we have presented our visions for microwave quantum networks in an article for the general public [2]. The demonstration of quantum teleportation between two dilution refrigerators placed in different labs certainly is one of the key highlights of the QMiCS project.

The second key experiment in the QMiCS project, namely quantum-radar-type illumination based on frequency-nondegenerate microwave entanglement, has been performed at partner ENSL. Both WMI and ENSL also have successfully tested parametric devices fabricated by partner VTT and analyzed the fundamental noise limits in parametric amplification [3]. In another exciting experiment, ENSL demonstrated squeezing beyond the usual 3 dB-threshold inside a resonant microwave mode [4].

Overall, the QMiCS project has been a great success. The cryolink set up at WMI is meanwhile used for a variety of interesting experiments like quantum communication over thermal channels [5], microwave quantum key distribution [6], entanglement distribution, or the realization of remote gates for distributed superconducting quantum computation.

References

[1] K. G. Fedorov, M. Renger, S. Pogorzalek, R. Di Candia, Q. Chen, Y. Nojiri, K. Inomata, Y. Nakamura, M. Partanen, A. Marx, R. Gross, and F. Deppe, Science Advances **7**, eabk0891 (2021).

[2] F. Deppe, K. G. Fedorov, and A. Marx, Akademie Aktuell **Heft 2**, 36–38 (2021).

[3] M. Renger, S. Pogorzalek, Q. Chen, Y. Nojiri, K. Inomata, Y. Nakamura, M. Partanen, A. Marx, R. Gross, F. Deppe, and K. G. Fedorov, npj Quantum Inf. **7**, 160 (2021).

[4] R. Dassonneville, R. Assouly, T. Peronnin, A. Clerk, A. Bienfait, and B. Huard, Phys. Rev. X Quantum **2**, 020323 (2021).

[5] M. Renger, S. Pogorzalek, F. Fesquet, K. Honasoge, F. Kronowetter, Q. Chen, Y. Nojiri, K. Inomata, Y. Nakamura, A. Marx, F. Deppe, R. Gross, and K. G. Fedorov, Physical Review A **106**, 052415 (2022).

[6] F. Fesquet, F. Kronowetter, M. Renger, Q. Chen, K. Honasoge, O. Gargiulo, Y. Nojiri, A. Marx, F. Deppe, R. Gross, and K. G. Fedorov, arXiv **2203.05530** (2022).

The Horizon Europe Project OpenSuperQPlus

S. Filipp, H. Hübl, C. Schweizer, M. Werninghaus [1]

In 2018, the European Union (EU) launched the Quantum Flagship projects (www.qt.eu) to invest massively in quantum technologies. In the field of superconducting quantum circuits, the WMI coordinated the project ***Quantum microwave communication and sensing (QMiCS)*** (see report on page 36). The realization of a superconducting qubit based quantum processor has been the goal of the OpenSuperQ project. After completion of this first round of funding, the European Union is now continuing its support of quantum technologies and has set up a framework to develop the relevant technologies for a scalable quantum computing system.

Figure 1: OpenSuperQPlus Logo

The WMI plays a key role in this effort: In 2022 the OpenSuperQPlus Framework Partnership Agreement (FPA) with the WMI as one of the major players has been given the green light to develop the roadmap towards a Quantum Processor Unit (QPU) based on superconducting qubits. Its ambitious goal is to reach up to 1000 qubits in a scalable architecture by creating a competitive, yet realistic, roadmap for a full-stack superconducting quantum computing system until 2029 and beyond. The framework program consists of two phases: In the first phase, OpenSuperQPlus 100 plans to reach 100 qubits by 2025 and to develop relevant technological components and solutions for the second phase, in which OpenSuperQPlus 1000 aims at systems of 1000 qubits and more by 2029.

OpenSuperQPlus100, which is planned to start in March 2023 and runs for 3.5 years, combines the quantum engineering and technology expertise of universities, RTOs, and SMEs to demonstrate quantum advantage and fault-tolerant quantum computing. Within this project the Quantum Processor Unit (QPU) design and fabrication technology, as well as the system integration and enabling technology capabilities are developed to reach the metrics required for useful quantum computing. By complementing the funding from national and private sources it further focusses the European community toward developing and deploying a scalable, high-performance European quantum computing platform. The OpenSuperQPlus 100 partnership builds on the expertise and technologies developed by the OpenSuperQ consortium, as well as by new partners with a long history of collaboration, e.g., via SOLID (2009-2012) and ScaleQIT (2012-2016).

In the OpenSuperQPlus100 project the WMI sets out to develop a QPU based on alternative, fluxonium-type qubits. In the first step a small number of fluxonium qubits are connected and their performance is compared to a standard transmon-type QPU, which is developed within the MQV projects (see report on page 34). The WMI focus lies on high-quality operations and on the scalability of the alternative-qubit platform with the main objective to make an informed decision on the platform for the next-generation 1000-qubit QPU. To reach this milestone, the WMI combines basic and exploratory research on novel devices with the technology development required for scalability. It will investigate novel materials and fabrication recipes to reach highest quality superconducting quantum circuits with small footprints. In addition, the WMI will explore ways to optically control qubits, such mitigating the imminent bottleneck created by the large number of individual control and readout lines for thousand and more qubits. Finally, the WMI plans to provide remote access to the QPUs and to develop system integration capabilities in collaboration with the Leibniz Rechenzentrum (LRZ).

[1] We acknowledge support by the EU Horizon Europe Project OpenSuperQPlus100 (Grant No. 101080139).

The EU-Project «Exploring Nonclassical States of Center-of-Mass Mechanical Motion with Superconducting Magneto- and Levitomechanics» (SuperMEQ)

H. Huebl, A. Marx, and R. Gross [1]

The EU Project «Exploring non-classical states of center-of-mass mechanical motion with superconducting magneto- and levitomechanics» (SuperMEQ) (coordinator: Witlef Wiczorek, Chalmers University of Technology) started in October 2022. Within this project, WMI collaborates with partners from Chalmers University of Technology, the University of Vienna, the University of Innsbruck, the Austrian Academy of Sciences, the Karlsruhe Institute of Technology, and the Universitat Autonòma de Barcelona as well as the industry partner Infineon.

SuperMeQ addresses three basic science goals in quantum technologies, targeting to gain new insights into quantum control over the center-of-mass motion of mechanical resonators: (i) We will push to the limits of decoherence mechanisms of massive objects, (ii) we will maximize the vacuum coupling of the center-of-mass motion of a mechanical resonator to a quantum system, and (iii) we will generate useful nonclassical states such as squeezed states or states with a negative Wigner function, which have direct relevance for quantum-enhanced force and inertial sensing. Our project follows a unique approach by realizing two complementary experimental platforms that are tailored to our goals and that are mutually beneficial through parallel development: (a) magnetically levitated superconducting microparticles that access a mass regime spanning more than seven orders of magnitude between picogram and sub-milligram masses, and that are expected to exhibit ultra-low mechanical decoherence, and (b) integrated clamped magnetic or superconducting mechanical resonators that are expected to reach strong vacuum coupling rates, two orders of magnitude larger than the state-of-the-art. Key in each of these approaches is that we will couple both types of mechanical resonator inductively to superconducting quantum circuits, which allow for full quantum control over the center-of-mass degree of freedom of the mechanical resonators. Our project results will lead to a breakthrough in the development and growth of novel quantum sensing technologies and give new insights into foundational aspects of quantum physics.

The WMI contributes to this project the following areas: (i) pushing optomechanics to the strong single photon coupling regime, (ii) the development of superconducting quantum circuits for the readout of massive objects, and (iii) the generation of non-classical states for sensing. The established nano-electromechanical systems based on nano-strings developed within the WMI in combination with the inductive readout technique developed at WMI provide an exquisite starting position for the sucessful realization of the goals of SuperMEQ. In addition, the long-standing and established know-how of the institute in areas such as low-temperature technology and vibration isolation techniques contribute further to those key challenges.

[1]This project has receives funding via the Horizon Europe 2021-2027 Framework Programme under grant agreement No. 101080143.

Basic Research

Magnetic Quantum Oscillations in a Molecular Conductor Near and Away from the Mott Transition

S. Erkenov, W. Biberacher, R. Gross, M.V. Kartsovnik [1]

The Mott metal-insulator transition (MIT) is a hallmark of strong electronic correlations in a metal, closely related to unconventional superconductivity and other exotic quantum states. Thorough knowledge of the metallic ground state properties in direct proximity to the MIT is indispensable for understanding these phenomena. We have recently demonstrated the high efficiency of the magnetic quantum oscillation technique in tracing the evolution of the quasi-two-dimensional (quasi-2D) conduction system of the molecular conductor κ-(BEDT-TTF)$_2$Cu[N(CN)$_2$]Cl (hereafter κ-Cl) tuned very close to the MIT by means of precisely controlled pressure in the range below 1 kbar [1]. The most surprising result of our study was an unexpectedly strong pressure dependence of the effective cyclotron mass, $m_c(P)$, which was even further accelerated in the transitional region, where the metallic and Mott-insulating phases coexist. A comparison with the theoretical predictions of the effective mass renormalization caused by electron-electron interactions near the MIT [2, 3] reveals an order-of-magnitude discrepancy [1]. To clarify whether some other mechanisms, irrelevant to the MIT, such as electron-phonon interactions, contribute to the $m_c(P)$ dependence, we have carried out a quantum oscillation study in the extended pressure range $0.5\,\text{kbar} \leq P \leq 15\,\text{kbar}$, covering both the close proximity of the MIT and a "good metal" region far away from the transition.

Figure 1(a) shows examples of the quantum (Shubnikov-de Haas, SdH) oscillations in the interlayer resistance of κ-Cl at different pressures, at $T = 0.4\,\text{K}$. The oscillatory component of the resistance R_{osc} is normalized to the non-oscillating field-dependent background R_{bg}. Two fundamental SdH frequencies are observed. The frequency $F_\alpha \simeq 600\,\text{T}$ is determined by the size of the closed pocket α of the Fermi surface, whereas the frequency $F_\beta \simeq 4\,\text{kT}$ is associated with the magnetic-breakdown orbit encompassing the entire 2D Fermi surface with an area equal to the first Brillouin zone area [1, 4]. The β oscillations exhibit beats originating most likely from a weak warping of the Fermi surface in the interlayer direction [1].

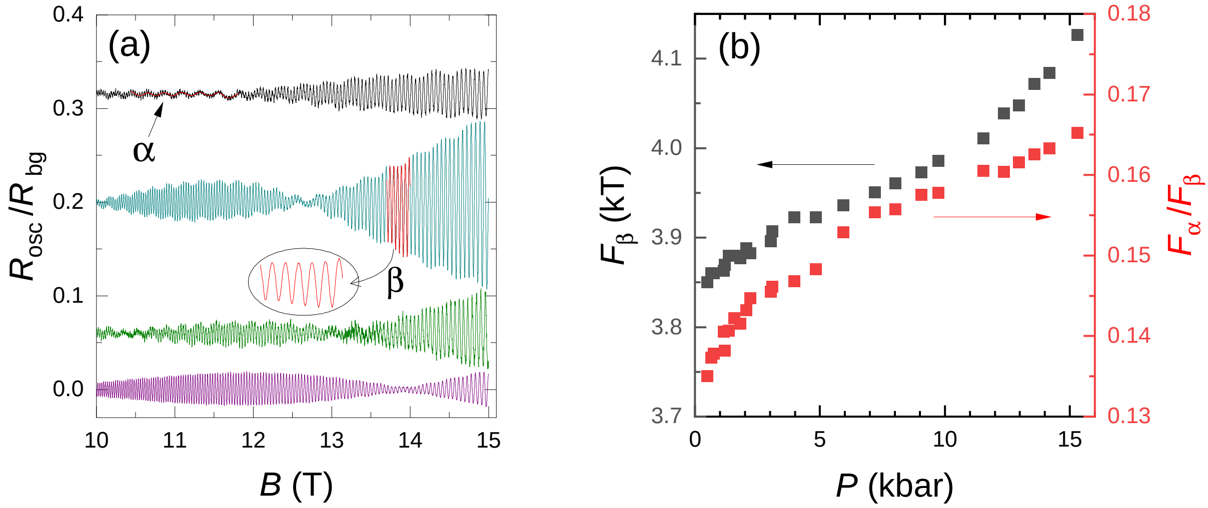

Figure 1: (a) SdH oscillations in the interlayer resistance of κ-Cl at $T = 0.4\,\text{K}$, at (top to bottom) $P = 1.3\,\text{kbar}$, 4.8 kbar, 7.2 kbar, and 14.2 kbar. The curves are vertically shifted for clarity. The fragments marked by red color emphasize the presence of slow (α) and fast (β) oscillations. (b) Pressure dependence of the β-oscillation frequency F_β (black symbols, left-hand axis) and of the frequency ratio F_α/F_β (red symbols, right-hand scale).

[1] The work is supported by the German Research Foundation, grants KA 1652/5-1 and GR 1132/19-1.

The pressure-induced compression of the crystal lattice leads to an expansion of the Brillouin zone, hence, to an increase of F_β [cf. Fig. 1(b), black squares]. The area of the Fermi pocket α increases even faster with pressure, which is reflected in a growing ratio F_α/F_β [cf. red symbols in Fig. 1(b)]. This data contains information about the P-dependence of the effective in-plane transfer integrals t and t' within the triangular-lattice Hubbard model [5]. The analysis aimed at evaluation of the frustration ratio t/t', one of the key parameters of the MIT in the presence of magnetic ordering instabilities, is currently in progress.

One of our main objectives was to trace the effective cyclotron mass in a broad pressure range spanning the phase diagram between the MIT and the "good metal" region. The mass was evaluated from the T-dependence of the SdH amplitude, using the standard Lifshitz-Kosevich formula [6]. The results are shown in Fig. 2 for the masses corresponding to the β and α cyclotron orbits. In the whole pressure range, the α mass is half the size of the β-mass. Remarkably, the band structure calculations neglecting many-body renormalization effects [7] yield considerably smaller values for the cyclotron masses but the same relationship, $m_{\beta,\,\mathrm{band}} \approx 2m_{\alpha,\,\mathrm{band}}$. This coincidence strongly suggests that the renormalization effects are the same for both orbits, i.e. independent of the electron momentum.

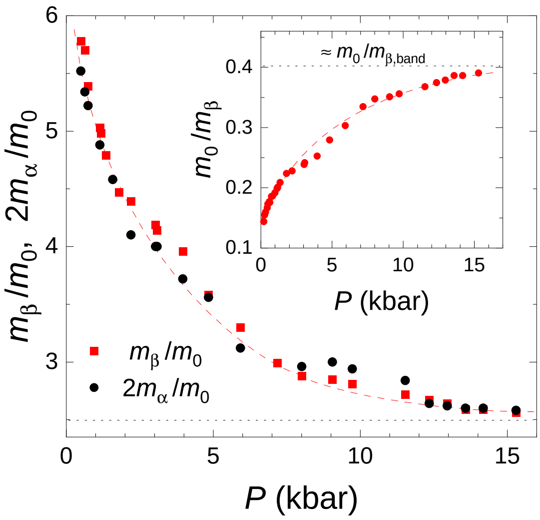

Figure 2: Effective cyclotron masses $2m_\alpha$ and m_β, normalized to the free electron mass m_0, plotted versus pressure. The dashed line is a guide to the eye. The P-dependence saturates at high pressures, at the level corresponding to the band cyclotron mass $m_{\beta,\,\mathrm{band}} \approx 2.5m_0$ (dotted line). The inset shows the inverse of the β mass to illustrate the saturation trend more clearly.

The P-dependence of the mass, being steep at low pressures, flattens out at $P \geq 10$ kbar. The saturation value, $\simeq 2.5m_0$, is close to the calculated band mass $m_{\beta,\,\mathrm{band}}$ [8], suggesting that the mass renormalization becomes negligibly weak as the system is driven away from the MIT. This is exactly what one expects from the renormalization caused by electron-electron interactions in a metal with the Mott-insulating instability. By contrast, the electron-phonon interactions are not expected to vary dramatically upon approaching the MIT. Moreover, the applied pressure of several kbar is too low to induce a considerable change in electron-phonon coupling. Therefore, we conclude that the anomalously steep P-dependence of the effective mass at pressures below 1 kbar, i.e. in the direct proximity of the purely Mott-insulating state, is most likely caused by electron-electron interactions. Clarifying the detailed nature of this dependence and its drastic violation of the existing theoretical predictions is expected to significantly advance our understanding of the Mott transition physics.

References

[1] S. Oberbauer, S. Erkenov, W. Biberacher, N. D. Kushch, R. Gross, and M. Kartsovnik, arXiv:2208.03230 (2022).
[2] W. Brinkman, and T. Rice, Phys. Rev. B **2**, 4302 (1970).
[3] A. Georges, G. Kotliar, W. Krauth, and J. Rozenberg, Rev. Mod. Phys. **68**, 13 (1996).
[4] M. V. Kartsovnik, W. Biberacher, K. Andres, and N. D. Kushch, JETP Lett. **62**, 905 (1995).
[5] F. Pratt, Physica B: Condensed Matter **405**, S205 (2010).
[6] D. Shoenberg. *Magnetic Oscillations in Metals* (Cambridge University Press, Cambridge, 1984).
[7] J. Merino, and R. H. McKenzie, Phys. Rev. B **62**, 2416 (2000).
[8] Y.-N. Xu, W. Y. Ching, Y. C. Jean, and Y. Lou, Phys. Rev. B **52**, 12946 (1995).

Microwave Single-Shot Quadrature Measurements

F. Fesquet, F. Kronowetter, M. Renger, A. Marx, R. Gross, K. G. Fedorov [1]

The security of modern classical data encryption usually relies on computationally hard to solve problems. A possible way to improve this approach is to apply techniques which take advantage of the laws of quantum physics to enable the secure exchange of information. Typical examples are unconditionally secure quantum key distribution (QKD) or unforgeable quantum tokens. In continuous variable (CV) quantum communication efficient single-shot field quadrature measurement (QM) are required to implement various QKD protocols or to perform entanglement swapping operations. In the microwave regime, single-shot QM can be performed via phase-sensitive amplification [1]. The latter has been demonstrated to be efficiently implemented with Josephson parametric amplifiers (JPAs) [2]. Here, we show the realization of a JPA-based QM of displaced squeezed microwave states propagating through a thermal channel. We analyze the measured data by computing the classical mutual information (MI) between a sender (Alice) and a receiver (Bob).

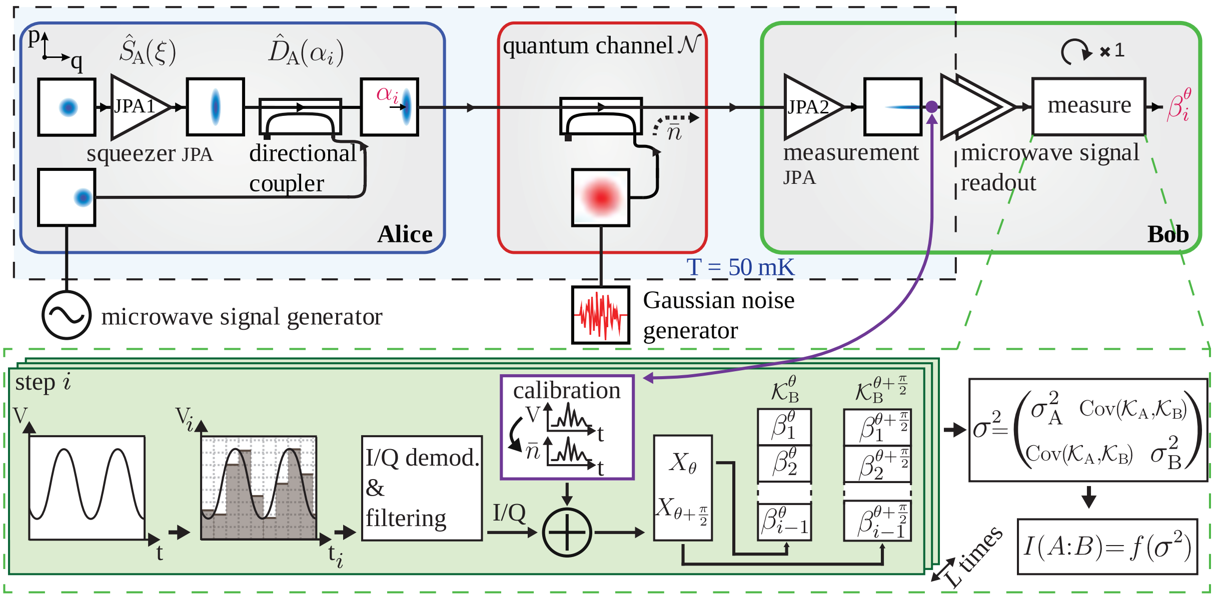

Figure 1: Experimental implementation of a microwave QM with propagating displaced squeezed microwave states. Color plots in black boxes represent quantum states in quasi-probability Wigner phase space spanned by field quadratures q and p. The thermal quantum channel $\mathcal{N}$ is implemented with a directional coupler adding $\bar{n}$ noise photons to the incoming signals. QMs are realized by a JPA operated in the phase-sensitive regime. For each quadrature measurement, the data is filtered and I/Q demodulated. The MI between Alice and Bob is computed from the tomography data.

Our experimental implementation, shown in Fig. 1, relies on superconducting flux-driven JPAs for the generation of squeezed microwave states [2]. The latter are displaced by a complex displacement amplitude α_i with a cryogenic directional coupler [3]. A second directional coupler emulates a thermal quantum communication channel by adding a controlled average noise photon number $\bar{n}$ to incoming signals. Subsequently, a second JPA, operated in the degenerate regime, enables single-shot QMs by strongly amplifying one quadrature (X_θ) while deamplifying a corresponding orthogonal quadrature ($X_{\theta+\frac{\pi}{2}}$). The statistics of the measured quadratures are used to compute the classical MI $I(A:B)$ between Alice's ensemble $\mathcal{K}_A = \{\alpha_i\}_{i\in[1,L]}$ and

[1] We acknowledge support by the German Research Foundation via Germany's Excellence Strategy (EXC-2111-390814868), and the German Federal Ministry of Education and Research via the project the project QuaMToMe (Grant No. 16KISQ036). This research is part of the Munich Quantum Valley, which is supported by the Bavarian state government with funds from the Hightech Agenda Bayern Plus.

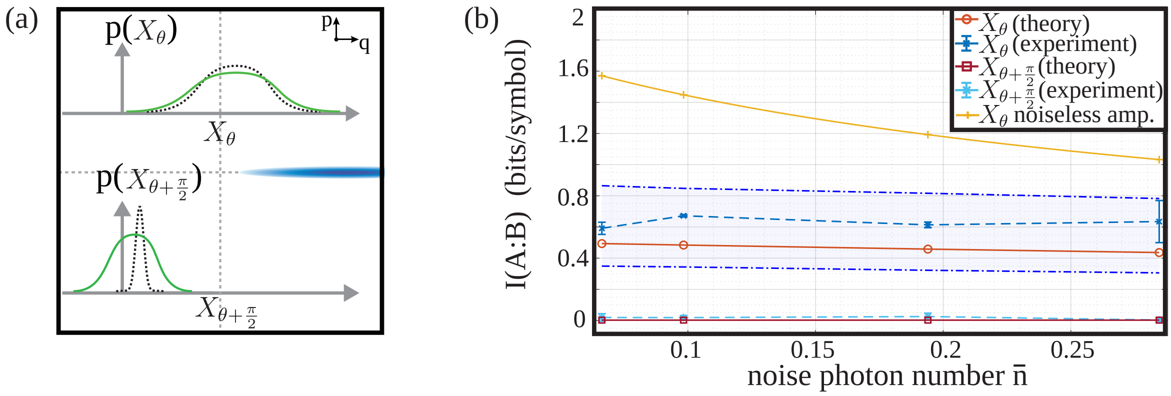

Figure 2: Measurements of the classical mutual information $I(A : B)$ between Alice and Bob. (a) Transformation of quadrature probability distributions during phase-sensitive amplification (green solid line corresponds to the initial state, grey dashed line corresponds to amplified and noisy distributions). The amplified quadrature X_θ is weakly disturbed by the detection noise. On the contrary, the deamplified quadrature $X_{\theta+\frac{\pi}{2}}$ is strongly affected by the detection noise. The corresponding MI for each quadrature is shown on panel (b) for both theory and experiment. The yellow solid line shows the theoretical MI for noiseless amplification.

Bob's ensemble $\mathcal{K}_B^\theta = \{\beta_i^\theta\}_{i\in[1,L]}$ (amplified quadrature) or $\mathcal{K}_B^{\theta+\pi/2} = \{\beta_i^{\theta+\pi/2}\}_{i\in[1,L]}$ (deamplified quadrature). This MI is related to the signal-to-noise ratio (SNR) of the experimental setup as

$$I(A : B) = \frac{1}{2}\log_2(1 + \mathrm{SNR}). \tag{1}$$

The SNR depends on the statistics of the measured quadratures and is strongly influenced by the noise properties of the measurement JPA. We characterize the noise of our measurement chain using the quantum efficiency $\eta = 1/(1 + 2n_{\mathrm{amp}})$, with n_{amp} the input noise photons added by the amplfiers [4]. In our experiment, we obtain the quantum efficiency of $38\,\% \pm 2\,\%$, corresponding to ~ 0.8 noise photons. In Fig. 2, we show the resulting classical MI. We observe a good agreement between the theory and the experiment. In particular, the MI for the deamplified quadrature is nearly zero, demonstrating the almost complete loss of information when projecting (amplifying) the conjugate quadrature. As a result, we model the amplification with the measurement JPA as a noisy quadrature projection operation. As illustrated in Fig. 2, the discrepancy between the experimentally implemented projection and an ideal projection can be regarded as the difference between the measured MI for X_θ and the same MI computed for an ideal noiseless measurement JPA.

In summary, our results demonstrate the successful realization of a single-shot QM in the microwave regime using JPAs. These results provide the basis for realizing more complex quantum communication protocols, such as microwave QKD, entanglement swapping, or entanglement distillation.

References

[1] F. Mallet, M. A. Castellanos-Beltran, H. S. Ku, S. Glancy, E. Knill, K. D. Irwin, G. C. Hilton, L. R. Vale, and K. W. Lehnert, Phys. Rev. Lett. **106**, 220502 (2011).

[2] L. Zhong, E. P. Menzel, R. Di Candia, P. Eder, M. Ihmig, A. Baust, M. Haeberlein, E. Hoffmann, K. Inomata, T. Yamamoto, Y. Nakamura, E. Solano, F. Deppe, A. Marx, and R. Gross, New J. Phys. **15**, 125013 (2013).

[3] K. G. Fedorov, L. Zhong, S. Pogorzalek, P. Eder, M. Fischer, J. Goetz, E. Xie, F. Wulschner, K. Inomata, T. Yamamoto, Y. Nakamura, R. Di Candia, U. Las Heras, M. Sanz, E. Solano, E. P. Menzel, F. Deppe, A. Marx, and R. Gross, Phys. Rev. Lett. **117**, 020502 (2016).

[4] M. Renger, S. Pogorzalek, Q. Chen, Y. Nojiri, K. Inomata, Y. Nakamura, M. Partanen, A. Marx, R. Gross, F. Deppe, and K. G. Fedorov, npj Quantum Inf. **7**, 160 (2021).

Towards a Practical Microwave Quantum Radar

F. Kronowetter, F. Fesquet, M. Handschuh, K. Honasoge, Y. Nojiri, M. Renger, A. Marx, R. Gross, K. G. Fedorov [1]

Theory predicts that radar techniques based on quantum illumination (QI) can substantially outperform the ideal classical radar by providing a 6 dB gain in the error probability exponent [1]. However, this quantum advantage can only be achieved in a specific parameter regime, namely at a low number of signal photons in combination with a bright thermal background and a weakly reflecting target. Since the implementation of the quantum receiver providing the full 6 dB advantage is highly complicated, alternative receiver schemes based on off-the-shelf components have been proposed [2]. These low-complexity approaches typically yield a theoretical quantum advantage of 3 dB. In order to experimentally realize such a scheme, we analyze practical implementations of the microwave quantum radar scheme with the goal to maximize the advantage in the error probability with respect to the ideal classical radar. In a second step, we analyze the effect of a reduced efficiency of the photon counter used in this scheme.

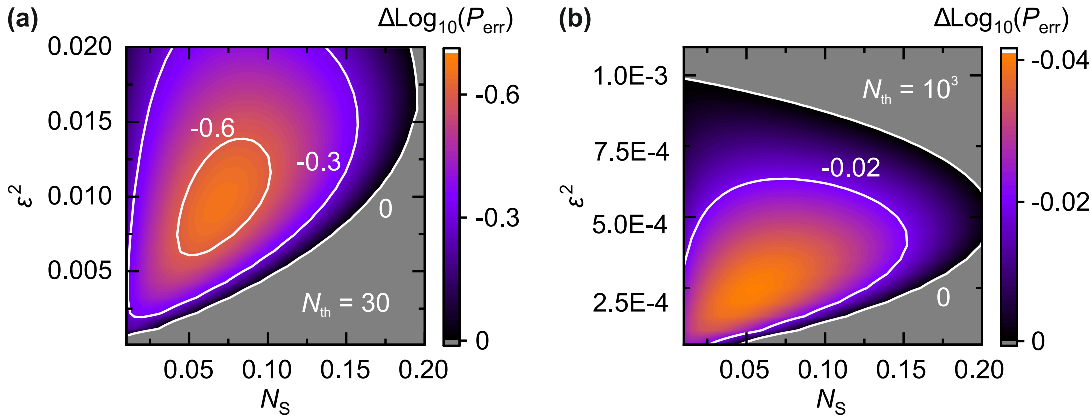

Figure 1: Contour plot of the logarithmic difference $\Delta \log_{10}(P_{\rm err}) = \log_{10}(P_{\rm err,Q}) - \log_{10}(P_{\rm err,C})$ between the QI error probability $P_{\rm err,Q}$ and the ideal classical error probability $P_{\rm err,C}$ as a function of the mean signal photon number $N_{\rm S}$ and the receiver gain $G = 1 + \epsilon^2$ for $\kappa = 0.01$, $M = 10^6$, **(a)** $N_{\rm th} = 30$ and **(b)** $N_{\rm th} = 1000$. The region where the QI scheme does not outperform the classical scheme is greyed out. While $N_{\rm S,ideal} = 0.07$ (orange color) is robust against $N_{\rm th}$, the ideal receiver gain $G = 1 + \epsilon^2$ decreases with increasing $N_{\rm th}$.

In the context of the quantum radar scheme [2], we consider entangled signal-idler modes with a mean photon number $N_{\rm S} \ll 1$ per mode. Under the hypothesis H_0 (object absent), the signal mode is lost and the return mode is a purely thermal state with a mean photon number $N_{\rm th} \gg 1$. Under the hypothesis H_1 (object present), the signal mode is weakly reflected (modeled by a beam splitter with low reflectivity, $\kappa \ll 1$) and superimposed with a thermal state. In contrast to the classical reference scheme based on coherent states, QI yields thermal states with zero mean under both hypotheses. The decisive resource for the enhanced QI performance are remaining intermode correlations reflected by non-zero anti-diagonal entries in the covariance matrix $V = \langle [\,\hat{a}_{\rm S}\,\hat{a}_{\rm I}\,\hat{a}_{\rm S}^\dagger\,\hat{a}_{\rm I}^\dagger]^T\,[\,\hat{a}_{\rm S}^\dagger\,\hat{a}_{\rm I}^\dagger\,\hat{a}_{\rm S}\,\hat{a}_{\rm I}]\,\rangle$, where $\hat{a}_{\rm S,I}$ are the bosonic operators of the signal and idler modes, respectively [1]. The transformation of the incoming signal and idler modes enables one to access these remaining correlations in measurements of the photon number

$$N = \langle \hat{b}_1^\dagger \hat{b}_1 \rangle = G\hat{a}_{\rm I}^\dagger \hat{a}_{\rm I} + (G-1)\hat{a}_{\rm S}\hat{a}_{\rm S}^\dagger + \sqrt{G(G-1)}(\,\hat{a}_{\rm I}^\dagger \hat{a}_{\rm S}^\dagger + \hat{a}_{\rm S}\hat{a}_{\rm I}), \quad (1)$$

[1] We acknowledge support by the German Research Foundation via Germany's Excellence Strategy (EXC-2111-390814868), and the German Federal Ministry of Education and Research via the project QUARATE (Grant No. 13N15380). This research is part of the Munich Quantum Valley, which is supported by the Bavarian state government with funds from the Hightech Agenda Bayern Plus.

where $\hat{b}_1$ is a single mode entering the photon counter. The last term in Eq. (1) contains the introduced anti-diagonal entries of V, which are nonzero under H_1 and vanish under H_0. For a total number of M mode copies following a thermal distribution with mean $M \cdot N$ and variance $M \cdot N(N+1)$, the ideal decision strategy to distinguish H_0 and H_1 is to count the overall number of photons and compare it with a threshold value. Here, we derive the latter by using the Bayesian decision rule [1]. We analytically solve for the total error probability $P_{\mathrm{err,Q}}$ of the QI scheme and compare against the analytically solved error probability $P_{\mathrm{err,C}}$ of the ideal classical scheme.

Fig. 1 shows a contour plot of the logarithmic error difference $\Delta \log_{10}(P_{\mathrm{err}}) = \log_{10}(P_{\mathrm{err,Q}}) - \log_{10}(P_{\mathrm{err,C}})$ as a function of N_S and ϵ^2 (receiver gain $G = 1 + \epsilon^2$) for $\kappa = 0.01$ and $M = 10^6$. Fig. 1(a) depicts the results for $N_{\mathrm{th}} = 30$, a level which is typically assumed for QI at optical frequencies in order to fulfill $N_{\mathrm{th}} \gg 1$. Note that realistic ambient noise values in the THz regime are $N_{\mathrm{th}} \approx 10^{-6}$ [1]. Fig. 1(b) illustrates the findings for $N_{\mathrm{th}} = 10^3$ which is a realistic noise value for microwave frequencies of several GHz. In the grey region, the QI scheme does not provide an advantage over the classical approach. While $N_{\mathrm{S,ideal}} = 0.07$ is robust against noise, $\epsilon^2_{\mathrm{ideal}}$ significantly decreases with increasing N_{th}.

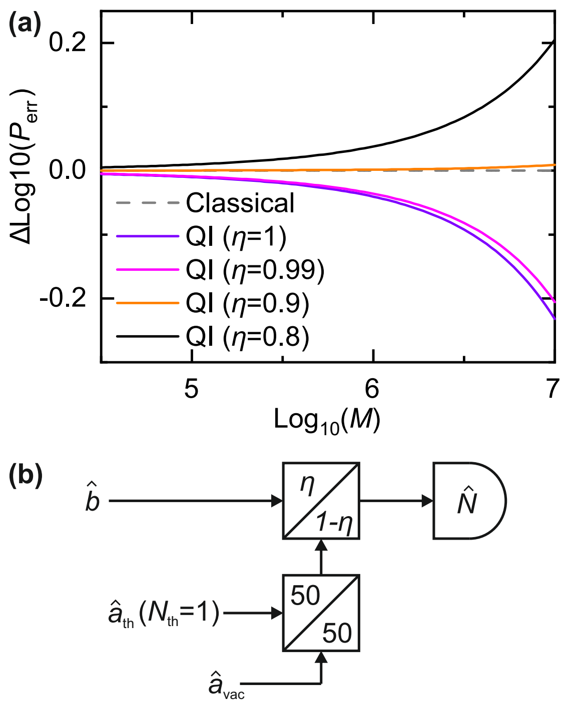

Figure 2: (a) Logarithmic difference $\Delta \log_{10}(P_{\mathrm{err}})$ as a function of the number of mode copies $\log_{10}(M)$ for different efficiencies η of the photon counter at the ideal working point according to Fig. 1(b) for $N_{\mathrm{th}} = 10^3$. (b) The finite photon counter efficiency is modeled by a beam splitter with transmissivity η. The effects of dark counts and missed incidents are modeled via a thermal state $\hat{a}_{\mathrm{th}}$ with $N_{\mathrm{th}} = 1$ and vacuum $\hat{a}_{\mathrm{vac}}$ incident to a second beam splitter with splitting ratio 50 : 50.

As the second step, we investigate the effect of non-ideal photon counting based on the same model. Fig. 2(a) depicts $\Delta \log_{10}(P_{\mathrm{err}})$ as a function of the mode copies $\log_{10}(M)$ for different efficiencies of the photon counter. The finite efficiencies are modelled by inserting a beam splitter with transmissivity η before the photon counter as schematically shown in Fig. 2(b). The second beam splitter enables independent modelling of dark counts ($\hat{a}_{\mathrm{th}}$ with $N_{\mathrm{th}} = 1$) and non-detected incidents ($\hat{a}_{\mathrm{vac}}$). Fig. 2(a) shows that $\eta > 0.9$ is required for realizing a quantum advantage for the microwave quantum radar, while $\eta = 0.8$ already results in an error probability inferior to the optimal classical scheme.

In conclusion, we have analyzed the QI scheme in several realistic parameter regimes including different numbers of noise photons and finite photon detection efficiencies. These findings provide valuable insights into the requirements for achieving a finite quantum advantage in microwave-based quantum radar.

References

[1] G. Sorelli, N. Treps, F. Grosshans, and F. Boust, IEEE Aerospace and Electronic Systems Magazine **37**, 68–90 (2022).

[2] U. Las Heras, R. Di Candia, K. G. Fedorov, F. Deppe, M. Sanz, and E. Solano, Scientific reports **7**, 9333 (2017).

Cooling Limits in Inductively Coupled Electromechanics

T. Luschmann, A. Marx, R. Gross, H. Huebl [1]

The coupling of electromagnetic fields to mechanical motion, studied in the field of cavity opto-mechanics [1], led to a remarkable success in the investigation of mechanical systems close to the quantum limit. However, in thermal equilibrium low-frequency modes of mechanical systems are populated with hundreds on phonons even when cooled down to mK-temperatures. Therefore, cooling these systems into the quantum regime, remains a big challenge. However, it is mandatory to solve this task before other challenges, such as the generation of non-classical states of mechanical motion, can be addressed. With the recent advent of inductively coupled electro-mechanics, where the opto-mechanical interaction is implemented as the transduction of mechanical displacement into a change of the (microwave) resonator's inductance, a new class of devices has been realized. They provide significantly larger coupling rates than their capacitively coupled counterparts [2–4]. At the same time, the inductive circuit element causes an inherent non-linearity of the microwave resonator, which needs to be taken into account. Here, we present the realization of an inductively coupled electro-mechanical device and use the large single-photon opto-mechanical coupling rate of up to $g_0/2\pi \approx 55\,\mathrm{kHz}$ to demonstrate sideband cooling of the nanostring's mechanical motion down to a few quanta of motion using less than a single photon in the microwave cavity.

The device investigated in this study consists of a $\lambda/4$ superconducting coplanar waveguide (CPW) resonator short-circuited to ground via a direct-current superconducting quantum interference device (dc-SQUID) (see Fig. 1). The SQUID can be considered as a flux-sensitive inductor and hence the resonance frequency of this flux-tunable microwave resonator (FTR) becomes sensitive to the magnetic field and the loop area of the SQUID. By suspending the SQUID loop, we form two nano-mechanical string oscillators and hereby implement the opto-mechanical interaction, i.e. a change in the resonance frequency by a displacement of a nano-string [3]. In contrast to Ref. [3], we use a combination of the out-of-plane and in-plane static magnetic fields, to control the coupling rate g_0. The former allows us to tune the static inductance of the SQUID by controlling the flux Φ_b, while the latter (B_{IP}) is used to control the strength of electro-mechanical interaction (see Fig. 1 c). The experiments are performed in a dilution refrigerator at $T \approx 80\,\mathrm{mK}$. Cooling mechanical resonators towards the quantum regime can be achieved following the well studied protocol of sideband cooling [1] (cf. Fig. 1**d**). A microwave pump tone is applied with $\omega_p = \omega_c - \Omega_m$, i.e. detuned from the microwave cavity frequency by exactly the eigenfrequency of the mechanical oscillator. In this case, microwave photons which are inelastically scattered into the anti-Stokes field are removed by the microwave resonator. This corresponds to a phonon annihilation process leading to the cooling of the mechanical mode [1].

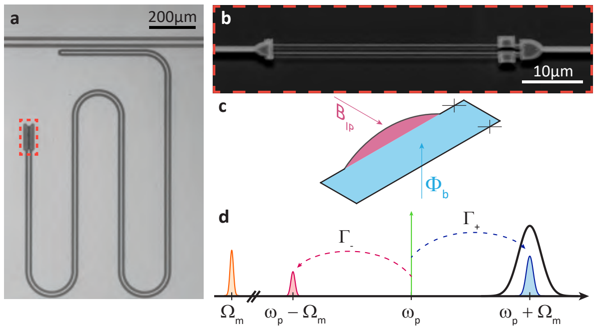

Figure 1: **a** Optical micrograph image of the $\lambda/4$ coplanar-waveguide resonator coupled to a feedline (top) and short-circuited to ground via a dc-SQUID (red box). **b** Tilted scanning electron micrograph image of a suspended SQUID structure similar to the one used in this work. **c** Schematic of the dc-SQUID with applied magnetic field components. The motion of one nanostring oscillator and the corresponding area change (purple) are highlighted. **d** Illustration of the sideband cooling measurement scheme with all relevant microwave tones.

[1]This project is funded by the European Union's Horizon 2020 program (No. 736943) and the German Research Foundation under Germany's Excellence Strategy (EXC-2111-390814868).

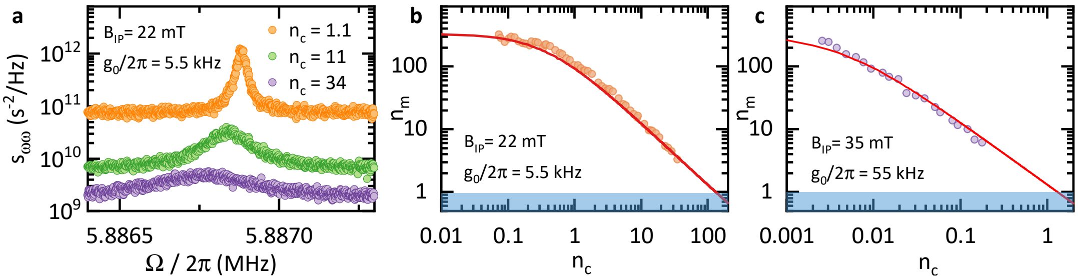

Figure 2: **a** Thermal displacement noise spectra of the investigated nano-string oscillator during a sideband cooling experiment for three different pump powers. **b,c** Phonon occupancy of the mechanical mode over the course of two separate sideband cooling experiments along with a model calculation based on Ref. [5]. Starting from thermal equilibrium, the occupancy decreases with increasing pump power.

The results obtained by applying the sideband cooling protocol to our device are shown in Fig. 2. In panel **a**, we show thermal displacement noise spectra of the nano-string oscillator, acquired as function of the microwave pump tone power, which we express here as the average photon occupation of the microwave cavity, n_c. The measurement was performed using $B_{\mathrm{IP}} = 22\,\mathrm{mT}$, which results in an (independently determined) opto-mechanical coupling rate of $g_0/2\pi \approx 5.5\,\mathrm{kHz}$. The peak area of the displacement noise spectra is proportional to the number of phonons populating the mechanical mode and to its displacement amplitude. Therefore, as we observe a decrease in peak area with increasing pump power, we can infer that the experimental protocol does indeed *cool* the motion of the nano-string. The cooling effect can be quantified by the evaluation of the peak area and comparison with the thermal equilibrium phonon occupation. The results are presented in panel **b**, along with a theoretical model (cf. Ref. [5]) based on the known sample parameters. We find that the investigated mode of the nanostring oscillator has been cooled to an average occupation of just above 3 phonons, using a pump power equivalent to $n_c \approx 34$ photons. This is also supported by the almost vanishing peak signature in panel **a** for this pump power (purple). The theoretical model further predicts that a pump power just above 100 photons would be sufficient to cool the system below 1 phonon, i.e. its motional quantum ground state. Unfortunately, the inherent non-linearity of the dc-SQUID in our device also sets a limit to the pump power above which the FTR frequency becomes unstable. Presently, this prevents us from investigating this regime. We perform a second experimental run, operating the device at $B_{\mathrm{IP}} = 35\,\mathrm{mT}$ and $g_0/2\pi \approx 55\,\mathrm{kHz}$ (see Fig. 2**c**). Using this larger coupling strength, the mechanical motion is cooled to an occupation of 6 phonons, using a pump power equivalent below 0.2 photons (or less than 1 fW), until the experiment once again becomes limited by non-linearity.

In summary, our experiments demonstrate the versatility of the inductively coupled architecture. Using different control fields, the opto-mechanical coupling strength can be tuned over a wide range, which directly translates into different power regimes required for cooling the mechanical motion down to the regime of individual quanta.

References

[1] M. Aspelmeyer, T. J. Kippenberg, and F. Marquardt, Reviews of Modern Physics **86**, 1391–1452 (2014).
[2] I. C. Rodrigues, D. Bothner, and G. A. Steele, Nature Communications **10**, 5359 (2019).
[3] P. Schmidt, M. T. Amawi, S. Pogorzalek, F. Deppe, A. Marx, R. Gross, and H. Huebl, Communications Physics **3**, 233 (2020).
[4] D. Zoepfl, M. L. Juan, C. M. F. Schneider, and G. Kirchmair, Physical Review Letters **125**, 023601 (2020).
[5] J. D. Teufel, T. Donner, D. Li, J. W. Harlow, M. S. Allman, K. Cicak, A. J. Sirois, J. D. Whittaker, K. W. Lehnert, and R. W. Simmonds, Nature **475**, 359–363.

Superconducting 3D-Cavity Architecture for Microwave Single-Photon Detection

Y. Nojiri, K. E. Honasoge, D. Bazulin, F. Fesquet, M.-T. Handschuh, F. Kronowetter, M. Renger, A. Marx, K. G. Fedorov, R. Gross [1]

Microwave single-photon detectors (SPDs) are essential devices in quantum technology, particularly required in a large variety of quantum communication [5, 6] and quantum computation protocols. First microwave SPDs have been realized with the help of superconducting qubits and resonators. Here, we experimentally study a SPD design compatible with a superconducting 3D cavity architecture. We exploit the multi-mode nature of horseshoe-shaped aluminum cavities in combination with transmon qubits to experimentally realize efficient detection of single microwave photons. We analyze the performance of such devices and discuss possible ways to improve them.

Our SPD scheme (see Fig. 1a) is based on the irreversible conversion of an incoming photon into a pair of qubit-cavity excitations [1]. We experimentally realize this approach by exploiting a multi-mode aluminum 3D cavity in a horseshoe geometry [2, 3] coupled to a superconducting transmon qubit (see Fig. 1b).

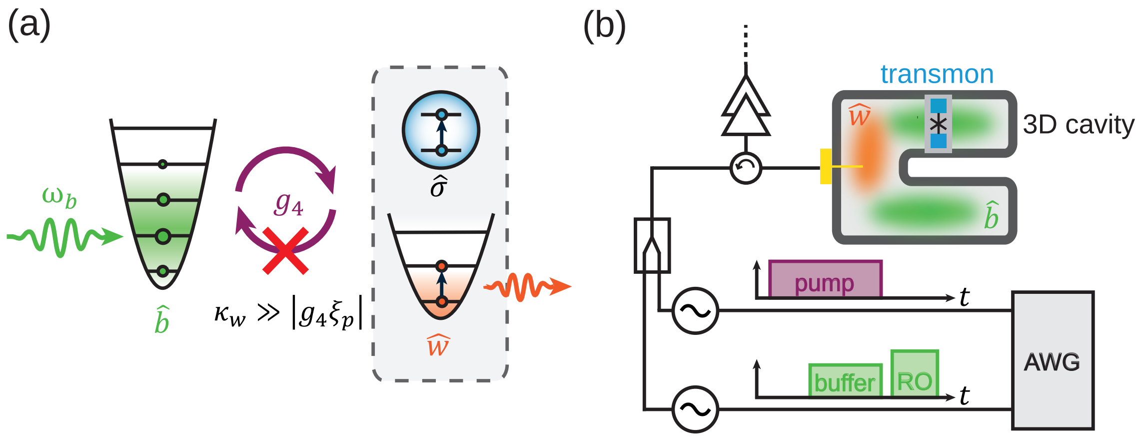

Figure 1: (a) Principle of the microwave single-photon detection. A coherent incoming microwave signal (green wave) is absorbed by a buffer mode, $\hat{b}$, and is converted into a pair of qubit mode, $\hat{\sigma}$, and waste mode, $\hat{w}$, with interaction strength g_4. Due to the engineered high dissipation rate of the waste mode, $\kappa_w \gg |g_4\xi_p|$, the reverse process ($\hat{b}^\dagger\hat{\sigma}\hat{w}$) is effectively suppressed. (b) Schematics of the experimental setup. A transmon qubit is mounted in a 3D superconducting cavity coupled to the cavity waste/buffer mode (orange/green shaded area representing its electric field distribution in the cavity). The weak incoming and the readout signals are produced by a microwave generator at the buffer frequency (green). The strong pump signal is produced by another generator at the frequency $\omega_p = \omega_q + \omega_w - \omega_b$ (purple). Both generators are modulated by the arbitrary wave generator (AWG) for the time-domain experiments.

The effective Hamiltonian of our system under a strong drive can be written as

$$\hat{H}_{\text{eff}} = g_4\xi_p\hat{b}\hat{\sigma}^\dagger\hat{w}^\dagger + g_4^*\xi_p^*\hat{b}^\dagger\hat{\sigma}\hat{w}, \tag{1}$$

where g_4 is the four-wave mixing interaction strength, ξ_p is the steady state mean field pump amplitude, and $\hat{b}, \hat{w}, \hat{\sigma}$ are the annihilation operators of the buffer, waste, and qubit mode, respectively. The key feature of this detector is the engineered fast decay rate of the waste

[1]We acknowledge support by the German Research Foundation via Germany's Excellence Strategy (EXC-2111-390814868), and the German Federal Ministry of Education and Research via the project QUARATE (Grant No. 13N15380). This research is part of the Munich Quantum Valley, which is supported by the Bavarian state government with funds from the Hightech Agenda Bayern Plus.

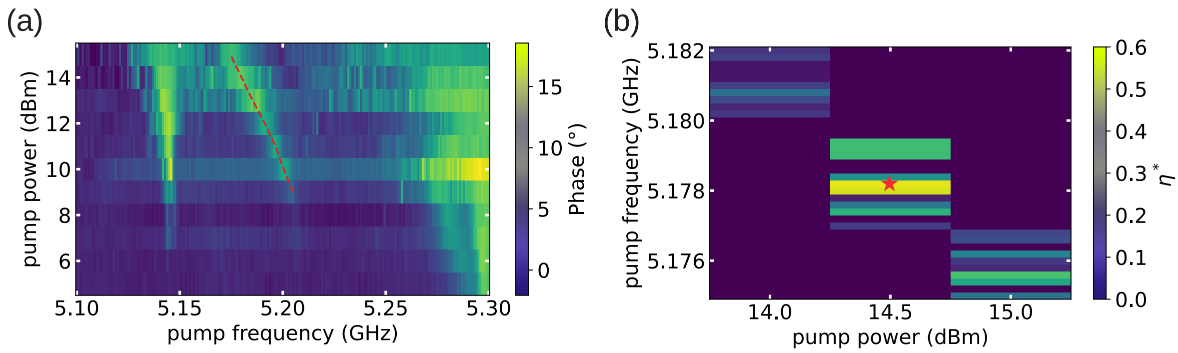

Figure 2: (a) Triple-tone spectroscopy of the coupled transmon-resonator system. An inclined feature (red dashed line) indicates the 4-wave mixing process. The peaks around 5.14 GHz and 5.30 GHz correspond to multi-photon transitions of the qubit, $f_{04}/4$ and $f_{14}/3$, respectively. (b) The detection efficiency η^* as a function of the pump power and pump frequency. The red star indicates the maximally observed efficiency of $\eta^* \simeq 0.56$

mode, $\kappa_w \gg |g_4 \xi_p|$, which enables an irreversible qubit-photon coupling. The time evolution of the qubit excitation follows

$$p_e(t) = 1 - \exp\left(-\eta \, |b_{\text{in}}|^2 \, t\right), \tag{2}$$

where η is the conversion efficiency, $|b_{\text{in}}|^2$ is the photon flux, and t is the temporal length of the incoming signal.

Fig. 2 shows experimental results of the SPD protocol. We apply a weak coherent microwave signal at the buffer mode frequency simultaneously with a strong pump tone followed by a readout signal (see Fig. 1b for details). The resulting triple-tone spectroscopy demonstrates the presence of the 4-wave mixing process as it can be seen in Fig. 2a. Finally, we fit the transmon dynamics for various pump parameters according to Eq. (2) and extract the SPD efficiency, η. The detection efficiency, $\eta^* = \eta \cdot \max(p_e)$, is plotted in Fig. 2b versus the frequency and power of the pump tone. We find the maximum detection efficiency around $\eta^* \simeq 0.56$.

In conclusion, we have successfully implemented the microwave SPD exploiting the multi-mode feature of the superconducting 3D-cavity with a detection efficiency exceeding 50%. Our preliminary analysis indicates that these efficiencies are limited by the transmon ionization and can be potentially suppressed by using an extra compensation tone [4]. The demonstrated SPD results open a path for more complex techniques, such as number-resolved photon-counters by making use of the cavity storage mode. High-efficiency microwave SPDs are essential for various quantum sensing applications, as well as the measurement-based quantum computing.

References

[1] R. Lescanne, S. Deléglise, E. Albertinale, U. Réglade, T. Capelle, E. Ivanov, T. Jacqmin, Z. Leghtas, and E. Flurin, Phys. Rev. X **10**, 021038 (2020).
[2] E. Xie, F. Deppe, M. Renger, D. Repp, P. Eder, M. Fischer, J. Goetz, S. Pogorzalek, K. G. Fedorov, A. Marx, and R. Gross, Appl. Phys. Lett. **112**, 202601 (2018).
[3] J. Lamprich. *Optimized Geometry for a Compact 3D Quantum Memory*. Master's thesis, Technische Universität München (2020).
[4] C. Lledó, R. Dassonneville, A. Moulinas, J. Cohen, R. Shillito, A. Bienfait, B. Huard, and A. Blais. Cloaking a qubit in a cavity. arXiv:2211.05758 (2022).
[5] F. Fesquet, F. Kronowetter, M. Renger, Q. Chen, K. Honasoge, O. Gargiulo, Y. Nojiri, A. Marx, F. Deppe, R. Gross, and K. G. Fedorov. Perspectives of microwave quantum key distribution in open-air. arXiv:2203.05530 (2022).
[6] K. G. Fedorov, M. Renger, S. Pogorzalek, R. Di Candia, Q. Chen, Y. Nojiri, K. Inomata, Y. Nakamura, M. Partanen, A. Marx, R. Gross, and F. Deppe, Sci. Adv. **7**, eabk0891 (2021).

Fractional State Transfer on a Superconducting Qubit Chain [1]

Federico Roy, Maximilian Nägele, Christian Schweizer, Leon Koch, Niklas Bruckmoser, Niklas Glaser, Max Werninghaus, Joao Romeiro, Malay Singh, Gleb Krylov, Stefan Filipp [1]

Superconducting circuits are a promising candidate for quantum computation due to their high coherence times and high-fidelity control.However, qubit connectivity is limited to nearest-neighbour local interactions. Nonetheless, recent studies show that simultaneous local interactions can be harnessed to efficiently generate multi-qubit operations and many-body entanglement [2]. A prime example of such a method is perfect (fractional) state transfer along a qubit chain, where an excitation at an initial location is fully (partially) transferred to a final location along the chain [3]. The Hamiltonian of a qubit chain with length N is given by

$$H_N = \sum_{n=1}^{N} \Delta_n \sigma_n^+ \sigma_n^- + \sum_{n=1}^{N-1} J_n \left(\sigma_n^+ \sigma_{n+1}^- + \text{h.c.}\right). \tag{1}$$

Here, $\sigma_n^{\mp}$ are the qubit lowering (raising) operators, Δ_n is the frequency of qubit n and J_n the coupling strength between qubits n and $n+1$. By setting J_n and Δ_n according to analytical solutions given in Ref. [1], one is able to implement fractional state transfer, where evolving the state $|n\rangle$ under H_N for a transfer time τ results in a rotation by an angle θ in the two-qubit subspace of qubit n and its mirror qubit on the chain, qubit $N+1-n$, i.e.

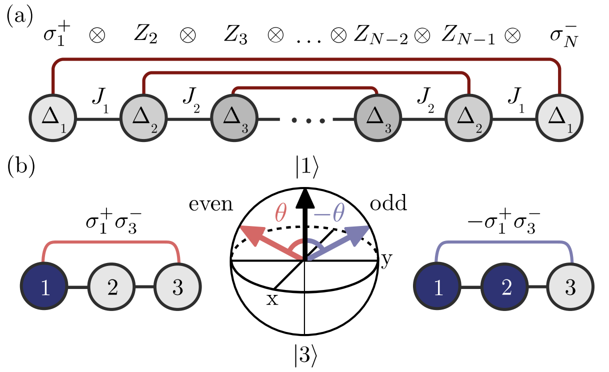

Figure 1: Qubit chain and effective parity-dependent couplings. (a) Chain of qubits (circles) with frequencies Δ_n and direct couplings J_n. Dark red lines indicate effective non-local interactions that stroboscopically arise for specific parameter choices of Δ_n and J_n. The effective interaction results in a rotation in the subspaces spanned by $|n\rangle$ and $|N+1-n\rangle$, where n denotes the location of the excitation. The orientation of the rotation vector depends on the parity of the qubits between each pair, $\otimes_{k=n+1}^{N-n} Z_k$. (b) Illustration of a chain with length $N=3$. A single excitation is prepared at site 1 and partially transferred to site 3 with effective interaction $\sigma_1^+\sigma_3^- + \text{h.c.}$ (left chain), which rotates the state by an angle θ on the Bloch-sphere spanned by the states $|1\rangle$ and $|3\rangle$ (red arrow). If an additional excitation is prepared at site 2 (right chain), the effective interaction changes sign, so that the state is rotated by an angle $-\theta$ on the Bloch-sphere (blue arrow).

$$e^{-iH_N\tau}|n\rangle = e^{-i\phi}\left(\cos\left(\frac{\theta}{2}\right)|n\rangle - i\sin\left(\frac{\theta}{2}\right)|N+1-n\rangle\right). \tag{2}$$

Furthermore, as we have detailed in our paper [1], the phase accumulated by the states during a transfer process will depend on the number of excitations in the chain. Indeed, the time-evolution under H_N can be mapped to the dynamics of an effective non-local Hamiltonian

$$\begin{aligned} G_N =& \sigma_1^+ \otimes Z_2 \otimes Z_3 \otimes \ldots \otimes Z_{N-2} \otimes Z_{N-1} \otimes \sigma_N^- \\ &+ I_1 \otimes \sigma_2^+ \otimes Z_3 \otimes \ldots \otimes Z_{N-2} \otimes \sigma_{N-1}^- \otimes I_N + \ldots + \text{h.c.} \end{aligned} \tag{3}$$

with parity-dependent couplings between mirror-symmetric qubit sites as illustrated in Fig. 1.

[1] We acknowledge support by the European Union, agreements No. 765267 (QuSCo), No. 828826 (FET-Open Quromorphic) and No. 754388 (LMUResearchFellows), the BMBF program No 13N15680 (GeCQoS), and by the DFG (EXC2111-390814868 and FI 2549/1-1.)

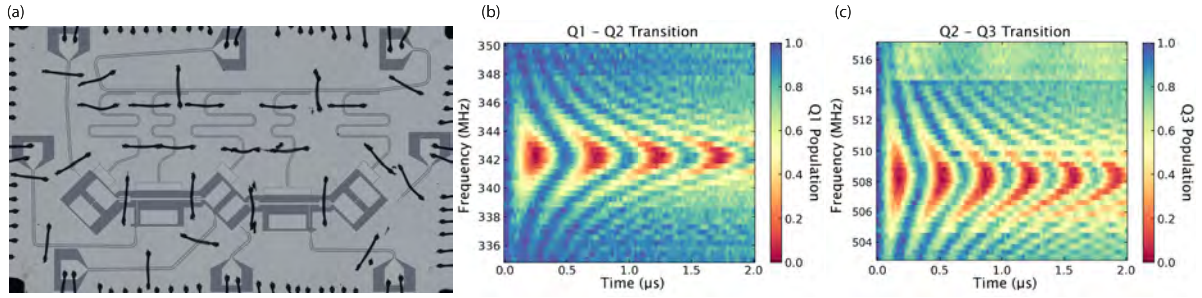

Figure 2: Experimental setup and two-qubit interactions. (a) Microscope picture of the sample. Black lines are wire bonds to connect the ground planes and the coplanar waveguides to external cabling. The three qubits and two interleaved couplers are transmon-like. The couplers and the center qubit are frequency-tunable through a dedicated flux line. All elements have an individual read-out resonator. (b, c) Effective couplings between adjacent qubits are activated by parametrically driving the coupler between them at their difference frequency.

We use a superconducting circuit system composed of three transmon-type qubits, Q1, Q2 and Q3, coupled along a chain via two flux-tunable transmon-type elements [Fig. 2(a)]. We activate effective interactions between adjacent qubit pairs by parametrically driving the coupler at the difference frequency of the two neighboring qubits [4]. The occupation dynamics of a single excitation is shown in Fig. 2(b) and 2(c). We control the effective interaction strength J_n and the effective detuning Δ_n between the qubits by tuning the drive strength and the drive frequency, respectively. In our experiment, we apply resonant drives on both couplers simultaneously with driving strengths resulting in equal effective interactions between neighboring qubits. This enables us to study perfect state transfer, see Fig. 3(a), where excitations travel from one side of the chain to the other and back. Simultaneously detuning both drives shifts the effective frequency of the center qubit Δ_2 and fractional state transfer can be observed, which exhibits smaller transfer angles at shorter times for larger detunings [Fig. 3(b), (c)]. Experimental results agree well with theoretical predictions.

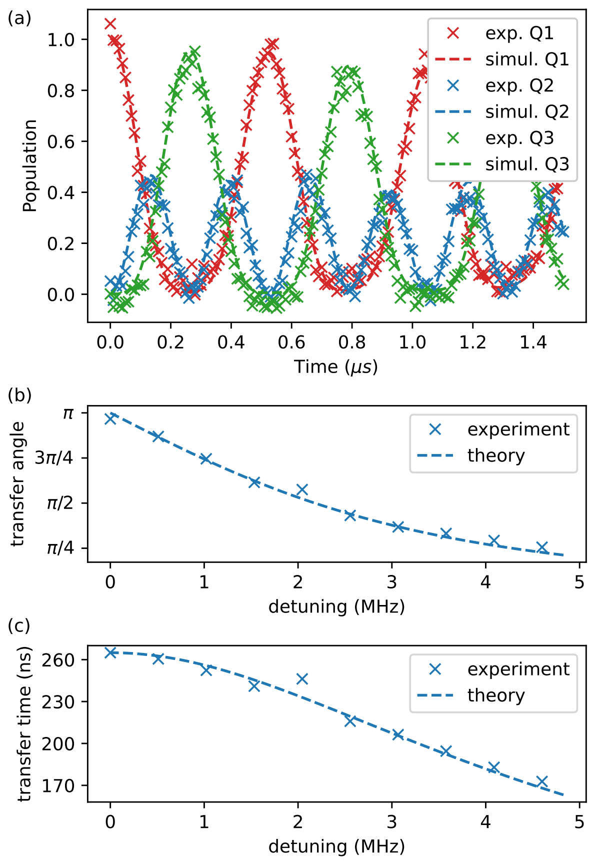

Figure 3: Experimental state transfer on a three-qubit chain. (a) Dynamics of repeated perfect state transfers between the qubits at the end of the chain. Measured populations of Q1, Q2 and Q3 are shown in red, green and blue crosses respectively. We prepare an excitation on qubit Q1 and apply parametric drive on each coupler element to activate effective direct couplings between qubit pairs, Q1-Q2 and Q2-Q3. Simulated dynamics are shown in dashed lines. Extracted transfer angle (b) and transfer time (c) are as a function of the effective detuning of the center qubit from the rest of the chain, as implemented by equally detuning both parametric drives. Theory curves have no fitting parameters.

References

[1] M. Nägele, C. Schweizer, F. Roy, and S. Filipp, Phys. Rev. Research **4**, 033166 (2022).

[2] X. Gu, J. Fernández-Pendás, P. Vikstål, T. Abad, C. Warren, A. Bengtsson, G. Tancredi, V. Shumeiko, J. Bylander, G. Johansson, and A. F. Kockum, PRX Quantum **2**, 040348 (2021).

[3] M. Christandl, N. Datta, A. Ekert, and A. J. Landahl, Phys. Rev. Lett. **92**, 187902 (2004).

[4] D. C. McKay, S. Filipp, A. Mezzacapo, E. Magesan, J. M. Chow, and J. M. Gambetta, Phys. Rev. Applied **6**, 064007 (2016).

Magnon transport in $Y_3Fe_5O_{12}$/Pt nanostructures with reduced effective magnetization

J. Gückelhorn, T. Wimmer, M. Müller, S. Geprägs, H. Huebl, R. Gross, M. Althammer [1]

Over the last years we dedicated our research focus on the transport and manipulation of (spin) angular momentum in magnetically ordered insulators by the quantized excitations of the magnetic lattice. These quantized excitations, i.e. magnons, carry finite spin and enable diffusive transport of spin information over micrometer distances, which can be parameterized by the magnon spin conductance [1]. We showed that this magnon spin transport in yttrium iron garnet (YIG)/platinum nanostructures can be manipulated by the combined action of the charge-to-spin current conversion process in Pt via the spin Hall effect (SHE) and the spin-transfer torque across the YIG/Pt interface via a charge current applied to the Pt layer. At large enough charge current values, we can compensate the intrinsic magnon decay rate in the YIG layer and achieve an enhancement in the magnon spin conductance [2, 3].

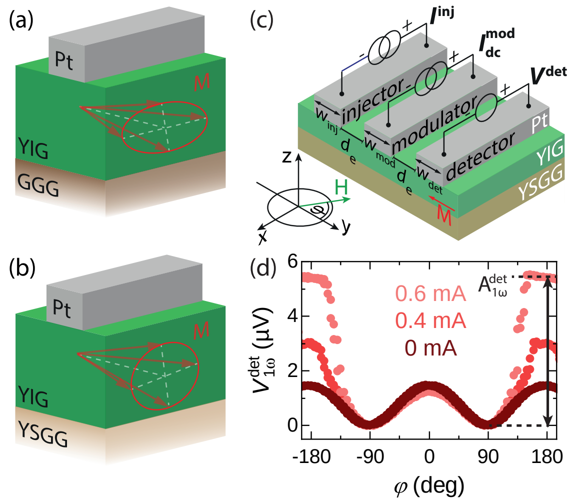

Figure 1: (a) Sketch of the elliptical magnetization precession in YIG thin films grown on lattice-matched GGG. (b) In biaxially strained YIG thin films grown on YSGG, the ellipticity is minimized. (c) Sketch of the sample configuration for a three-terminal device and the coordinate system with the in-plane rotation angle φ of the applied magnetic field $\mu_0\mathbf{H}$. (d) Detector signal $V^{det}_{1\omega}$ of a three terminal magnon transport structure plotted versus the magnetic field orientation with constant magnitude $\mu_0 H = 50\,$mT for various modulator currents I^{mod}_{dc}.

An important aspect for damping processes of magnon modes are nonlinear processes induced by the finite ellipticity of the precession of the magnetic moments in the magnetically ordered systems (see Fig. 1(a)). Especially for thin film samples, the shape anisotropy related to the saturation magnetization M_s and the perpendicular magnetic anisotropy fields H_k are important contributions to the finite ellipticity and is described by the effective magnetization $M_{eff} = M_s - H_k > 0$. To analyze the role of ellipticity on diffusive magnon transport, we realized large H_k and reduced M_s in biaxially strained YIG films epitaxially grown on yttrium scandium gallium garnet ($Y_3Sc_2Ga_3O_{12}$, YSGG) by magnetoelastic coupling effects. This allows us to approach the limit $M_{eff} = 0$ and thus a circular magnetization precession is expected (cf. Fig. 1(b)). We characterized these biaxially strained YIG films by broadband ferromagnetic resonance and extract $\mu_0 M_{eff} = 56\,$mT, which is three times smaller than in epitaxial high-quality YIG films grown on lattice-matched gadolinium gallium garnet (GGG) substrates [2]. Moreover, from distance-dependent all-electrical magnon transport experiments, we find $\lambda_m \approx 1\,\mu$m in good agreement with YIG films grown on lattice-matched GGG [2]. These results indicate that our strained YIG films are perfectly suited for the charge current based manipulation of magnon spin transport. For this task, we use three-terminal devices, which allow us to manipulate the magnon transport between injector and detector via the center Pt strip acting as the modulator (see Fig. 1(c)). In this configuration, we apply a low-frequency AC charge current to the injector strip, while a constant DC charge current I^{mod}_{dc} is applied to the modulator strip. The detector voltage V^{det}

[1] We acknowledge financial support from the German Research Foundation under Germany's Excellence Strategy - EXC-2111 - 390814868 and project "AL 2110/2-1".

is recorded via lock-in detection, where the first harmonic voltage signal $V_{1\omega}^{\mathrm{det}}$ can be assigned to the transport of magnons generated via the SHE at the injector [2, 3]. We measure $V_{1\omega}^{\mathrm{det}}$ as a function of the magnetic field orientation φ for different external magnetic field magnitudes and different modulator currents $I_{\mathrm{dc}}^{\mathrm{mod}}$. The results are plotted in Fig. 1(d). In agreement with our previous reports [2, 3], we observe a significant enhancement of $V_{1\omega}^{\mathrm{det}}$ at $\varphi = \pm 180°$ for $I_{\mathrm{dc}}^{\mathrm{mod}} > 0$. This result can be attributed to a magnon accumulation underneath the modulator caused by the SHE-induced magnon chemical potential and thermally generated magnons due to Joule heating. This accumulation increases the magnon conductivity, resulting in a larger voltage signal $V_{1\omega}^{\mathrm{det}}$.

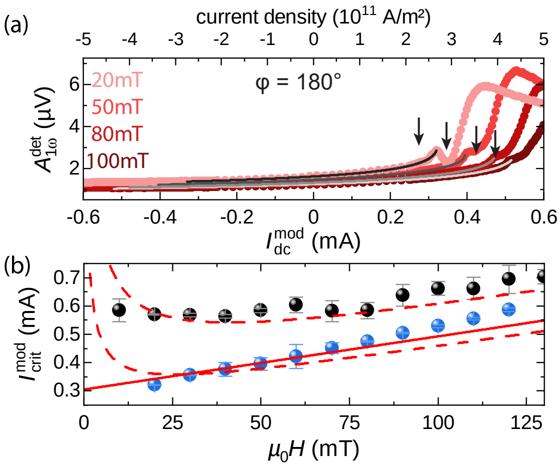

Figure 2: (a) The voltage amplitudes $A_{1\omega}^{\mathrm{det}}$ versus the DC charge current $I_{\mathrm{dc}}^{\mathrm{mod}}$. The gray lines indicate fits for current values below the threshold current $I_{\mathrm{crit}}^{\mathrm{mod}}$ to extract $I_{\mathrm{crit}}^{\mathrm{mod}}$ indicated by black arrows. (b) Extracted critical currents $I_{\mathrm{crit}}^{\mathrm{mod}}$ as a function of the magnetic field magnitude $\mu_0 H$ (blue circles). For comparison, the black data points are taken from our previous work, for YIG thin film grown on a lattice-matched GGG substrate [2]. The dashed lines correspond to fits with a finite M_{eff}, while the solid line is a fit to the data in the limit of $M_{\mathrm{eff}} = 0$.

For a more quantitative analysis, we extract the signal amplitudes $A_{1\omega}^{\mathrm{det}}(+\mu_0 H)$ at $\varphi = 180°$ and plot them as a function of the modulator current $I_{\mathrm{dc}}^{\mathrm{mod}}$ for different $\mu_0 H$ in Fig. 2(a). For $|I_{\mathrm{dc}}^{\mathrm{mod}}| <$ 0.25 mA, we observe the expected superposition of a linear and quadratic $I_{\mathrm{dc}}^{\mathrm{mod}}$ dependence corresponding to SHE-induced magnons and thermally generated magnons due to Joule heating, respectively [2, 3]. However, for larger $I_{\mathrm{dc}}^{\mathrm{mod}}$ a clear deviation from this behavior is observed. In particular, we observe a strongly increased signal amplitude $A_{1\omega}^{\mathrm{det}}$. This observation can be attributed to an enhanced effective magnon conductivity underneath the modulator, which is explained by a compensation of the magnon decay rate underneath the modulator [2]. The onset current $I_{\mathrm{crit}}^{\mathrm{mod}}$ for nonlinear effects is indicated by black arrows. We compare the dependence of $I_{\mathrm{crit}}^{\mathrm{mod}}$ with $\mu_0 H$ in Fig. 2(b) for epitaxially strained and unstrained YIG films. For the epitaxially strained YIG film (blue circles), we observe a linear increase of the critical current $I_{\mathrm{crit}}^{\mathrm{mod}}$ with applied magnetic field for $\mu_0 H > 20\,\mathrm{mT}$. This is in contrast to the observations in Ref. [2] (black circles), where a linear increase in $I_{\mathrm{crit}}^{\mathrm{mod}}$ with $\mu_0 H$ is only observed for $\mu_0 H > 50\,\mathrm{mT}$. If we account for the case $M_{\mathrm{eff}} \approx 0$, and use material parameters extracted from independent experiments we can fit our data and extract the spin mixing conductance $g^{\uparrow\downarrow} = 9.9 \times 10^{18}\,\mathrm{m}^{-2}$. Similar values were obtained on previous YIG/Pt samples [2].

In summary, we showed that a reduction in M_{eff} and ensuing less elliptical magnetization precession is reflected in unique signatures in all-electrical magnon transport experiments. More details on the data analysis and further results on the all-electrical magnon transport in epitaxially strained YIG films are available in our publication in Physical Review B [4].

References

[1] M. Althammer, Phys. Stat. Sol. (RRL) **15**, 2100130 (2021).
[2] T. Wimmer, M. Althammer, L. Liensberger, N. Vlietstra, S. Geprägs, M. Weiler, R. Gross, and H. Huebl, Phys. Rev. Lett. **123**, 257201 (2019).
[3] J. Gückelhorn, T. Wimmer, S. Geprägs, H. Huebl, R. Gross, and M. Althammer, Appl. Phys. Lett. **117**, 182401 (2020).
[4] J. Gückelhorn, T. Wimmer, M. Müller, S. Geprägs, H. Huebl, R. Gross, and M. Althammer, Phys. Rev. B **104**, L180410 (2021).

Reduced effective Magnetization and Damping by Slowly-Relaxing Impurities in Strained γ-Fe_2O_3 Thin Films

M. Scheufele, M. Müller, J. Gückelhorn, L. Flacke, H. Huebl, S. Geprägs, R. Gross, M. Althammer [1]

M. Weiler [2]

Magnetic insulators, where spin information is transported by the quantized excitations of the spin system called magnons, are promising candidates for the implementation of logic circuits based on angular momentum transport [1]. At present, the majority of studies in the field is focused on yttrium iron garnet ($Y_3Fe_5O_{12}$, YIG), as its low Gilbert damping $\alpha \simeq 10^{-5}$ [2] is one of the key parameters for spin-wave based devices. However, apart from its superior damping properties, the growth of YIG requires high deposition and annealing temperatures and expensive gadolinium gallium garnet ($Gd_3Ga_5O_{12}$) substrates, making alternative magnetic insulators with low Gilbert damping desirable. To this end, a promising material platform are spinel ferrites, which are compatible with conventional substrate materials such as MgO and exhibit a low Gilbert damping $\alpha \simeq 10^{-3}$ [3].

Here, we investigated the epitaxial growth as well as the static and dynamic magnetic properties of the spinel-type room temperature ferrimagnetic insulator γ-Fe_2O_3 (maghemite) [4]. The γ-Fe_2O_3 thin films were grown via pulsed laser deposition on MgO (001) substrates. The structural properties and the strain state of the γ-Fe_2O_3 thin films were analyzed by high-resolution X-ray diffraction. Exemplarily, a reciprocal space map around the γ-Fe_2O_3 (408) reflection is shown in Fig. 1(a). We have observed a pseudomorphic growth with a tensile epitaxial strain within the film plane (ip) of $\epsilon_{xx} = 1.1\,\%$ and an unexpectedly small out-of-plane (oop) strain of $\epsilon_{zz} = -0.05\,\%$, which we assign to an oxygen deficiency in our samples.

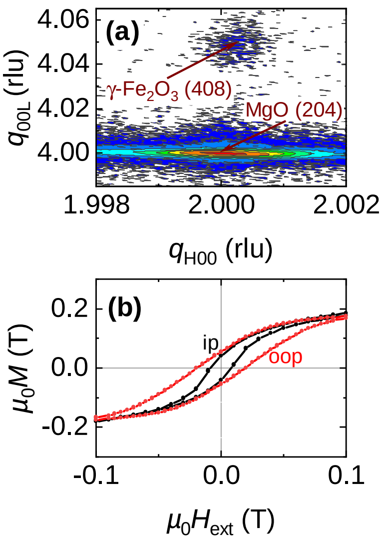

Figure 1: (a) Reciprocal space map around the γ-Fe_2O_3 (408) and MgO (204) X-ray reflections. The units are given in reciprocal lattice units (rlu) with respect to the MgO substrate. (b) Room temperature magnetization versus applied magnetic field for a γ-Fe_2O_3 thin film measured with the magnetic field applied in- and out-of-plane.

To characterize the static magnetic properties of our thin films, we have performed SQUID magnetometry measurements and have observed a hysteretic behavior in $M(H)$ for the external magnetic field H_{ext} applied both ip and oop [see Fig. 1(b)]. This indicates an extra magnetic anisotropy contribution in addition to the ip shape anisotropy, which we attribute to the strain present in the maghemite film in combination with magnetoelastic coupling [5].

To determine the dynamic magnetic properties of our maghemite samples, we performed broadband ferromagnetic resonance (bbFMR) experiments. In particular, we recorded the complex microwave transmission parameter S_{21} for fixed microwave frequencies f as a function of the static magnetic field H_{ext} applied along the oop direction using a vector network analyzer. Thereby, we extract the resonance field H_{res} and the linewidth ΔH as a function of f as shown in Fig. 2(a) and (b).

[1] Financial support by the German Research Foundation via Germany's Excellence Strategy "EXC-2111-390814868" is gratefully acknowledged.

[2] Fachbereich Physik and Landesforschungszentrum OPTIMAS, Technische Universität Kaiserslautern, Germany

In Fig. 2(a) the extrapolated negative H_{res} value at $f = 0$ translates into an effective magnetization $M_{eff} = M_s - H_k < 0$, which clearly indicates a dominant oop easy-axis anisotropy described by the uniform uniaxial oop anisotropy field H_k. Furthermore, we observe a non-linear $\Delta H(f)$ dependence in Fig. 2(b) that differs from a linear Gilbert damping mechanism. Such a non-linear behavior of $\Delta H(f)$ can be attributed to the slowly relaxing impurity mechanism [6], where an additional contribution to magnetization damping is induced by the exchange coupling between the magnetization of the thin film and the electron spin of impurity atoms. Here, a plausible candidate for the slowly relaxing impurity are unpaired Fe^{2+}-ions generated by an oxygen deficiency in our samples [7].

Figures 2(c) and (d) show M_{eff} and the slowly relaxing impurity parameter $CF(T)$ extracted by fitting the data of our bbFMR experiments as a function of temperature T. We find a small $\mu_0 M_{eff} \approx -12$ mT at room temperature [see panel (c)], which gradually increases with decreasing temperature. M_{eff} changes sign at $T_{cross} \approx 200$ K. We attribute the change in sign to a transition from an oop easy-axis to an ip easy-plane anisotropy induced by the reduced strain in γ-Fe_2O_3 for reduced temperatures.

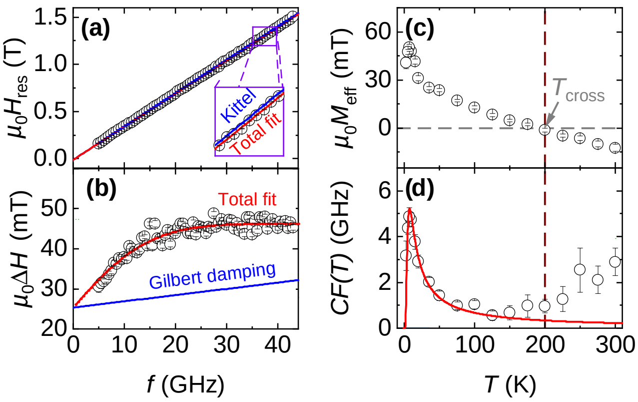

Figure 2: BbFMR data of a 52.6 nm thick γ-Fe_2O_3 thin film taken with the external magnetic field applied oop. (a), (b) Room temperature raw data of the extracted resonance field H_{res} and resonance linewidth ΔH together with fits including the slow-relaxor mechanism (red lines). The inset in (a) shows the small difference between the linear Kittel contribution (blue line) and the total fit (red line). The linear, blue line in (b) corresponds to the Gilbert damping contribution to the total fit. (c) Effective magnetization M_{eff} as a function of T. (d) Magnitude of slowly relaxing impurity contribution $CF(T)$ together with a theoretical fitting curve in red.

Additionally, we observe a maximum of $CF(T)$ at $T \simeq 7$ K followed by a decrease up to $T \approx 150$ K [cf. Fig. 2(d)]. For $T > 150$ K the magnitude of $CF(T)$ increases again up to room temperature. The peak-behavior at low T is characteristic of damping effects due to slowly relaxing impurities. For $T > 150$ K, we speculate that the increase is caused by electrons hopping between Fe^{2+} and Fe^{3+} ions in our oxygen-deficient films giving rise to additional damping due to the valence-exchange mechanism [7].

In summary, we found a strain-induced, near-zero effective magnetization in our strained, epitaxial γ-Fe_2O_3 thin films rendering maghemite a promising material platform for magnonic devices of magnetically ordered insulators [1]. Moreover, we observe a non-linear evolution of the FMR linewidth $\Delta H(f)$ and explain it within the so-called slow relaxor model [6].

References

[1] A. Brataas, B. van Wees, O. Klein, G. de Loubens, and M. Viret, Phys. Rep. **885**, 1–27 (2020).
[2] E. G. Spencer, R. C. LeCraw, and A. M. Clogston, Phys. Rev. Lett. **3**, 32–33 (1959).
[3] S. Emori, D. Yi, S. Crossley, J. J. Wisser, P. P. Balakrishnan, B. Khodadadi, P. Shafer, C. Klewe, A. T. N'Diaye, B. T. Urwin, K. Mahalingam, B. M. Howe, H. Y. Hwang, E. Arenholz, and Y. Suzuki, Nano Lett. **18**, 4273–4278 (2018).
[4] M. Müller, M. Scheufele, J. Gückelhorn, L. Flacke, M. Weiler, H. Huebl, S. Geprägs, R. Gross, and M. Althammer, Journ. Appl. Phys. **132**, 233905 (2022).
[5] E. Popova, N. Keller, F. Gendron, L. Thomas, M.-C. Brianso, M. Guyot, M. Tessier, and S. S. P. Parkin, J. Vac. Sci. Technol. A **19**, 2567–2570 (2001).
[6] H. T. Nembach, T. J. Silva, J. M. Shaw, M. L. Schneider, M. J. Carey, S. Maat, and J. R. Childress, Phys. Rev. B **84**, 054424 (2011).
[7] P. Hansen, W. Tolksdorf, and J. Schuldt, Journ. Appl. Phys. **43**, 4740–4746 (1972).

Saturation Recovery Spectroscopy of ^{167}Er:$^{7}LiYF_4$ in Zero Magnetic Field

A. Strinic, J. Chen, R. Gross, N. Kukharchyk [1]

Quantum memories, i.e. devices which are able to store a quantum state for a given time and retrieve it afterwards, are an important building block of many quantum devices such as quantum repeaters [1]. Most of current research on quantum memories is dedicated to optical quantum memories, required for the realization of long-distance quantum communication. However, a quantum memory which operates in a frequency regime compatible with superconducting quantum circuits would be valuable as it could be directly interfaced with a superconducting quantum processor. By such a direct interfacing losses due to frequency transduction can be avoided. An environment compatible with superconducting devices requires (i) microwave frequencies, (ii) millikelvin temperatures and (iii) near-zero magnetic field. The advantages of interfacing quantum processors and quantum memories have already been discussed in various studies on hybrid quantum systems [2, 3]. A detailed study on the performance of a hybrid architecture with respect to integer factorization indicated that a significant reduction of the size of the processor unit compared to standard architectures can be achieved [4]. These results outline the importance of implementing hybrid architectures in the field of quantum computing.

Rare earth spin ensembles are attractive candidates for realizing solid state microwave quantum memories, as they exhibit long optical and spin coherence times [5]. While many quantum memory schemes are based on coupling the spin ensemble to a resonator, a cavity-free approach allows for broadband accessibility of the hyperfine transitions, which is favorable in regard of an atomic frequency comb protocol in the microwave range. In our transmission line based approach, a rare earth doped crystal is placed on top of a meander-shaped superconducting coplanar waveguide leading to an inductive coupling of the spin ensemble to the microwave field, as depicted in Fig. 1.

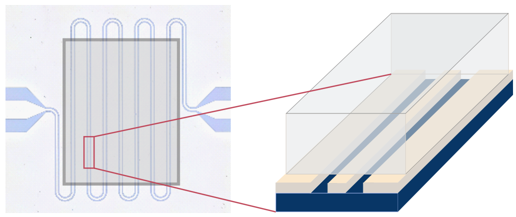

Figure 1: Schematic picture of the meander shaped transmission line with the sample crystal placed on top.

We have conducted microwave spectroscopy on an isotopically purified ^{167}Er:$^{7}LiYF_4$ crystal in zero magnetic field, i.e. in a magnetically shielded environment and without the application of an external magnetic field. In order to identify the hyperfine transitions, we measure the transmission spectrum (S_{21}) for different input powers in the range from -40 to 0 dBm and normalize each recorded spectrum by subtracting the spectrum recorded with the lowest power (-40 dBm). The normalized spectra in the range from 2.97 to 2.99 GHz are plotted in Fig. 2. With increasing power, the transmission at the absorption features increases, as the lower lying energy levels become depopulated. The transmission returns to its initial state after a given time, which is associated with the relaxation rates of the involved hyperfine levels. As a first step towards characterizing the hyperfine transitions, we conducted saturation recovery measurements to probe the relaxation time of the spins.

To measure the saturation recovery, a short high-power pump pulse is applied by a signal generator at the center frequency of the absorption to saturate the spins. The falling edge of the pump pulse triggers the vector network analyzer to start a continuous-wave time sweep at the probe frequency (f_{probe}) with a low-power probe signal in order to sense the recovery

[1] We acknowledge support by the German Research Foundation via Germany's Excellence Strategy (EXC-2111-390814868).

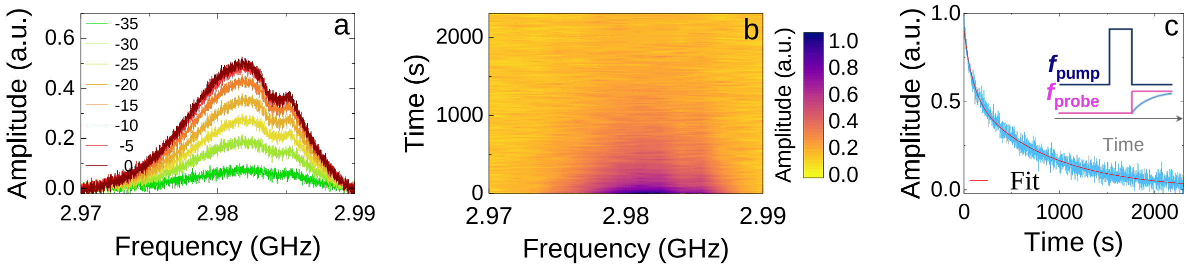

Figure 2: (a) Normalized transmission amplitude S_{21} from 2.97 to 2.99 GHz for powers between −35 and 0 dBm, as indicated in the legend. Normalization is performed via subtraction of the −40 dBm spectrum. (b) Saturation recovery at f_{pump} = 2.981 GHz and f_{probe} from 2.97 to 2.99 GHz. (c) Measured time-dependence of the saturation recovery at f_{probe} = 2.981 GHz, and its double-exponential fit. Inset shows the saturation recovery measurement scheme.

of the saturated transition versus time. The full sweep of f_{probe} in the range from 2.97 to 2.99 GHz with a pump frequency f_{pump} = 2.981 GHz is plotted in Fig. 2(b), while the scheme of the applied signals is shown in the inset of Fig. 2(c).

A double exponential fit of the decay measured at f_{probe} = 2.981 GHz, corresponding to a vertical slice of Fig. 2 (b), is shown in Fig. 2(c). The fit reveals a short relaxation time constant of t_1 = 96 s and long relaxation time constant of 14 min (t_2 = 841 s). The reason for a double instead of a single exponential decay could be the fact that different levels involved in the relaxation have different relaxation times and/or that different relaxation processes contribute with different relaxation rates.

In general, the electron spin lifetime (T_1) of the rare earth ions at sub-Kelvin temperatures is limited by the spin-spin interaction governed by flip-flops between the pairs with anti-parallel spins and the direct spin-lattice relaxation (SLR) process [6]. As the direct process scales with B^5, the flip-flop process dominates at low magnetic fields. Since spin flips due to SLR are a source of decoherence for the electron spins, the measurement of T_1 is crucial for investigating the spin dynamics. In the future, measurements of T_1 and T_2 as a function of magnetic field and temperature should shed light on the involved relaxation processes. This is particulary important regarding clock-transitions in the low magnetic field range, which exhibit long coherence times due to a reduced sensitivity to magnetic field fluctuations.

In summary, we have investigated an ^{167}Er spin ensemble coupled to a microwave transmission line in a magnetically shielded environment via microwave spectroscopy at 10 mK. We have identified hyperfine transitions at 2.981 GHz via the power dependence, while saturation recovery revealed a long spin relaxation time of 14 min. Since T_1 sets the upper limit of T_2, the measured long T_1-time is promising for taking advantage of long coherence times of ^{167}Er-ions doped into ^{7}LiYF$_4$ for microwave quantum memories. Furthermore, our results set the basis for a thorough investigation of the spin dynamics of rare earth ions at mK temperatures.

References

[1] A. Ortu, J. V. Rakonjac, A. Holzäpfel, A. Seri, S. Grandi, M. Mazzera, H. de Riedmatten, and M. Afzelius, Quantum Sci. Technol. 7, 035024 (2022).
[2] G. Kurizki, P. Bertet, Y. Kubo, K. Mølmer, D. Petrosyan, P. Rabl, and J. Schmiedmayer, Proc. Natl. Acad. Sci. U.S.A. **112**, 3866–3873 (2015).
[3] A. A. Clerk, K. W. Lehnert, P. Bertet, J. R. Petta, and Y. Nakamura, Nat. Phys. **16**, 257–267 (2020).
[4] E. Gouzien, and N. Sangouard, Phys. Rev. Lett. **127**, 140503 (2021).
[5] M. Zhong, M. P. Hedges, R. L. Ahlefeldt, J. G. Bartholomew, S. E. Beavan, S. M. Wittig, J. J. Longdell, and M. J. Sellars, Nature **517**, 177–180 (2015).
[6] E. Z. Cruzeiro, A. Tiranov, I. Usmani, C. Laplane, J. Lavoie, A. Ferrier, P. Goldner, N. Gisin, and M. Afzelius, Phys. Rev. B **95**, 205119 (2017).

Finite-energy Microwave Quantum Teleportation Over Thermal Channels

W. K. Yam, M. Renger, S. Gandorfer, F. Fesquet, K. Honasoge, F. Kronowetter, Y. Nojiri, A. Marx, F. Deppe, R. Gross, K. G. Fedorov [1,2]

Quantum communication utilizes the fundamental laws of quantum physics to surpass the performance of classical communication protocols in efficiency and security. One of the most famous quantum communication protocols is quantum teleportation, where an unknown quantum state is transferred between two distant communication parties using a shared entangled resource and a classical feedforward channel. Experimental quantum teleportation with propagating microwaves has recently been demonstrated at WMI [1]. This motivates the study of teleportation resilience against experimental imperfections being unavoidable in realistic application scenarios. To this end, we analyze the effects of finite-energy codebooks and thermal noise on the performance of quantum teleportation of coherent states.

As a result of the no-cloning theorem, quantum teleportation promises unconditionally secure exchange of information between remote parties when teleportation fidelities reach values beyond the no-cloning threshold F_{nc} [2]. In the limit of an infinitely large and uniformly distributed codebook, the no-cloning threshold approaches the asymptotic value $F_{\mathrm{nc}} \to 2/3$. However, in realistic application scenarios, it is not possible to teleport coherent states with arbitrarily large photon numbers due to finite energy capacities and various related technical limitations. As a compromise between the known theory and practical constraints, we consider a truncated Gaussian codebook making use of finite-energy states, as shown in Fig. 1(a). We derive an upper bound on the no-cloning threshold for the truncated Gaussian codebook

$$F_{\mathrm{TG}} \leq \begin{cases} \frac{4\sigma^2+2}{6\sigma^2+1} + 2e^{-N_{\mathrm{S}}/2\sigma^2}, & \sigma^2 \geq \frac{1}{2} + \frac{1}{\sqrt{2}}, \\ \frac{1}{(3-2\sqrt{2})\sigma^2+1} + 2e^{-N_{\mathrm{S}}/2\sigma^2}, & \sigma^2 \leq \frac{1}{2} + \frac{1}{\sqrt{2}}, \end{cases} \quad (1)$$

which is found by estimating an upper bound for the deviation between the truncated and full Gaussian distributions [3]. Quantum teleportation using a truncated Gaussian codebook is unconditionally secure if the measured fidelity exceeds this threshold. Fig. 1(b) shows the no-cloning threshold F_{TG} as a function of the codebook variance σ^2 and truncation photon number N_{S}. The gray region, where $F_{\mathrm{TG}} > 1$, implies a physically unattainable regime. In the limit of $N_{\mathrm{S}} \to \infty$, F_{TG} approaches the Gaussian no-cloning fidelity $F_{\mathrm{nc}} = 2/3$.

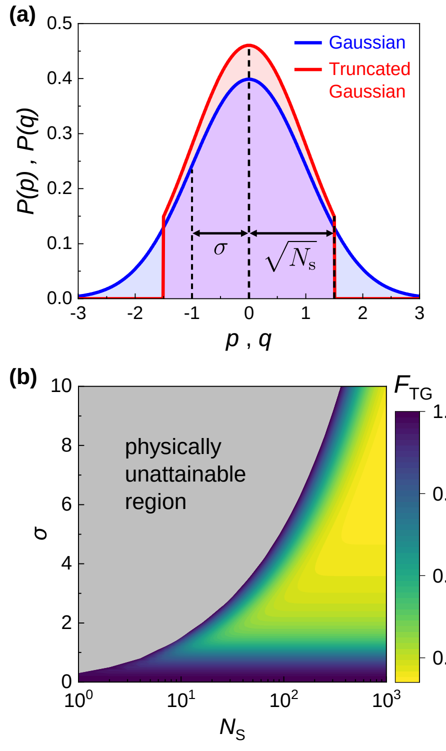

Figure 1: (a) The truncated Gaussian codebook is constructed by truncating a Gaussian codebook with variance σ^2 at a cutoff photon number N_{S} and then rescaling it for normalization. Variables p and q represent the quadrature components of the codebook states. (b) Dependence of the no-cloning threshold F_{TG} on the codebook variance σ^2 and truncation photon number N_{S}.

[1] We acknowledge support by the German Research Foundation via Germany's Excellence Strategy (EXC-2111-390814868), the EU Flagship project QMiCS (Grant No. 820505), and the German Federal Ministry of Education and Research via the projects QUARATE (Grant No. 13N15380) and QuaMToMe (Grant No. 16KISQ036). This research is part of the Munich Quantum Valley, which is supported by the Bavarian state government with funds

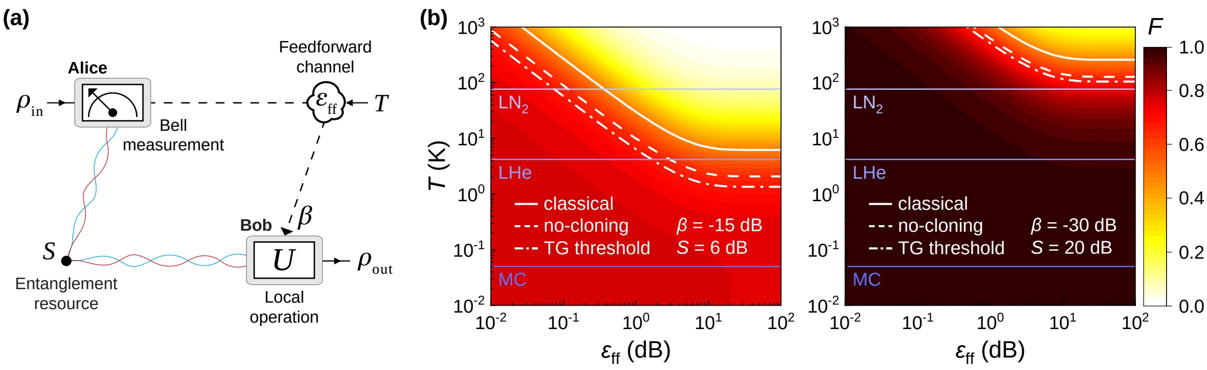

Figure 2: (a) Scheme of the quantum teleportation protocol. An entangled state with resource squeezing S is shared between sender Alice and receiver Bob. Alice performs a Bell measurement on the input state ρ_{in} and her entangled state and then sends the result to Bob through the feedforward channel, which is coupled via losses ε_{ff} to the ambient temperature T. Bob performs a local operation by coupling with strength β the feedforward signal to his entangled state and thereby produces the output state ρ_{out}. (b) Quantum teleportation fidelity F as a function of the feedforward losses ε_{ff} and ambient temperature T. Solid lines represent the asymptotic classical threshold $F = 1/2$, dashed lines represent the asymptotic no-cloning threshold $F = 2/3$, and dash-dotted lines represent the truncated Gaussian no-cloning threshold F_{TG} for $N_{\text{S}} = 100$. Reference lines MC, LHe, and LN_2 indicate mixing chamber, liquid helium, and liquid nitrogen temperatures, respectively.

In realistic application scenarios, communication channels in the teleportation protocol may be noisy. In this regard, we investigate the influence of thermal noise coupled to the feedforward channel. We follow Ref. 1 to model the analog quantum teleportation protocol and consider power losses ε_{ff} and ambient temperature T in the feedforward channel as shown in Fig. 2(a). With an ideal shared entangled resource and an ideal Bell measurement, the fidelity of the coherent state quantum teleportation can be expressed as

$$F = \frac{2}{2 + \beta\varepsilon_{\text{ff}} \coth\left(\frac{\hbar\omega}{2k_{\text{B}}T}\right)} = \frac{1}{1 + \beta\varepsilon_{\text{ff}} f(\omega, T)}, \tag{2}$$

where β is the feedforward coupling and $f(\omega, T)$ is the thermal power spectrum at mode frequency ω. Teleportation is resilient against thermal noise in the feedforward channel when $\beta\varepsilon_{\text{ff}} f(\omega, T) \to 0$, which is achieved if a sufficiently small coupling β suppresses the noise contribution $\varepsilon_{\text{ff}} f(\omega, T)$. Fig. 2(b) shows the simulation results for our quantum teleportation protocol. For our experimentally attainable parameters, $\beta = -15$ dB and resource squeezing $S = 6$ dB, the teleportation fidelity can exceed the truncated Gaussian no-cloning threshold for feedforward channel temperatures up to 300 K. Implementing a smaller coupling β extends the high-fidelity region and generating more squeezing S improves the overall fidelity values. It is thus possible to correct for arbitrarily large losses and noise in the feedforward channel.

In conclusion, our theoretical analysis demonstrates that quantum teleportation can guarantee security for finite-energy codebooks and is asymptotically robust against feedforward losses and noise. These results demonstrate the potential for microwave quantum communication over thermal channels, including those corresponding to ambient room temperatures.

References

[1] K. G. Fedorov, M. Renger, S. Pogorzalek, R. D. Candia, Q. Chen, Y. Nojiri, K. Inomata, Y. Nakamura, M. Partanen, A. Marx, R. Gross, and F. Deppe, Sci. Adv. 7, eabk0891 (2021).
[2] F. Grosshans, and P. Grangier, Phys. Rev. Lett. **88**, 057902 (2002).
[3] P. T. Cochrane, T. C. Ralph, and A. Dolińska, Phys. Rev. A **69**, 042313 (2004).

from the Hightech Agenda Bayern Plus.
[2]We would like to thank Roberto Di Candia for helpful discussions.

Application–Oriented Research

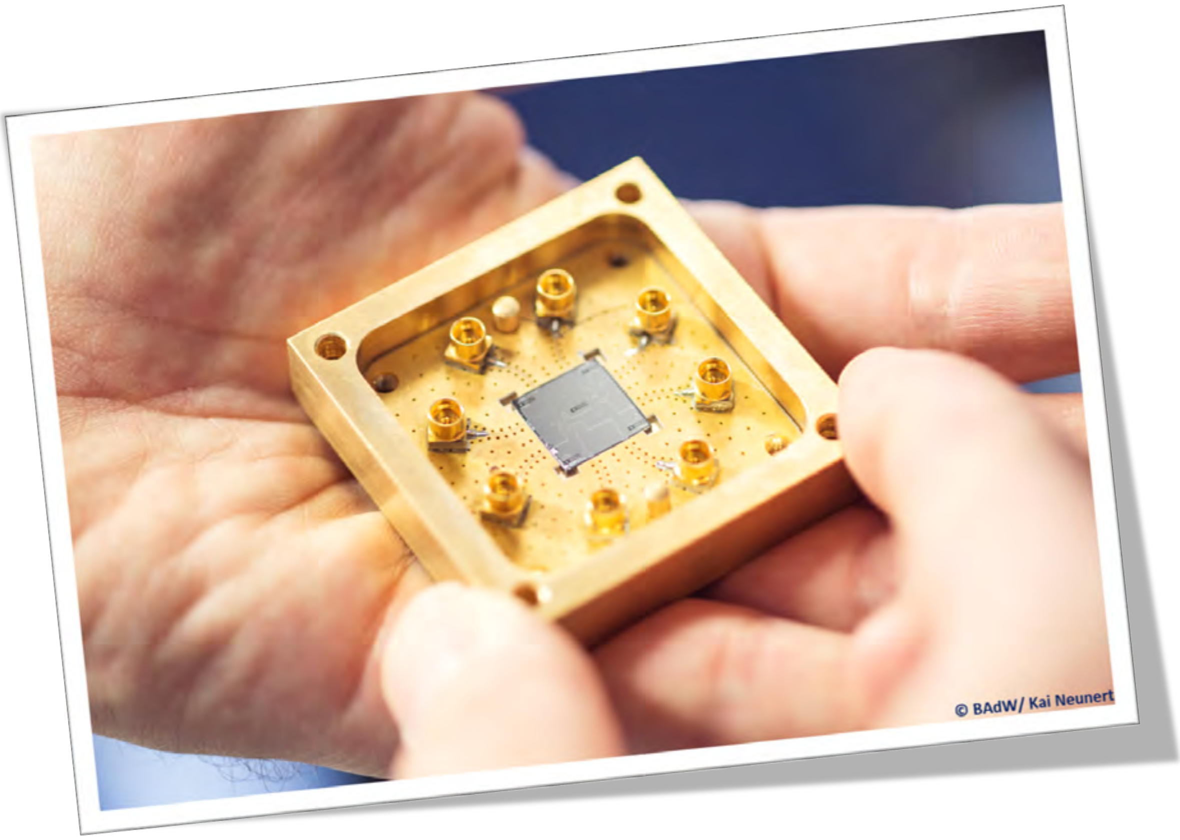

Calibration of Superconducting Qubits

N. J. Glaser, J. Romeiro, C. Schweizer, M. Singh, G. Krylov, C. Broocks, M. Werninghaus, S. Filipp [1]

The coherent control of superconducting qubits requires the interplay of a range of devices. Arbitrary waveform generators are used to control the pulse shapes of microwave pulses for qubit excitation, which can be short with durations of tens of nanoseconds. For qubit–qubit coupling, baseband pulses are utilized for dynamic frequency control of qubits. In both cases, the pulse shapes have to be calibrated and the qubit parameters characterized to achieve high-performance control operations. Here, we present our framework for qubit control, characterization, and calibration.

In order to achieve the correct timing of the short pulses with high repetition rates, we closely cooperate with Zurich Instruments. They provide dedicated hardware and develop the software package LabOneQ, which enables well synchronized control of many devices. On top of LabOneQ an internal software package (wmiqc) has been developed, which serves as an abstraction layer to facilitate the operation and reproducibility for experimentalists. This abstraction layer enables the user to write experiments in a gate-based generalized scheme instead of specifying all individual pulses. The scheme is inspired by the quantum assembly language (QASM), which enables the support for experiment submission through higher-level frameworks like Qiskit for experiment design.

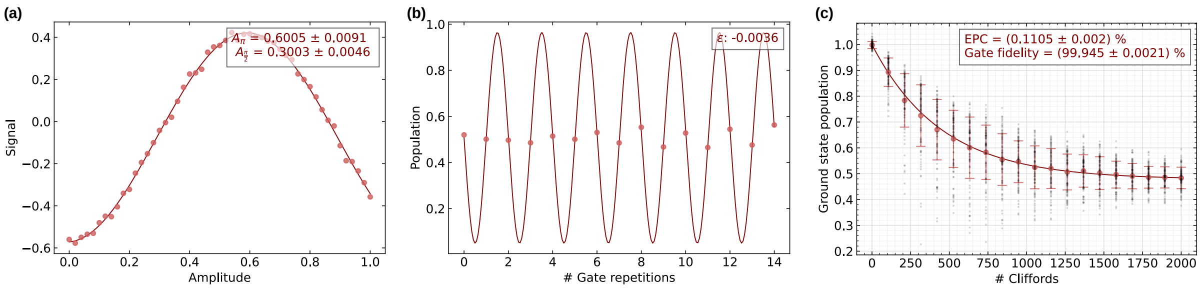

Figure 1: Exemplary single-qubit tuneup routines and single-qubit randomized benchmarking. (a) Measured Rabi oscillation used for the amplitude calibration of single-qubit gates. (b) Error amplification sequence used for the fine calibration of pulse amplitudes. After an initial $\pi/2$-rotation n π-rotation gates are executed. For perfect π-pulses the qubit population will remain at 0.5. The fitted value ε is the relative over rotation, utilized for the iterative optimization. (c) Randomized benchmarking after tuneup sequence. From the decay we can extract a gate fidelity of 99.945(2) %.

To calibrate the pulse shapes required for high-fidelity quantum gates, the established framework includes calibration routines for automatic tuneup of single- and two-qubit gates. Most routines consist of multiple stages and start with a sequence to find a rough estimate for the parameters and end with a method for precise fine calibration. For example, the amplitude of single-qubit gates will be first roughly calibrated by a Rabi experiment. Here, the population after a single pulse will be measured for a range of amplitudes to extract the required amplitude for specific rotations [Fig. 1(a)]. Next, an error amplification sequence is used, where after an initial $\pi/2$-pulse consecutive π-rotations are applied to the qubit [3]. This leads to a high accuracy as the sequence is very sensitive to over and under rotations [Fig. 1(b)]. After tuneup, single-qubit gates have fidelities well above 99.9 % close to the coherence limit [Fig. 1(c)] and two-qubit gates > 99 %.

[1] We acknowledge support by the European Union, No. 828826 (FET-Open Quromorphic) and No. 754388 (LMUResearchFellows), the BMBF program No. 13N15680 (GeCQoS), by the DFG (EXC2111-390814868 and FI 2549/1-1.), and by the Munich Quantum Valley, which is supported by the Bavarian state government with funds from the Hightech Agenda Bayern Plus and the BMBF program GeQCoS No. 13N15680.

To verify pulse calibrations, Randomized benchmarking (RB) is an important characterization technique for qubits and also the performance of quantum processors [1]. In RB, a long, uniformly sampled sequences of quantum operations, namely Clifford gates, is applied that change the qubit states but returns them back to their initial states in case operations are working perfectly. Any imperfections alter the result and can therefore be quantified. RB measurements are readily implemented in Qiskit and are therefore directly executable on our framework. Three multi-qubit RB routines were implemented in the in-house control and analysis software and tested on two-qubit samples with calibrated two-qubit and single-qubit gates. These are conventional RB [Fig. 1(c)], interleaved RB [1] for assessing the error of a specific gate, and simultaneous RB [2] for assessing cross-talk and unwanted interactions in single-qubit gates.

Quantum gates with even higher fidelity can be found when using pulse parametrizations with more degrees of freedom. For the optimization of mutually dependent pulse parameters we use black-box optimization with proper fidelity measures, such as ORBIT [4] tests, Bayesian optimizers, such as the TPE optimizer [5], and optimizers based on sampling from an evolving covariance matrix, i.e., CMA-ES [6]. In order to efficiently use such optimization strategies a fast feedback between individual iterations is required to minimize the experiment downtime. Our efforts to improve the effective optimization speed include submitting experiments as batches and minimizing the exchange of waveform data on the actual experiments, which significantly reduces the device communication time. Initial results show successful optimizations with good convergence for various simple pulse parametrizations of a two-qubit CPHASE gates, even with the expected experimental noise in the sampling landscape summarized in Fig. 2. We are thus confident to further improve the fidelity of our gates with this strategy.

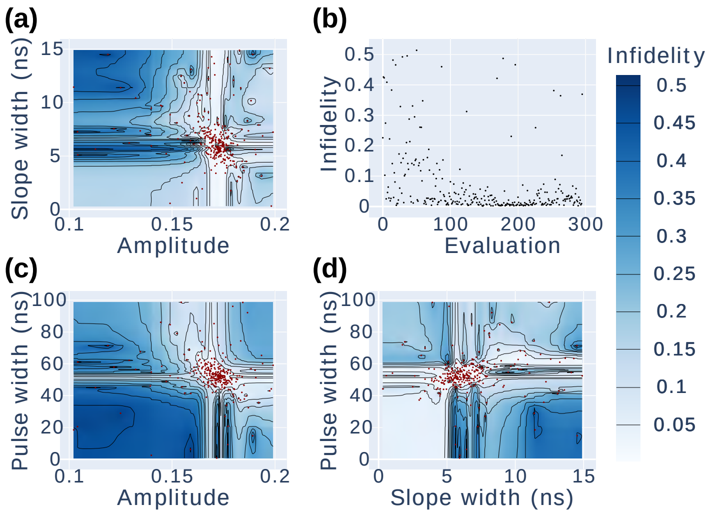

Figure 2: Cost function optimization of baseband CPHASE gate. By tuning the frequency of a tunable coupler between two qubits a CPHASE gate can be realized. Based on a custom gate fidelity the pulse shape parameters are tuned. (a,b,c) Landscape of the infidelity as functions of amplitude, slope and width of the flux pulse. The contours are estimated based on the evaluated red points. (b) Optimization history of the optimizer, showing fast convergence to low infidelities. Best evaluated point at 0.0015.

References

[1] E. Magesan, J. M. Gambetta, and J. Emerson, Physical Review Letters **106**, 180504 (2011).

[2] J. M. Gambetta, A. D. Córcoles, S. T. Merkel, B. R. Johnson, J. A. Smolin, J. M. Chow, C. A. Ryan, C. Rigetti, S. Poletto, T. A. Ohki, M. B. Ketchen, and M. Steffen, Physical Review Letters **109**, 240504 (2012).

[3] S. Sheldon, L. S. Bishop, E. Magesan, S. Filipp, J. M. Chow, and J. M. Gambetta, Physical Review A **93**, 012301 (2016).

[4] J. Kelly, R. Barends, B. Campbell, Y. Chen, Z. Chen, B. Chiaro, A. Dunsworth, A. Fowler, I.-C. Hoi, E. Jeffrey, A. Megrant, J. Mutus, C. Neill, P. O'Malley, C. Quintana, P. Roushan, D. Sank, A. Vainsencher, J. Wenner, T. White, A. Cleland, and J. M. Martinis, Physical Review Letters **112**, 240504 (2014).

[5] J. S. Bergstra, R. Bardenet, Y. Bengio, and B. Kégl 9.

[6] N. Hansen. The CMA Evolution Strategy: A Tutorial. ArXiv:1604.00772 [cs, stat] (2016).

Fabrication of Flux-Pumped Josephson Traveling Wave Parametric Amplifiers

D. E. Bazulin, K. E. Honasoge, L. Koch, N. Bruckmoser, Y. Nojiri, T. Luschmann, A. Marx, S. Filipp and K. G. Fedorov [1]

Scalable quantum computing with superconducting qubits relies on efficient and fast readout of multiple qubits. This goal can be achieved by exploiting broadband Josephson Traveling Wave Parametric Amplifiers (JTWPAs). They are typically based on arrays of superconducting non-linear elements, such as various types of superconducting quantum interference devices (SQUIDs). Here, we investigate the fabrication and characterization of a specific type of JTWPAs based on aluminum Superconducting Nonlinear Asymmetric Inductive eLements (SNAILs) [1] exploiting the 3-wave mixing down-conversion process. With this approach we plan to circumvent many inherent JTWPA problems with phase-matching and are able to spatially separate signal and pump paths. Last but not least, the pump mode propagating through a spatially separated transmission line is expected to enhance the overall JTWPA performance by mitigating the back-action amplification processes and avoiding the pump depletion problem [2].

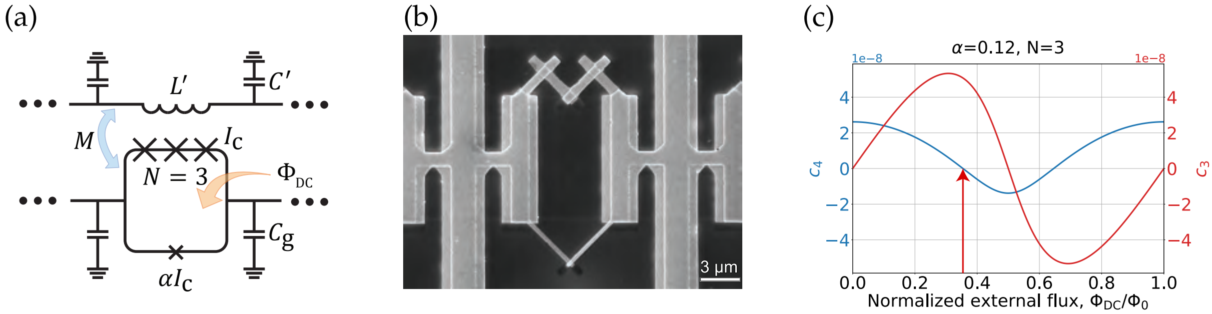

Figure 1: (a) Circuit of a flux-pumped SNAIL as a basic element of the nonlinear transmission line. Pump transmission line is inductively coupled to the SNAIL chain. (b) Scanning electron microscope image of a SNAIL fabricated with WMI Al double-angle shadow evaporation process. (c) Dependence of 3-wave (red) and 4-wave (blue) non-linear coefficients of a SNAIL with the asymmetry ratio $\alpha = 0.12$ and number of large junctions $N = 3$ as a function of the external magnetic flux. Red arrow indicates the magnetic flux value corresponding to the pure 3-wave mixing process.

In general, amplification requires some kind of nonlinear medium to enable coupling between a weak signal, that has to be amplified, and a strong external source of energy. By connecting individual SNAILs (see Fig. 1(a, b)) in long chains one can create such a nonlinear medium in the microwave regime. The main feature of the SNAIL is the possibility to suppress unwanted higher-order nonlinearities by biasing them with a specifically chosen magnetic flux (see Fig. 1(c)). This property allows to enable a pure 3-wave mixing process in the SNAIL chains in contrast to symmetric SQUIDs or individual Josephson junctions. The behavior of the non-linear coefficients depends on the asymmetry parameter α (defined as the ratio between critical currents of small and large Josephson junctions) and the number of large Josephson junctions N.

Here, we fabricate the 3-wave JTWPAs with a single-mask double-angle shadow evaporation process. We use the Manhattan-type Al/AlOx/Al Josephson junctions. In contrast to

[1] We acknowledge support by the German Research Foundation via Germany's Excellence Strategy (EXC-2111-390814868), by the German Federal Ministry of Education and Research via the project GeCQoS (FKZ 13N15680), the project QUARATE (Grant No. 13N15380). This research is part of the Munich Quantum Valley, which is supported by the Bavarian state government with funds from the Hightech Agenda Bayern Plus.

other designs, this approach greatly simplifies the fabrication process by avoiding the usage of multiple masks and extra metal or dielectric layers [3, 4]. Fabricated JTWPAs have two spatially separated waveguides (see Fig. 2(a)): a coplanar waveguide for the pump mode and a waveguide consisting of an array of SNAILs for the signal mode (Fig. 2(c)).

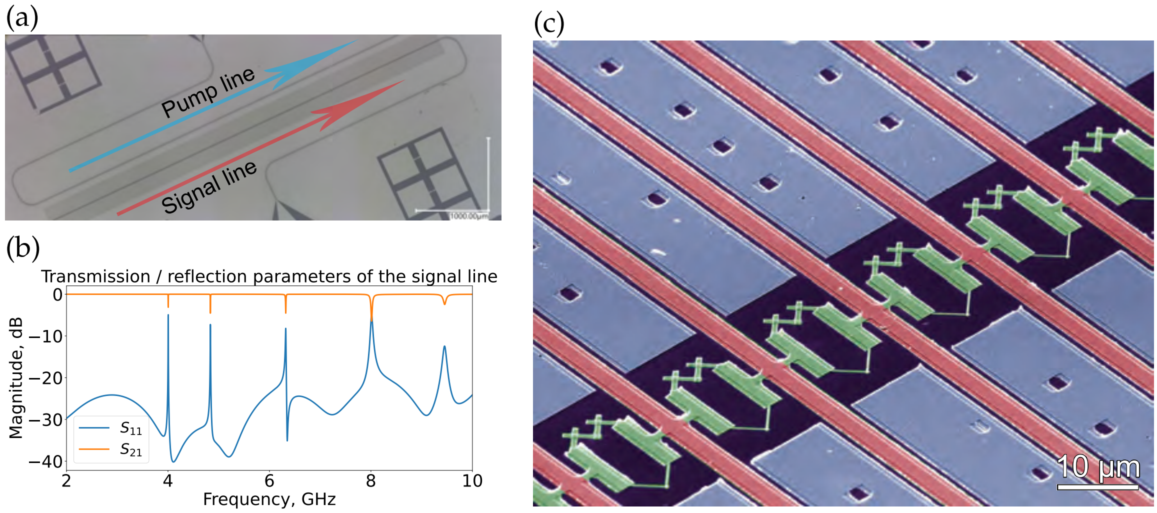

Figure 2: (a) Optical microscope image of the JTWPA fabricated at WMI. The signal line consists of SNAILs connected in series with added fish-bone capacitors for 50 Ω impedance matching. The pump line is spatially separated, being inductively coupled along the non-linear part of the signal line. (b) Simulated S11 and S21 parameters of the JTWPA signal line with implemented fish-bone capacitors. (c) False-color scanning electron microscope image of the the central signal line. It consists of nominally identical SNAILs (shown in green) shunted with symmetric fish-bone capacitors (red color). The ground plane with flux-traps is shown in blue.

As the characteristic impedance of the SNAIL chain greatly exceeds the 50 Ω standard, we have to introduce additional capacitive shunts into our design. Here, we choose to implement the so-called fish-bone capacitors [5] due to the possibility to fabricate them simultaneously with the Josephson junctions. This approach also avoids using extra dielectric layers, which are typical sources of losses and noise in JTWPAs. We simulate the scattering parameters of the fabricated sample and acquire a reasonable matching to the 50 Ω standard within the range 4-8 GHz, see Fig. 2(b). Resonances visible in the simulation results originate from the pump line presence and will be optimized in the future designs.

Preliminary characterization measurements of our devices indicate good impedance matching to the 50 Ω standard and excellent reproducibility of the SNAILs. One of the next steps for experimental demonstration of the quantum-limited broadband amplification with flux-driven JTWPAs is the precise targeting of Josephson critical current density. The latter can be achieved by careful calibration of oxidation parameters during the Josephson junctions fabrication and is currently investigated in detail.

References

[1] N. E. Frattini, U. Vool, S. Shankar, A. Narla, K. M. Sliwa, and M. H. Devoret, Appl. Physics Letters **110**, 222603 (2017).
[2] A. Zorin, Phys. Rev. Applied **12**, 044051 (2019).
[3] A. Ranadive, M. Esposito, L. Planat, E. Bonet, C. Naud, O. Buisson, W. Guichard, and N. Roch, Nat. Commun. **13** (2022).
[4] M. Perelshtein, K. Petrovnin, V. Vesterinen, S. H. Raja, I. Lilja, M. Will, A. Savin, S. Simbierowicz, R. Jabdaraghi, J. Lehtinen, L. Grönberg, J. Hassel, M. Prunnila, J. Govenius, G. Paraoanu, and P. Hakonen, Phys. Rev. Applied **18**, 024063 (2022).
[5] Y. Lu, W. Xu, Q. Zuo, J. Pan, X. Wei, J. Jiang, Z. Li, K. Zhang, T. Guo, S. Wang, C. Cao, H. Wang, W. Xu, G. Sun, and P. Wu, Appl. Physics Letters **120**, 082601 (2022).

Improving the Coherence of Superconducting Coplanar Waveguide Resonators

L. Koch, D. Bunch, N. Bruckmoser, K. E. Honasoge, T. Luschmann, D. Bazulin, C. Schneider and S. Filipp [1]

Realizing a fault-tolerant quantum computer is the goal of an ever-growing number of publicly funded and commercial research and development activities. Amongst many potential platforms, quantum computers based on superconducting circuits are a promising candidate. However, to get beyond the noisy intermediate scale quantum (NISQ) era, the fidelity of quantum bit (qubit) gate operations needs to further increase. Since fidelity is inherently limited by qubit coherence, fabrication methods need to be improved to reach this goal. In particular, decoherence in state-of-the-art devices arises from two-level systems (TLS) [1]. The interfaces between metal (M), substrate (S) and air (A), as visualized in Fig. 1 **(a)**, are regions that host a high TLS density and thus require optimization.

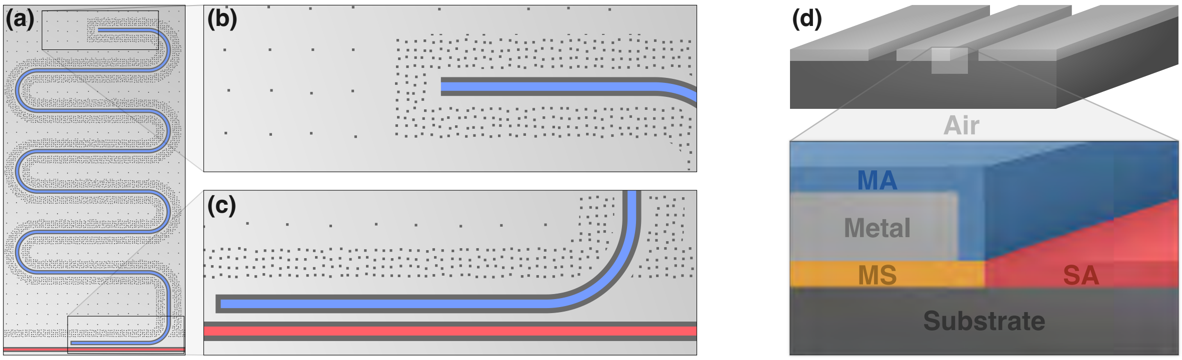

Figure 1: Layout of a superconducting coplanar waveguide (CPW) resonator. **(a)** Cross-section of a CPW. The inset highlights the different interfaces between materials. **(b)** Superconducting $\lambda/4$ CPW resonator (blue) coupled to a feedline colored in red. The resonator is shorted at the top **(c)** and open at the feed line **(d)**.

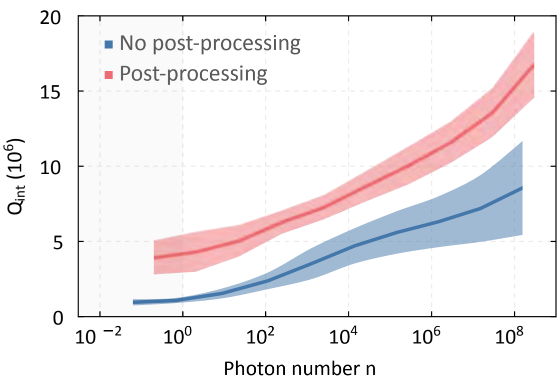

Figure 2: Dependence of the internal quality factor Q_{int} on the mean photon number for two different samples. The curves show the mean quality factor of the 13 resonances of each chip, the standard deviations are highlighted with the corresponding shade.

In order to establish a fabrication process for highly coherent quantum circuits, we optimize coplanar waveguide (CPW) resonators as a sensing system for TLS. A reduction in TLS density due to improved fabrication processes leads to a lower internal loss rate κ_{int} and therefore to a higher internal quality factor

$$Q_{int} = 2\pi f_r / \kappa_{int}$$

with the resonance frequency f_r [2]. An exemplary resonator layout is shown in Fig. 1 **(a)**. The $\lambda/4$ CPW resonator (blue) is capacitively coupled to a transmission line (red) with an impedance of $50\,\Omega$. This design allows for multiplexing more than 10 resonators to an individual

[1] This project has received support by the BMBF program No. 13N15680 (GeCQoS), the Munich Quantum Valley Quantum Computer Demonstrators - Superconducting Qubits (MUNIQC-SC; project number: 13N16188), and the Munich Quantum Valley, which is supported by the Bavarian state government with funds from the Hightech Agenda Bayern Plus.

transmission line. Thus, we can investigate a frequency span from 4 GHz to 8 GHz with a single two-port measurement. The transmitted signal of the feedline is measured around each resonance as a function of signal power and analyzed to extract Q_{int}.

To fabricate the samples, we clean high-resistivity silicon chips with a buffered oxide etch solution and sputter a 150 nm thick layer of niobium in a PLASSYS deposition system. After an optical lithography step using a direct laser writing process, the pattern is transferred onto the superconducting film by reactive ion etching. Since the interfaces to air are dominant loss channels, we extend our fabrication process by an additional subsequent wet-chemical post-processing step. To characterize the fabricated samples, we cool them to around 10 mK in dilution refrigerators and use a vector network analyzer for the transmission measurements.

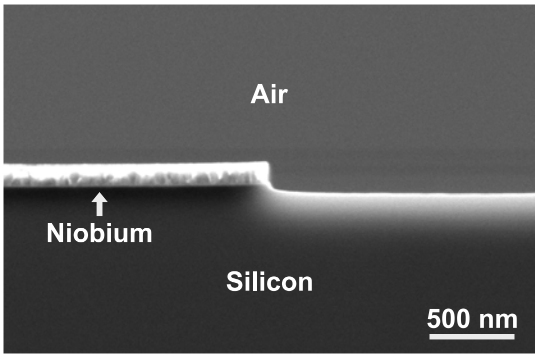

Figure 3: Scanning electron microscope picture of a CPW cross section. The niobium film is etched with an inductively coupled SF_6 plasma.

The comparison of the internal quality factor Q_{int} between a resonator sample without post-processing (blue) and post-processing (red) is shown in Fig. 2. At high photon numbers, TLS become saturated, thus leading to lower losses. In the quantum regime at low power, TLS losses are limiting the internal quality factor for both resonators. By removing lossy niobium oxides in the MA interface we were able to increase the mean Q_{int} at low power from $1 \cdot 10^6$ to $4 \cdot 10^6$, with individual resonators reaching $Q_{\mathrm{int}} = 6 \cdot 10^6$.

In addition, we optimized the reactive ion etching process to realize steep niobium etch walls and a small silicon roughness below 1 nm; an exemplary CPW cross section is shown in Fig. 3. The former is beneficial to reduce the coupling strength between the CPW and TLS and, thus, increases the quality factor. In addition, the latter is desirable to achieve a high uniformity of the Josephson junction area, which are added in a subsequent fabrication step when manufacturing superconducting qubits.

References

[1] C. Müller, J. H. Cole, and J. Lisenfeld, Reports on Progress in Physics **82**, 124501 (2019).

[2] C. R. H. McRae, H. Wang, J. Gao, M. R. Vissers, T. Brecht, A. Dunsworth, D. P. Pappas, and J. Mutus, Review of Scientific Instruments **91**, 091101 (2020). `https://doi.org/10.1063/5.0017378`.

Development of a wafer-scale Josephson junction fabrication process

L. Koch, T. Sievers, N. Bruckmoser, D. Bazulin, K. Honasoge, T. Luschmann, Y. Nojiri, C. Schneider, N. Fernandez, S. Filipp [1]

One of the major challenges for upscaling superconducting quantum processors is the reliable fabrication of high quality Josephson junctions that provide the necessary non-linearity in superconducting circuits. Here, a reproducible wafer-scale fabrication process is a key requirement to ensure well-separated resonance frequencies, high coherence, and predictable chip performance. Therefore, a reproducible wafer-scale fabrication process is a key enabling technique. Additionally, the fabrication of several layouts on the same wafer allows the investigation of design variations on the performance of quantum processors without errors due to differences in chip to chip fabrication. The critical current of a Josephson junction which defines the frequency of superconducting quantum bits (qubits) depends on the one hand on the oxide thickness between the two superconductors and on the other hand on the Josephson junction area. In our project, we focus on establishing a fabrication process for high yield and precise critical current targeting.

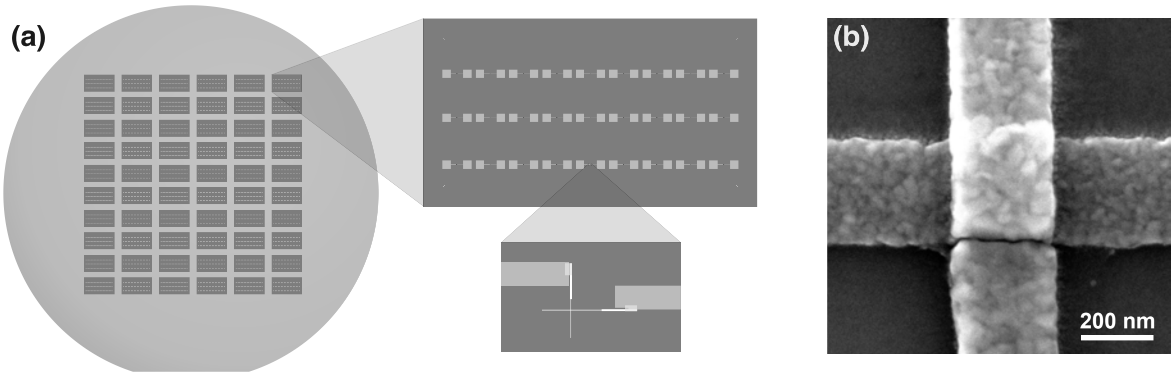

Figure 1: Layout of the wafer with a total of 1740 Josephson junctions. **(a)** Full wafer design. Niobium is visualized in light gray, silicon in dark gray. The first inset shows an individual die consisting of 27 Josephson junctions with Nb contact pads. The second inset displays a single junction which is located at the crossing of the aluminum arms shown in white. **(b)** Scanning electron microscope image of a Josephson junction with a side length of 200 nm.

The test layout consists of a total of 60 identical dies with 27 test Josephson junctions each. The layout is fabricated on a 4 inch high resistivity ($> 10\,\mathrm{k\Omega\,cm}$) silicon wafer shown in Fig. 1 **(a)**. To ensure direct comparability with our qubit fabrication process, we use dry-etched niobium probe pads and an additional ex-situ bandaging process to galvanically connect the junctions with the pads. We use Manhattan-style Josephson junctions with a shadow evaporation deposition to fabricate Al/AlOx/Al trilayer junctions. In contrast to the widely established Dolan bridge process, the Manhattan technique is less sensitive to height variations in the resist mask. This becomes especially important for complex circuits where so called air-bridges and through silicon vias lead to an uneven resist thickness across the sample. An exemplary Josephson junction is shown in Fig. 1 **(b)**.

Instead of characterizing the critical current spread by measuring transmon qubits, we utilize the Ambegaokar-Baratoff relation [1]

$$R_\mathrm{n} = \frac{\pi\Delta}{2eI_\mathrm{c}} \quad , \tag{1}$$

[1]This project is part of the Munich Quantum Valley, which is supported by the Bavarian state government with funds from the Hightech Agenda Bayern Plus and has received support by the Munich Quantum Valley Quantum Computer Demonstrators - Superconducting Qubits (MUNIQC-SC; project number: 13N16188).

where R_n is the normal state resistance, Δ is the superconducting gap of Al and I_c is the critical current across the Josephson junction and e is the electron charge. Using Eq. 1, we can estimate the qubit frequency by measuring the resistance between two pads with a four-wire measurement setup. The critical current is converted to the Josephson energy $E_J = \Phi_0 I_c/(2\pi)$ with the magnetic flux quantum Φ_0, leading to the qubit frequency for a fixed charge energy of $E_C = 250\,\mathrm{MHz}$. These results are shown in Fig. 2 for different junction sizes. The full width at half maximum of the fitted Gaussian distributions vary from 395 MHz for a junction area of $100 \times 100\,\mathrm{nm}^2$ to 649 MHz for $250 \times 250\,\mathrm{nm}^2$.

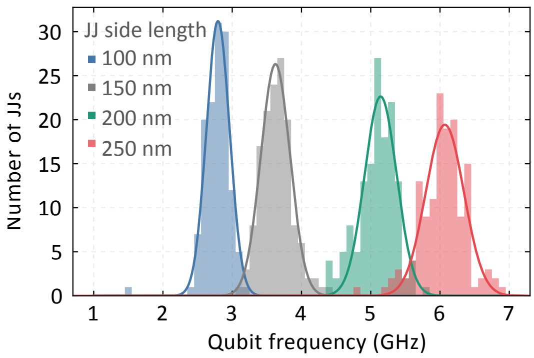

Figure 2: Estimated qubit frequency for a fixed value of $E_C = 250\,\mathrm{MHz}$. The different colors correspond to varying Josephson junction sizes with an area that is squared to the side length. Solid lines are Gaussian fits to the binned data.

In addition, different cleaning methods were investigated to improve the interface quality between the silicon surface and the evaporated aluminum nanowires. We were able to improve the Josephson junction yield on 4-inch wafer-scale from roughly 50 % to more than 99 %.

The next step will be to further minimize the spread of the critical current of our junctions by taking into account wafer bow, radial junction size dependence, line edge roughness of our Josephson junctions, and ideal oxidation parameters for uniform AlOx tunnel barriers.

References

[1] V. Ambegaokar, and A. Baratoff, Phys. Rev. Lett. **10**, 486–489 (1963).

Large-scale Fabrication of Josephson Parametric Amplifiers

M. Handschuh, K. E. Honasoge, Y. Nojiri, D. E. Bazulin, N. Bruckmoser, L. Koch, F. Fesquet, F. Kronowetter, M. Renger, W. K. Yam, A. Marx, R. Gross, K. G. Fedorov. [1]

The rapid progress in the field of quantum information processing with superconducting circuits has led to a demand in large-scale fabrication. The latter allows to increase fabrication efficiency, reproducibility, and brings down costs. Moreover, many advanced quantum applications and experiments rely on using multiple nominally identical chips, such as flux-driven Josephson parametric amplifiers (JPAs) [1]. To this end, a challenge of the growing number of quantum devices requires fabrication on a larger scale. Thus, we investigate fabrication of JPAs with Nb/Al-AlOx/Nb Josephson junctions on 4-inch wafers. A conservative distribution of samples around the center of the wafer provides us with approximately ~ 100 separate JPA chips in a single fabrication run (see Fig. 1).

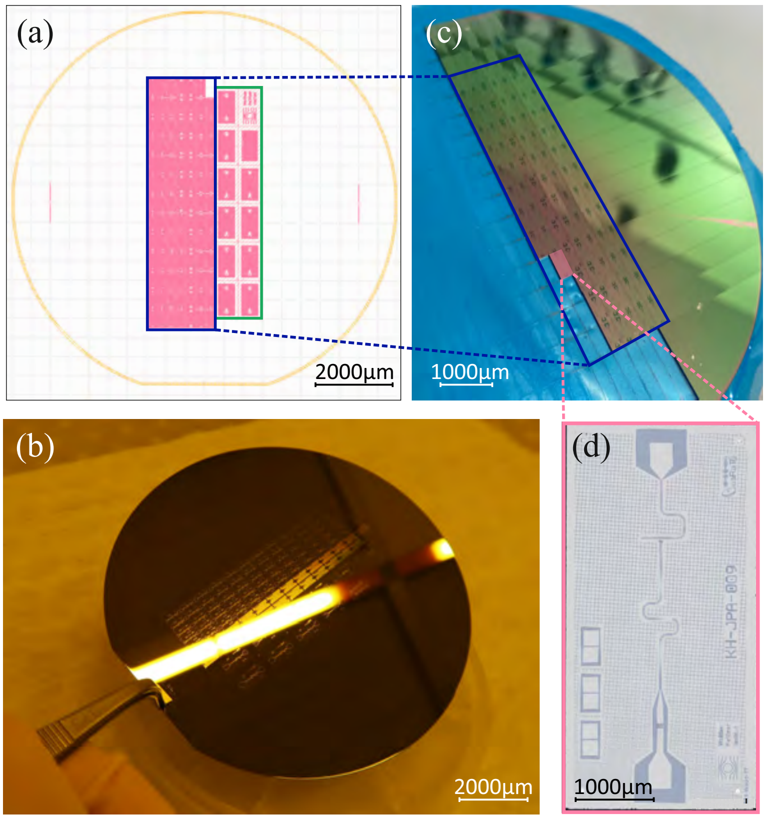

Figure 1: Illustration of the 4-inch wafer fabrication process: (a) the GDS design of the entire wafer with two different single chip sizes (2.5 mm$\times$5 mm and 6 mm$\times$10 mm), (b) a photo of the wafer with etched Nb structures, (c) the photo of the cut wafer for one chip size, (d) a microscope image of an individual 2.5 mm$\times$5 mm JPA sample.

The considered flux-driven JPA design is built on the basis of a superconducting bi-coplanar $\lambda/4$ resonator. The resonator is short-circuited to ground with a direct current superconducting interference device (dc-SQUID) consisting of two nominally identical Josephson junctions [2]. For our chip substrates we employ 525 µm thick intrinsic silicon. The resonator and pump line are formed by sputtering 150 nm thick niobium followed by an optical lithography and argon ion etching. The dc-SQUIDs are patterned using e-beam lithography followed by a double-angle aluminium shadow evaporation process. In our fabrication process, we use multiple cleaning steps which are intended to reduce microwave losses and increase the internal quality factor of the JPA fundamental mode. These steps will be described elsewhere (see contribution by K. E. Honasoge *et al.*, page 75 - 76). The fabrication process starts with a pre-cleaned wafer being placed into the PLASSYS MEB 550 S4-I UHV system for Nb deposition via sputtering.

[1]We acknowledge support by the German Research Foundation via Germany's Excellence Stratega (EXC - 2111 - 390814868), and the German Federal Ministry of Education and Research via the project QUARATE (Grant No. 13N15380). This research is part of the Munich Quantum Valley, which is supported by the Bavarian state government with funds from the Hightech Agenda Bayern Plus.

After deposition, the wafer is spin-coated with an optical resist and patterned with the PicoMaster 200 laser writer of 4 PICO. Then, we develop and dry-etch the wafer. This step is found to be rather sensitive to the etching parameters, due to the spatially inhomogeneous dry-etching process. The latter depends on the size of the chip/wafer because the ratio between the etch area and the resist coating is not negligible at wafer-scale.

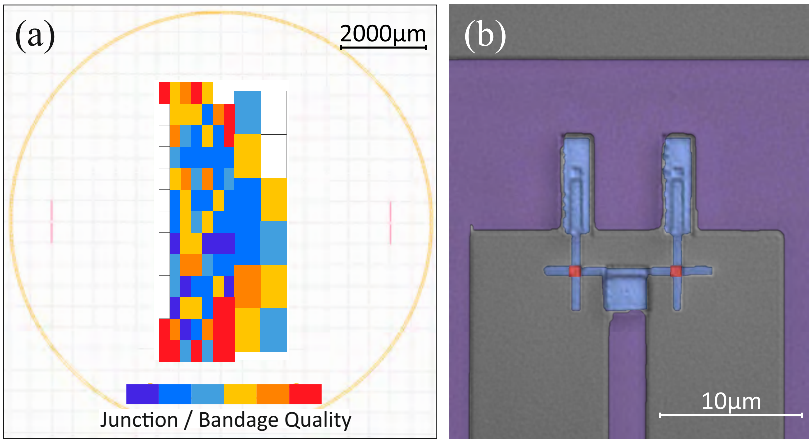

Figure 2: Panel (a) shows a distribution of fabrication yield of JPAs over the 4-inch wafer. Blue shades correspond to visually good or near-perfect samples. Yellow color indicates visible defects in dc-SQUIDs or bandages, such as dirt particles. Orange and red color indicates heavily damaged junctions or no Josephson junctions or bandages. Panel (b) shows a false-colored optical image of the JPA dc-SQUID. Here, purple color corresponds to Nb layer, red marks the Josephson junctions, blue the Al layer and grey the Si substrate.

After pattering of large structures (resonators, pump lines, contact pads, coupling capacitors), the wafer is cleaned again and spin-coated with an e-beam resist for dc-SQUID patterning. This step is implemented in our e-beam lithography nB5 machine of NanoBeam. The evaporation of the Al films for the Josephson junctions forming the dc-SQUID is performed in a PLASSYS MEB 550 S4-I UHV system. After lift-off, the last e-beam step takes place. It implements the so-called bandages, which galvanically connect the Al Josephson junctions to the Nb resonator and ground plane, thus, forming the dc-SQUID as shown in Fig. 2(b). Detailed characterization measurements of our JPA samples are the ongoing process. Nevertheless, optical characterization allows for limited conclusions about the quality of the fabricated samples as shown in Fig. 2. Here, one can observe a distribution of JPA quality over the wafer. As expected, the best samples are located near the wafer center. The area with multiple red-colored samples arises from resist inhomogeneities.

Our preliminary results on the fabrication process already indicate a reasonable yield and quality of the fabricated superconducting circuits. The next step is the investigation of the distribution of Josephson critical currents and internal quality factors over the wafer. Corresponding characterization measurements are currently ongoing. In the end, we plan to use the large-scale fabrication of the JPAs as a backbone for current and future experiments towards microwave quantum communication, quantum computing, and quantum sensing.

References

[1] K. G. Fedorov, M. Renger, S. Pogorzalek, R. D. Candia, Q. Chen, Y. Nojiri, K. Inomata, Y. Nakamura, M. Partanen, A. Marx, R. Gross, and F. Deppe, Sci. Adv. **7**, eabk0891 (2021).

[2] T. Yamamoto, K. Inomata, M. Watanabe, K. Matsuba, T. Miyazaki, W. D. Oliver, Y. Nakamura, and J. S. Tsai, Appl. Phys. Lett. **93**, 042510 (2008).

Fabrication of Low-Loss Josephson Parametric Circuits

K.E. Honasoge, Y. Nojiri, D.E. Bazulin, L. Koch, T. Luschmann, N. Bruckmoser, M.T. Handschuh, F. Fesquet, F. Kronowetter, M. Renger, A. Marx, R. Gross, K.G. Fedorov [1]

The emergence of quantum information processing with superconducting circuits has stimulated the development of various Josephson parametric devices. The latter offer a wide range of applications ranging from quantum-limited amplification to generation of entangled squeezed states of light [1]. One of the key challenges is to fabricate low-loss Josephson junction based superconducting circuits, directly leading to an improved performance of related applications and protocols. Here, we report on the optimization of the fabrication technique for low-loss Josephson parametric converters (JPCs) [2].

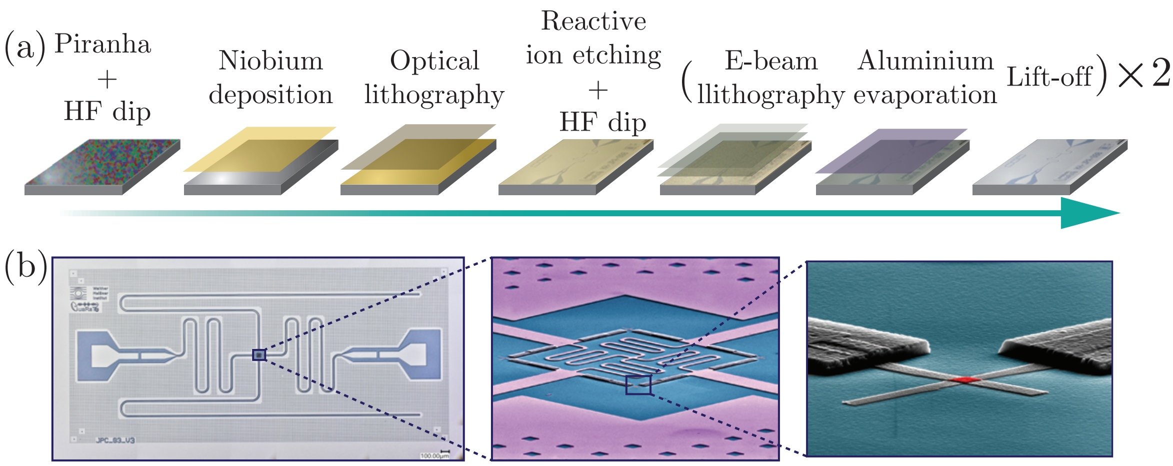

Figure 1: (a) Simplified illustration of our fabrication process, aiming at the mitigation of TLS losses at various interfaces. (b) Optical image of a Josephson parametric converter (JPC) fabricated with the fabrication process shown in panel (a). The center image shows a false-colored SEM micrograph of the JPC center element, which consists of four inductively shunted Josephson junctions. The right image shows an SEM close-up of one of the junctions. The color coding is: Nb-purple, Si-cyan, Al-grey, and Josephson junction-red.

The challenge in reaching low microwave losses and, respectively, high internal quality factors, Q_{int}, for superconducting circuits is to remove the various loss channels. One of the dominant loss channels is related to omnipresent two-level systems (TLSs). These TLSs may couple to internal microwave modes of the JPCs and lead to energy relaxation, significantly limiting Q_{int}. To mitigate losses from TLSs, we incorporate a series of surface treatment steps during the fabrication of our superconducting circuits.

Our fabrication process is illustrated in Fig. 1(b). It starts with treating pre-cleaned high resistivity ($R_\square > 10\,\mathrm{k\Omega}$) silicon (Si) substrates in a hot Piranha solution. This ensures the oxidized dissolution of any organic contaminants and additionally leaves the substrate with a thick surface oxide. This is followed by a buffered hydrofluoric acid solution (BOE) treatment of the substrate before surface metallization by sputter deposition of niobium (Nb). This BOE step strips the surface Si oxide, ensuring a clean metal-substrate interface. After deposition, the substrates are patterned with optical lithography and a sulfur hexafluoride dry etching process. Then, we apply another BOE step before the e-beam lithography step for Josephson junction patterning. This ensures a clean metal-surface interface for the two consecutive aluminium (Al) depositions, with an intermediate oxidation step that forms the Josephson

[1] We acknowledge support by the German Research Foundation via Germany's Excellence Strategy (EXC – 2111 – 390814868), and the German Federal Ministry of Education and Research via the project QUARATE (Grant No. 13N15380). This research is part of the Munich Quantum Valley, which is supported by the Bavarian state government with funds from the Hightech Agenda Bayern Plus.

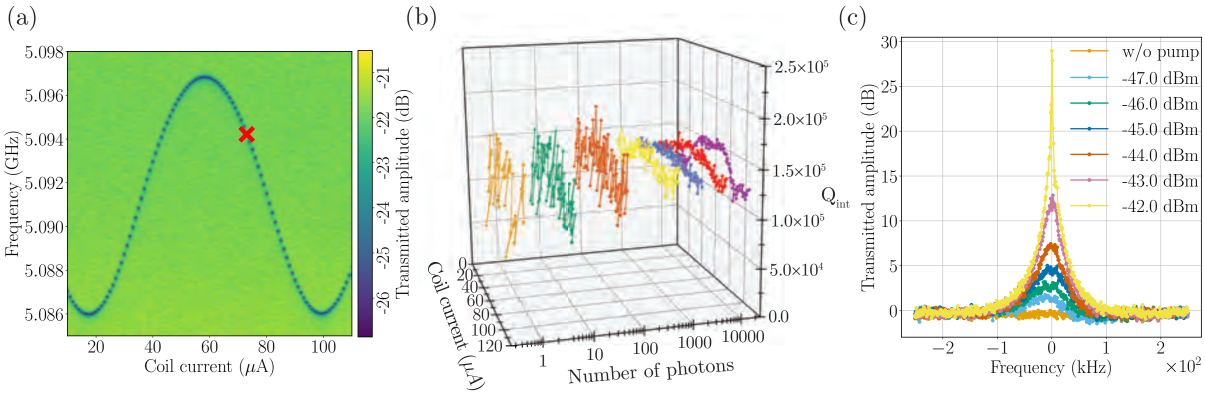

Figure 2: (a) Resonance frequency of the JPC as a function of current applied to the flux generating coil. (b) Dependence of the internal quality factor on the applied current and the photon number in the JPC cavity. (c) Phase insensitive gain of the JPC for various pump powers.

junctions. The last fabrication step includes argon ion milling to ensure clean metal-metal interfaces between Nb and Al layers. A typical JPC, fabricated according to the described procedures, is shown in Fig. 1(c).

Microwave measurements on the JPC are performed in a dilution refrigerator using a vector network analyzer (VNA). These measurements yield the complex scattering parameters as a function of frequency and power. The resonant frequency of the JPC can be tuned by varying the magnetic flux generated by feeding a current through a coil, see Fig. 2(a). We carry out multiple sweeps at different input powers and flux values in order to derive Q_{int} through an analytic fit [3]. The experimentally extracted values Q_{int} of the JPC exceed 1×10^5 in the single-photon regime and surprisingly stay rather independent of the power and flux, see Fig. 2(b). Additionally, we study the JPC amplification. The result is shown in Fig. 2(c). For this step, we apply an additional pump tone at twice the signal frequency (2ω) to induce the phase-sensitive parametric amplification process. We observe a respective gain of up to $\mathrm{G} = 25\,\mathrm{dB}$, with a corresponding gain-bandwidth product, $G \cdot BW \simeq 459.4\,\mathrm{kHz}$. Further characterization measurements of the JPCs, including their noise and compression properties, are ongoing.

The demonstrated internal quality factors in excess of 1×10^5 of the Josephson parametric circuits illustrate the state-of-the-art developments in our fabrication process. These techniques are readily applicable to the fabrication of other Josephson parametric devices, such as flux-driven Josephson parametric amplifiers (JPAs) and single-photon detectors (SPDs) required for various application in quantum sensing and quantum networks based on propagating quantum microwaves.

References

[1] K. G. Fedorov, M. Renger, S. Pogorzalek, R. Di Candia, Q. Chen, Y. Nojiri, K. Inomata, Y. Nakamura, M. Partanen, A. Marx, and R. Gross, Science advances **7**, eabk0891 (2021).

[2] E. Flurin. *The Josephson mixer: a Swiss army knife for microwave quantum optics*. Diploma thesis, Ecole normale supérieure-ENS PARIS (2014).

[3] S. Probst, F. Song, P. A. Bushev, A. V. Ustinov, and M. Weides, Review of Scientific Instruments **86**, 024706 (2015).

Coupler-mediated Unconditional Reset of Fixed-Frequency Superconducting Qubits

Gerhard Huber, Federico Roy, Max Werninghaus, Niklas Bruckmoser, Niklas Glaser, Leon Koch, Gleb Krylov, Joao Romeiro, Malay Singh, Ivan Tsitsilin, Stefan Filipp [1]

For the execution of quantum algorithms, the qubits in a quantum computer must be initialized in a known state. As coherence times of superconducting qubits increase, waiting passively for the natural decay to the ground state becomes inefficient. A method for fast and reliable reset allows to operate devices at high repetition rates and to implement mid-circuit measurements, needed for error correcting schemes. Here, we implement an unconditional reset protocol for fixed-frequency qubits in a flux-tunable multi-qubit coupler architecture building on the protocol proposed in Ref. [1].

In our setup, the flux tunable coupler is capacitively coupled to the qubit and the resonator, respectively, as shown in Fig. 1(a,b). The Hamiltonian of the coupled system is

$$
\begin{aligned}
H = & \sum_{i=q,r,c} \omega_i b_i^\dagger b_i + \sum_{i=q,c} \frac{\alpha_i}{2} b_i^\dagger b_i^\dagger b_i b_i \\
& - \sum_{ij=qr,qc,rc} g_{ij} (b_i^\dagger - b_i)(b_j^\dagger - b_j),
\end{aligned}
\tag{1}
$$

where subscripts refer to the qubit, the resonator and the coupler and ω, α and g are the respective frequencies, anharmonicities and pair-wise couplings. We modulate the Josephson energy $E_{J,c}$ of the coupler via an external flux to control the coupler frequency $\omega_c(t) = \sqrt{8E_J(t)E_c} - E_c(1 + \frac{11}{16}\varepsilon(t))$, the anharmonicity $\alpha(t) = E_c(1 + \frac{9}{16}\varepsilon(t))$ and the coupling $g_{ic}(t) \propto (E_J(t))^{\frac{1}{4}}$ where $\varepsilon(t) = \sqrt{\frac{2E_c}{E_J(t)}}$. Device parameters are listed in Tab. 2.

We activate effective resonant interactions between the qubit and the resonator by parametrically driving the coupler at half

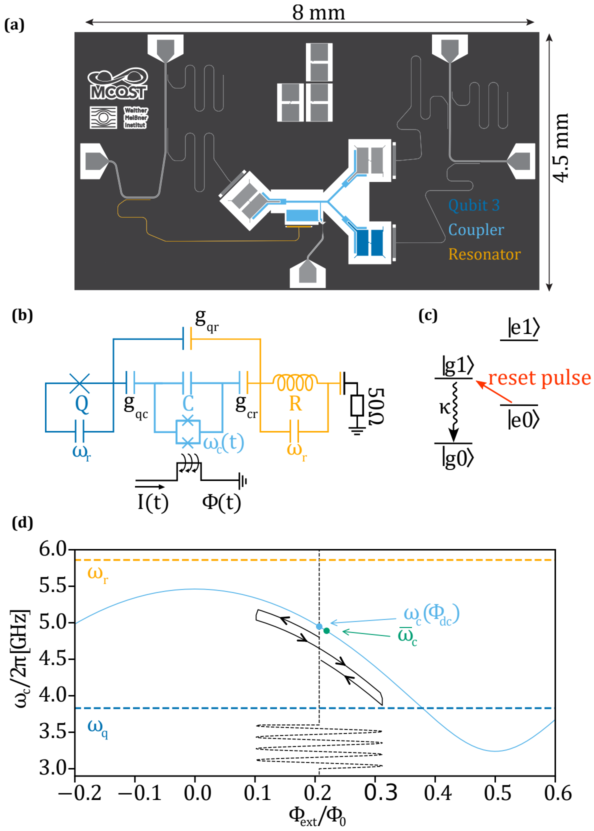

Figure 1: Experimental setup and reset protocol. (a) Three qubit coupler chip used in this work. Highlighted elements are the qubit coupler (light blue), the resonator connected to the smaller island of the coupler (orange) and the qubit used during the reset protocol (dark blue). Elements not used during the reset protocol are greyed out. (b) Simplified circuit diagram of the chip. The qubit is capacitively connected to the coupler (resonator) with coupling strength g_{qc} (g_{qr}). The coupler flux is controlled by a pulse in the flux line inductively coupled to the coupler squid loop. The resonator is coupled to the 50 Ω environment. (c) Level diagram of the first two qubit and resonator states, respectively. The reset pulse swaps the excitation in $|e0\rangle$ to $|g1\rangle$ where it decays into the environment with the resonator decay rate κ. (d) Energy diagram of the coupler as a function of the external flux in units of flux quanta Φ_0. The flux pulse is shown as a black dashed line, which is applied on top of the flux bias Φ_{dc}. The average coupler frequency $\overline{\omega}_c$ is marked in green. Uncoupled qubit and resonator frequencies are shown with dashed lines.

[1]We acknowledge financial support by the German Research Foundation via Germany's Excellence Strategy "EXC-2111-390814868", the Munich Quantum Valley, which is supported by the Bavarian state government with funds from the Hightech Agenda Bayern Plus and the BMBF program GeQCoS "No 13N15680"

	$\omega/2\pi$(GHz)	$\alpha/2\pi$(GHz)	$g_{i;c}/2\pi$(MHz)	$g_{q;r}/2\pi$(MHz)	T_1(µs)
Q	3.83	-0.21	114.7	6.6	45
R	5.86		77.6		0.20
C	3.24-5.46	-0.16			4

Table 2: The device parameters of the qubit (Q), resonator (R) and coupler (C) as shown in Fig. 1. Couplings and lifetimes were measured at the dc flux bias sweetspot $\Phi_{dc} = 0\,\Phi_0$. The T_1 time of the coupler is Purcell-limited at the sweet-spot, away from the sweetspot the coupler T_1 increases to $\approx 20\,\mu s$.

their difference frequency [2], where the effective coupling strength is controlled by the drive amplitude, as shown in Fig. 1(c,d). To calibrate the drive frequency at a given amplitude, we measure an initially excited state after a flux pulse for varying pulse lengths and frequencies as shown in Fig. 2(a). Depending on the drive amplitude we operate the reset either in an underdamped regime, where the excitation swaps between qubit and resonator or in an overdamped regime, where no oscillations occur as shown in Fig. 2(b). To characterize the reset fidelity, we measure the residual population in the qubit after a reset of length 180 ns using standard dispersive readout (Fig. 2(c)). Due to it's higher frequency, the resonator has a lower residual excited population than the qubit. The reset reduces the residual excitation in the qubit from 1.6 % ($T_{eff} \approx 45$ mK) to 0.3 % ($T_{eff} \approx 32$ mK), effectively cooling the qubit by ≈ 13 mK. Finally, we compare our reset protocol to passive reset achieved by waiting a fixed time (Fig. 2(d)). Our reset protocol prepares the ground state of the qubit with fidelities > 99% even for times much shorter than the qubit lifetime.

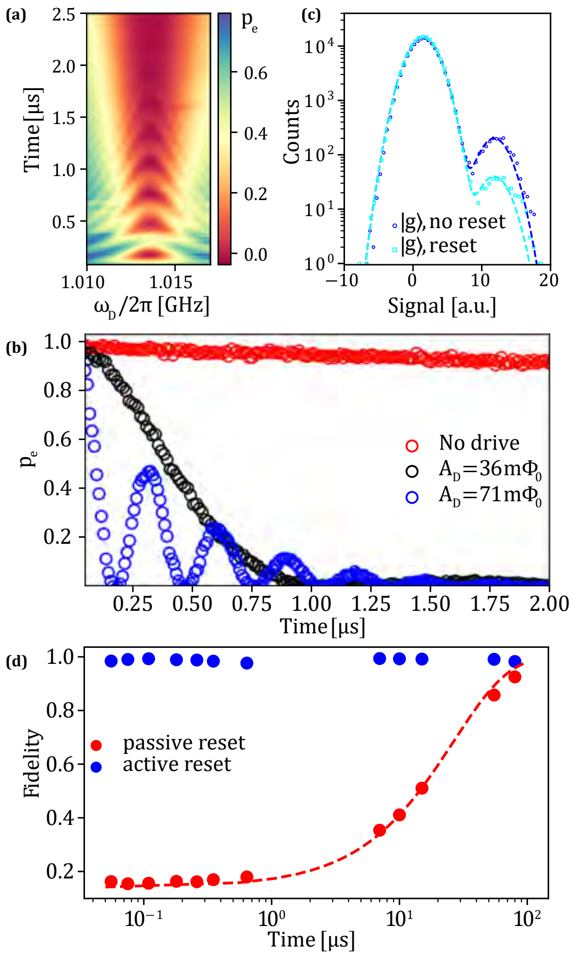

Figure 2: Measurement results of the qubit reset protocol. (a) Qubit population against reset pulse length and drive frequency. (b) The qubit population during flux modulation for different drive amplitudes. For no flux drive (red) the qubit decays with it's natural lifetime. For weak drive amplitudes the qubit lifetime is reduced but no oscillations of the population occur (black). For strong drives, the excitation swaps faster than it can decay in the resonator leading to a decaying oscillation (red). (c) Readout histogram of the ground state of the qubit without (blue) and with reset (cyan). (d) Fidelity of ground state preparation for passive and active reset. We first prepare the qubit in it's excited state and then either wait (red) or perform a reset pulse with the same length (blue). The red dashed line is the expected fidelity including the qubit lifetime and 4 µs measurement time.

References

[1] Y. Zhou, Z. Zhang, Z. Yin, S. Huai, X. Gu, X. Xu, J. Allcock, F. Liu, G. Xi, Q. Yu, H. Zhang, M. Zhang, H. Li, X. Song, Z. Wang, D. Zheng, S. An, Y. Zheng, and S. Zhang, Nat. Comms. **12**, 5924 (2021).

[2] D. C. McKay, S. Filipp, A. Mezzacapo, E. Magesan, J. M. Chow, and J. M. Gambetta, Phys. Rev. Appl. **6**, 064007 (2016).

Long-term performance and lifetime of a cryogenic millikelvin link

M. Renger, S. Gandorfer, W.K. Yam, F. Fesquet, K. Honasoge, F. Kronowetter, Y. Nojiri, A. Marx, R. Gross, K.G. Fedorov [1]

The rapidly growing field of superconducting quantum information processing requires quantum networks for secure and efficient information exchange between different quantum nodes. In order to avoid inefficient frequency conversion processes, it is advantageous to implement these netwoks directly in the microwave regime. Here, a straightforward approach requires temperatures below 100 mK which enables various quantum microwave communication protocols [1]. For this purpose, we have successfully realized a cryogenic link which connects two dilution cryostats, located in separate laboratories, over a distance of 6.5 m. A schematic illustration of our cryogenic link is provided in Fig. 1. With our system, we reach a base temperature of 52 mK in the center.

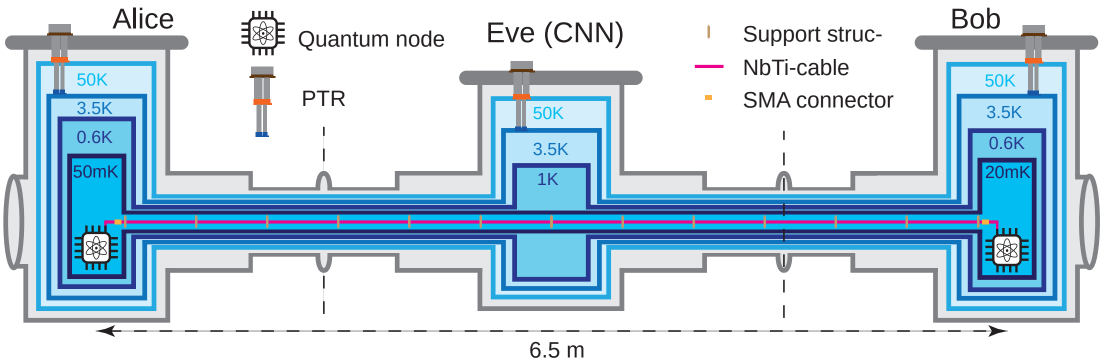

Figure 1: Schematic illustration of the cryogenic link connecting two dilution refrigerators. The center tube of the link contains a superconducting transmission line. A third cryostat, Eve, acts as a cold network node (CNN) and stabilizes the center temperature via an additional pulse tube refrigerator (PTR).

During operation of the cryogenic link, we observe that the effective cooling power at the first pulse tube (PT1) and at the second pulse tube (PT2) stage steadily decreases. This consecutive loss of cooling power manifests in an uptrend of the corresponding stage temperatures which eventually limits the operation time of our cryogenic link to 3 weeks. This temperature uptrend for the PT1 stage is plotted in Fig. 2(a) for 3 different cooldowns. The offset between different curves thereby results from the fact that between the cooldowns we have optimized the system with respect to radiative heat leaks. After warming up the system, we detect gas accumulation of 0.7 mbar in the cryogenic link volume. In the following, we follow the hypothesis that the gas consists mainly of water vapor which is either a result from trapped moisture in the superinsulation or from diffusion though our Viton O-rings. We assume that this water forms a layer of ice on top of the PT1 shield and thereby slowly forms a film with emissivity

$$\varepsilon_{\mathrm{f}}(t) = (1 - e^{-kt})\varepsilon_* + e^{-kt}\varepsilon_{\mathrm{s}}, \tag{1}$$

where ε_{s} denotes the emissivity of our Mylar superinsulation, ε_* is the emissivity of ice, k denotes the ice formation rate, and t is time. Since ice can be approximated as a black body for infrared wavelengths, this film significantly affects the heat balance of the system. In case we approximate the cooling power of the PT1 stage to be independent of temperature, it can

[1]We acknowledge support by the German Research Foundation via Germany's Excellence Strategy (EXC-2111-390814868), the EU Flagship project QMiCS (Grant No. 820505), the German Federal Ministry of Education and Research via the project QUARATE (Grant No. 13N15380), and the project QuaMToMe (Grant No. 16KISQ036). This research is part of the Munich Quantum Valley, which is supported by the Bavarian state government with funds from the Hightech Agenda Bayern Plus.

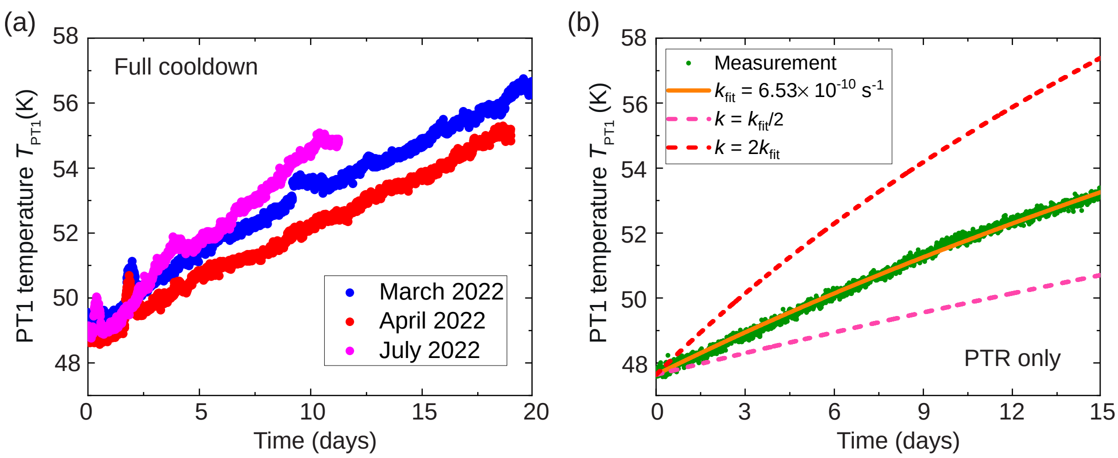

Figure 2: (a) Measured temperature uptrend for the PT1 stage for three different cooldowns. The corresponding thermometer has been fixed on top of Alice's PT1 plate. (b) Experimentally reproduced temperature uptrend in case we operate the cryogenic link with the PTRs only and keep all Helium cycles evacuated (green dots). The orange line corresponds to a fit according to Eq. 2 where we treat the quantity k as the only fit parameter.

be shown that the equlibrium PT1 temperature can be expressed as

$$T_{\mathrm{PT1}}^4(t) = T_\mathrm{r}^4 + (T_0^4 - T_\mathrm{r}^4)\eta(t), \qquad \eta(t) = 1 - \frac{\varepsilon_\mathrm{r}[\varepsilon_\mathrm{f}(t) - \varepsilon_\mathrm{s}]}{\varepsilon_\mathrm{f}(t)[\varepsilon_\mathrm{s} + \varepsilon_\mathrm{r}(N+2-\varepsilon_\mathrm{s})]}, \tag{2}$$

where T_r denotes room temperature, $T_0 = T_{\mathrm{PT1}}(0)$, $N = 40$ denotes the number of superinsulation layers and ε_r is the emissivity of the room temperature aluminum shields. We employ Eq. 2 to fit the temperature uptrend. The fit is shown in Fig. 2(b) and we observe good agreement with our observation. The experimental data thereby correspond to the scenario where we only operate the PTRs with evacuated Helium circuits such that the heat load is dominated by radiation.

Next, we analyze the source of water accumulation. We thereby investigate the hypothesis that the dominating source is diffusion through our Viton O-rings. This hypothesis is based on the significant amount of O-ring seals as well as on the fact that the slope of the temperature uptrend is higher for the cooldown in July, compared to March and April, as visible in Fig. 2(a). This observation can be explained by the temperature dependent partial pressure of water in atmosphere, as predicted by the August-Roche-Magnus equation. The permeation rate through our O-ring seals can be expressed as [2]

$$\dot{V} = \sum_y \sum_x g K_x p_x N_y f_y, \qquad f_y = \frac{\pi^2}{2} \frac{D_y + d_y}{d_y^2 \arccos\left(\frac{h_y^2 + g_y^2 + 2h_y g_y}{d_y^2}\right)} \sqrt{d_y^4 - (h_y + g_y)^4}, \tag{3}$$

where p_x (K_x) labels the partial pressure (permeation coefficient) for gas x, N_y (f_y) denotes the number of O-rings (form factor) for seal geometry y, and g accounts for lubrication. In Eq. 3, we express f_y in terms of the O-ring diameter D_y, cross-sectional diameter d_y, trench depth h_y, and clearance gap g_y under the assumption of elliptical O-ring distortion. Equation 3 predicts a gas accumulation of 1.3 mbar within 3 weeks [2]. Considering our measurement uncertainty as well as employed worst case approximations, this value is consistent with our observation.

Possible long-term solutions for the described problem include an upgrade of the cooling power of Alice and installation of cryogenic vapor traps.

References

[1] K. G. Fedorov *et al.*, Sci. Adv. **7**, eabk0891 (2021).
[2] P. Sturm *et al.*, Journal of Geophysical Research: Atmospheres **109**, D04309 (2004).

Materials, Thin Film and Nanotechnology, Experimental Techniques

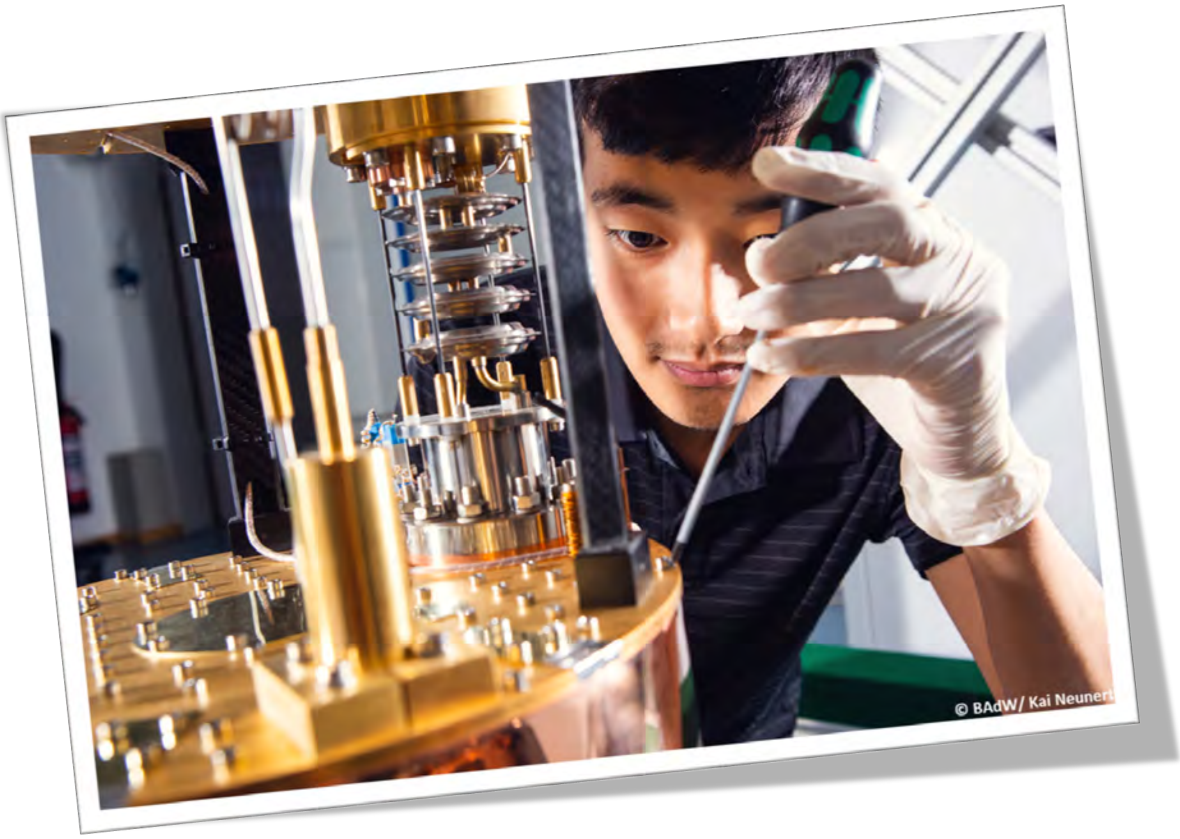

Magnetic Field Robust High Quality Factor NbTiN Superconducting Microwave Resonators for Electrons Spin Resonance Experiments

M. Müller, P. Oehrl, J. Franz, T. Luschmann, A. Faltermeier, S. Weichselbaumer, L. Koch, G. Huber, F. Deppe, A. Marx, S. Filipp, M. Althammer, R. Gross, H. Huebl [1]

H. W. Schumacher, N. Ubbelohde, D. Reifert, T. Scheller [2,3]

High-quality superconducting microwave resonators are a central building block for today's quantum information processing with superconducting circuit elements [1, 2]. A particular advantage of microwave resonators based on superconductors is the fact that resonators with high- and ultrahigh-quality factors Q can be realized even for planar designs, e.g. in the form of lumped-element or coplanar waveguide resonators [3]. While Al and Nb represent well-established materials in superconducting quantum technology, there are superconductors with higher critical temperatures T_c. Niobium titanium nitride (NbTiN) is one of the prime candidates, as it is a hard type II superconductor with a transition temperature of up to $T_c = 17\,K$, which offers an enhanced robustness against magnetic fields and elevated temperatures. These properties are useful to perform for electron spin resonance (ESR) with the goal in mind to realize quantum memory based on spin donors in Si [4].

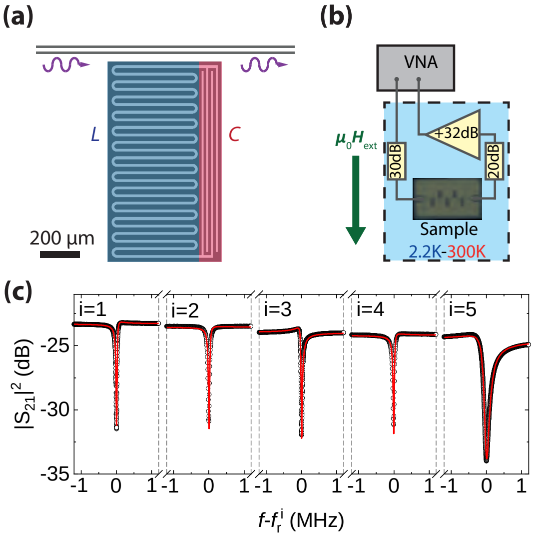

Figure 1: (a) Schematic illustration of the resonator design. (b) Schematic of the measurement setup. (c) Exemplary microwave transmission spectrum $|S_{21}(f)|^2$ of a NbTiN device grown on Si and measured at $T = 2.2\,K$ and a microwave power corresponding to $\simeq 10^7$ photons on average in the resonator. One can identify five resonances attributed to the resonators (R1-R5) patterned on the chip. Fits following the circle fit model [5] are shown as red lines. The resonance frequencies are $f_1 = 4.672\,GHz$, $f_2 = 4.806\,GHz$, $f_3 = 4.924\,GHz$, $f_4 = 5.026\,GHz$, and $f_5 = 5.133\,GHz$, respectively.

In our recent work [6], we investigate the performance of thin-film $Nb_{70}Ti_{30}N$ (NbTiN) lumped element microwave resonators from a materials perspective. Specifically, we focus on the preparation of the NbTiN thin-films and compare the quality factors for various substrate configurations. The superconducting resonators are patterned into NbTiN thin films grown by sputter deposition on both pristine (001) oriented, high-resistivity Si substrates and SiO_2 (1 μm) on Si substrates, respectively. We further compare characteristic properties of resonators with identical geometry fabricated from NbTiN thin films deposited on SiO_2 (150 nm) on Si substrates at the *Physikalisch-Technische Bundesanstalt* (PTB). In addition to the low temperature limit, which is of importance for applications in superconducting quantum technology, we investigate the performance of our resonators at elevated temperatures and at applied magnetic fields having their application for ESR in mind.

The NbTiN films are patterned into planar lumped element resonators using electron beam lithography and reactive ion etching. The investigated chip layout includes a microwave transmission line coupled in a hanger-type configuration to five lumped

[1]We acknowledge financial support by the German Research Foundation via Germany's Excellence Strategy "EXC-2111-390814868" and the Munich Quantum Valley, which is supported by the Bavarian state government with funds from the Hightech Agenda Bayern Plus

[2]Physikalisch-Technische Bundesanstalt, Braunschweig, Germany

[3]The work at PTB was co-funded by the German Research Foundation under Germany's Excellence Strategy "EXC-2123-390837967".

element microwave resonators which slightly differ in their capacitance C and, hence, their resonance frequency f_r. This configuration allows for a multiplexed readout scheme which we use to asses the resonator to resonator variance with respect to the Q-factor [see also Fig. 1(a) for the geometry of the resonator layout]. For measurements, the finalized chip is mounted in a sample box and inserted into a variable temperature helium cryostat. The microwave setup is depicted in Fig. 1(b). We connect the two ends of the central feed line to the two ports of a vector network analyzer and record the complex transmission parameter $S_{21}(f)$ close to the resonance frequency f_r for each resonator as shown in Fig. 1(c) at applied microwave powers that correspond to the high-photon limit of the resonators ($\langle n_{ph} \rangle \simeq 10^7$).

For resonators patterned on NbTiN grown on SiO_2 average internal quality factors of $Q_{int} \simeq (1-2) \cdot 10^4$ are achieved, while for those patterned on NbTiN on highly resistive Si we observe enhanced quality factors of $Q_{int} \simeq 2 \cdot 10^5$. Characterizing our resonators in terms of their robustness to elevated temperatures and external magnetic fields, NbTiN resonators grown on unoxidized Si exhibited a $Q_{int} \geq 10^5$ for $T \leq 4.8\,$K and $\mu_0 H_{ext} \leq 180\,$mT, greatly outperforming resonators made out of elementary Nb [7].

An exemplary ESR spectrum is shown in Fig. 2, where we plot the microwave transmission $|S_{21}|^2$ of a transmission line coupled to a NbTiN resonator on which a phosphorous-doped ^{nat}Si substrate with a concentration of [P]$= 2 \cdot 10^{17}\,\mathrm{cm}^{-3}$ is mounted. The transmission is reduced from $-6\,$dB to about $-14\,$dB when the excitation frequency is in resonance with the NbTiN resonator. We further observe a shift of the resonance frequency over the displayed magnetic field range, which we attribute to the magnetic field dependent kinetic inductance of the superconductor. The applied magnetic field leads to an increase in the kinetic inductance and, thereby, also the total inductance of the resonator changing the resonance frequency. Furthermore, we observe two distinct features at $\mu_0 H_{ext} = 145.6\,$mT and $\mu_0 H_{ext} = 149.8\,$mT, which are identified as the two hyperfine transitions of the P donors in Si. These initial experiments demonstrate the usefulness of our NbTiN resonators for ESR-experiments and reveal that they can serve as an appropriate base material platform towards the implementation of quantum memory based on spin donors in Si [4].

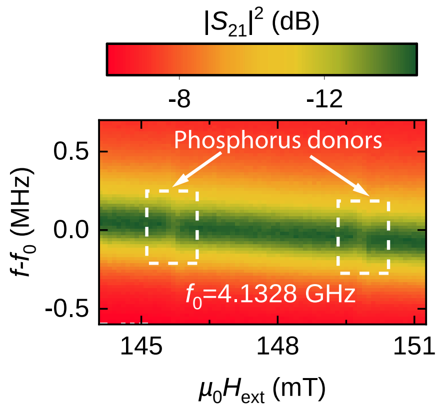

Figure 2: Microwave transmission $|S_{21}|^2$ as a function of the frequency and the applied magnetic field recorded at $T = 3.0\,$K and a microwave power $P = -105\,$dBm. The frequency-dependent absorption dip corresponds to the NbTiN resonator, while the two distinct features indicate the phosphorus hyperfine transitions.

References

[1] A. Wallraff, D. I. Schuster, A. Blais, L. Frunzio, R.-S. Huang, J. Majer, S. Kumar, S. M. Girvin, and R. J. Schoelkopf, Nature **431**, 162–167 (2004).
[2] I. Chiorescu, P. Bertet, K. Semba, Y. Nakamura, C. J. P. M. Harmans, and J. E. Mooij, Nature **431**, 159–162 (2004).
[3] C. W. Zollitsch, K. Mueller, D. P. Franke, S. T. B. Goennenwein, M. S. Brandt, R. Gross, and H. Huebl, Appl. Phys. Lett. **107**, 142105 (2015).
[4] C. Grezes, B. Julsgaard, Y. Kubo, M. Stern, T. Umeda, J. Isoya, H. Sumiya, H. Abe, S. Onoda, T. Ohshima, V. Jacques, J. Esteve, D. Vion, D. Esteve, K. Mølmer, and P. Bertet, Phys. Rev. X **4**, 021049 (2014).
[5] S. Probst, F. B. Song, P. A. Bushev, A. V. Ustinov, and M. Weides, Rev. Sci. Instrum **86**, 024706 (2015).
[6] M. Müller, T. Luschmann, A. Faltermeier, S. Weichselbaumer, L. Koch, G. B. P. Huber, H. W. Schumacher, N. Ubbelohde, D. Reifert, T. Scheller, F. Deppe, A. Marx, S. Filipp, M. Althammer, R. Gross, and H. Huebl, Mater. Quantum. Technol. **2**, 015002 (2022).
[7] S. E. de Graaf, A. V. Danilov, A. Adamyan, T. Bauch, and S. E. Kubatkin, Journ. Appl. Phy. **112**, 123905 (2012).

Cryogen-Free Dilution Refrigerator with Seven Hour Pulse Tube Shut-off – a Novel Design

K. Uhlig

Cryogen-free dilution refrigerators (CF-DR or dry DR) have become the workhorses for low temperature researchers with temperatures as low as 5 mK being commercially available [1]. Especially in the field of quantum technology dry DRs are indispensable. To precool CF-DRs, pulse tube cryocoolers (PTCs) are employed. As there are no moving parts in PTCs, their level of mechanical vibration is low and therefore they are ideally suited for this purpose. However, very small but finite vibrations and temperature variations of the PTCs do exist. They are either generated by the compressor of the PTC or by the streaming helium gas and the associated pressure variations [2]. For example, in STM or MRI applications these vibrations can be problematic. Of course there are measures to attenuate the vibrations, but the straightforward way to get rid of them would be to shut off the PTC during measurements. However, in standard dry DRs, after a shut-off period of the PTC of about 30 min, the temperature of the 2nd stage of PTC exceeds 10 K. Thus, the circulating ^{3}He is no longer adequately pre-cooled and the dilution process gets out of control.

Here we report on a dry DR where the PTC can be shut off temporarily, while the dilution circuit runs undisturbed during the shut-off time. Moreover, it continues to operate continuously when the PTC is turned on again. For cooling and condensing the ^{3}He flow during the shut-off time, a helium refrigeration circuit was installed in the cryostat. Its 1 K pot serves as a cold buffer for the circulating ^{3}He of the dilution unit. With this cold buffer the shut-off time of the PTC can be extended to 7 h but even longer shut-off times seem possible.

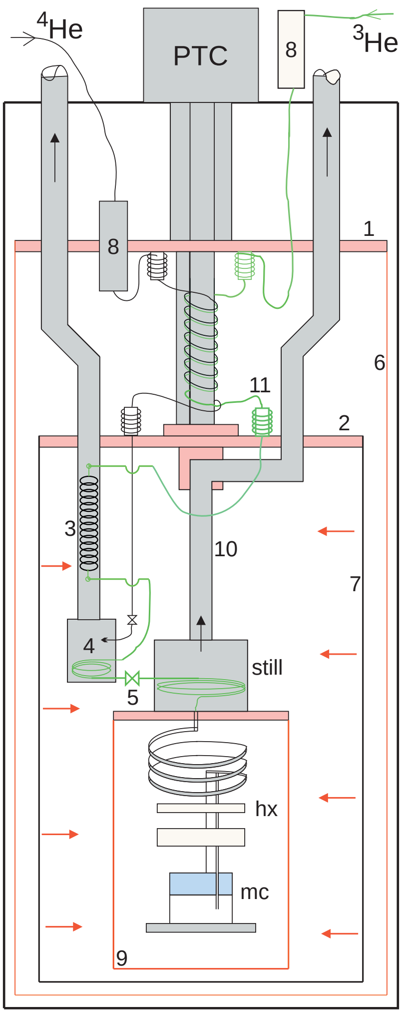

Figure 1: Section of the cryostat: 1 - 1st stage of PTC; 2 - 2nd stage of PTC; 3 - counterflow heat exchanger; 4 - pot of 1 K stage; 5 - flow restriction; 6 - rad. shield; 7 - inner vacuum can; 8 - charcoal trap; 9 - still rad. shield; 10 - still pumping line - mechanical suspension; 11 - heat exchanger.

In Fig. 1, a section of the cryostat is shown. It not only contains the dilution refrigeration unit, but also the 1 K helium circuit mentioned before [3]. Its pot has a volume of 100 cm^3 (for comparison, the volume of the mixing chamber is 125 cm^3). Before a PTC shut-off, the 1 K pot is filled with He_{liq} and afterwards the 1 K loop is operated in a single cycle mode. A peculiarity of the construction is that the inlet line of the dilution circuit is run through a counterflow heat exchanger (cfhx), which is placed in the pumping line of the 1 K stage for pre-cooling ("3" in Fig. 1) and through a heat exchanger in the pot ("4" in Fig. 1) for condensing. From here the ^{3}He flow is run through a restriction ("5" in Fig. 1) to the dilution unit.

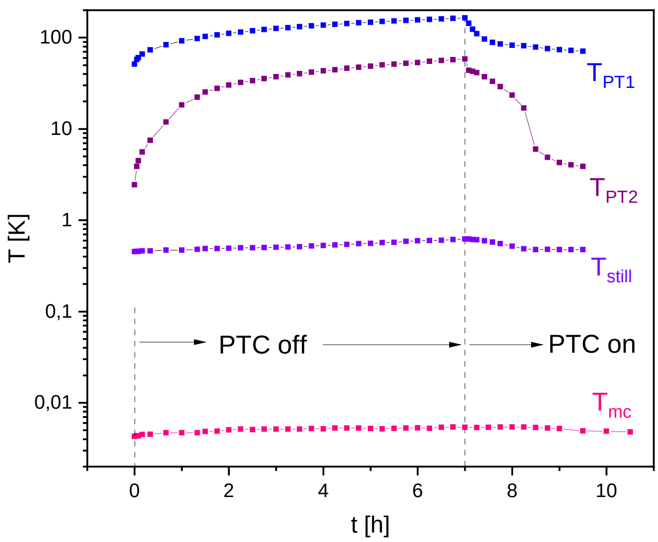

Figure 2: Temperatures of the DR during ($0 < t < 7$ h) and after (7 h $< t$) a PTC shut-off. The temperatures of the two stages of the PTC are given (T_{PT1}; T_{PT2}) and the temperatures of the still (T_{still}) and the mixing chamber (T_{mc}).

The relevant temperatures of the PTC, the still and the mixing chamber are shown in Fig. 2. Most importantly, the temperature of the mixing chamber is almost unchanged during a PTC shutoff, whereas the temperatures of the two stages of the PTC show a substantial rise caused by radiation and heat flow through the PTC, the pumping line and the trestle. The temperature of the 1st stage of the PTC rose from 53 K to 177 K and that of the 2nd stage from 2.5 K to 57 K. The radiant-heating load to the still shield, generated by the rising temperature of the inner vacuum can ("9" and "7" in Fig. 1), causes the still temperature to rise from 0.45 K to 0.6 K and a rise of the ^{3}He flow rate, which in turn results in a rise of the inlet pressure in the ^{3}He return line ($p_{cond} < 0.5 \times 10^5$ Pa). The rising ^{3}He flow finally entails a small rise in the mixing chamber temperature from 4.3 mK to 5.8 mK.

The dilution unit faces several heat sources that have to be compensated during a PTC-off:

1. The ^{3}He return flow of the dilution loop, after leaving the heat exchanger at PT2 ("11" in Fig. 1), is cooled by the cold ^{4}He gas pumped from the 1 K pot and condensed afterwards in a heat exchanger in the 1 K pot. The evaporation rate of the pot is self-regulating.
2. The pumping line of the still also serves as the suspension of the dilution unit. It is cooled by the cold ^{3}He gas stream pumped from the still – a gas-cooled suspension.
3. The radiation coming from the radiation shield of the second stage of the PTC ("8" and red arrows in Fig. 1) is cooled by the refrigeration power of the still.
4. The heat input through coaxial lines and electrical leads is also compensated by the cooling power of the still.
5. Heat flowing from the 2nd stage of the PTC through the pumping line of the 1 K stage towards the 1 K pot is absorbed by the cold ^{4}He gas pumped from the pot.

We note that even longer shut-off times of the PTC can be gained with the concept described above. However, several improvements to the system have to be done to achieve this. For example, the volume of the 1 K pot has to be increased, but also the size of the cfhx in the 1 K circuit has to be increased and adjusted to the highest temperatures of the back-streaming ^{3}He gas.

References

[1] H. Zu, Cryogenics **121**, 103390 (2022).
[2] A. D'Addabbo, Cryogenics **93**, 56–65 (2018).
[3] K. Uhlig, Cryogenics **66**, 6–12 (2015).

Development of Scalable Packaging for Multi-qubit Processors

J. Schirk, I. Tsitsilin, L. Koch, N. Bruckmoser, F. Haslbeck, F. Wallner and S. Filipp [1]

Building multi-qubit quantum processors based on superconducting qubits requires an efficient signal transport between chip and control hardware [1]. For this purpose, we develop microwave packages that route microwave signals from coaxial cables to the chip and vice versa while also offering protection against external radiation and magnetic fields.

The packaging comprises four parts: a printed circuit board (PCB) that transmits microwave signals to the chip, a surface mounted coaxial connector that allows connection to the PCB, a base-plate and a lid that together form a cavity protecting the QPU from vacuum decay and thermal photons [2]. A computer graphic of the assembled package for a two port chip is shown in Fig. 1 (a). The PCB material is made out of a low-loss Isola Astra MT77 dielectric and copper as a conductor which allows it to be produced using industry standard production methods. For these small scale packages we use two layer PCBs that transmit microwave signals with conductor backed coplanar waveguides which lowers production cost. The enclosing cavity is made from oxygen free, high conductivity copper (OFHC) to ensure good thermalization of all constituents of the package and has small openings to allow for the CPWs to enter the cavity. To verify transmission and crosstalk characteristics, the package is simulated using finite elements simulations, the results of which are shown in Fig. 2 (b). The package is designed to have a maximum of -1 dB of transmission attenuation and at most -20 dB of signal reflection in the frequency range of DC to 20 GHz. The maximum operating frequency of the package is given by the frequency of the fundamental cavity mode which is 17.8 GHz for a chip size of 6 mm x 10 mm.

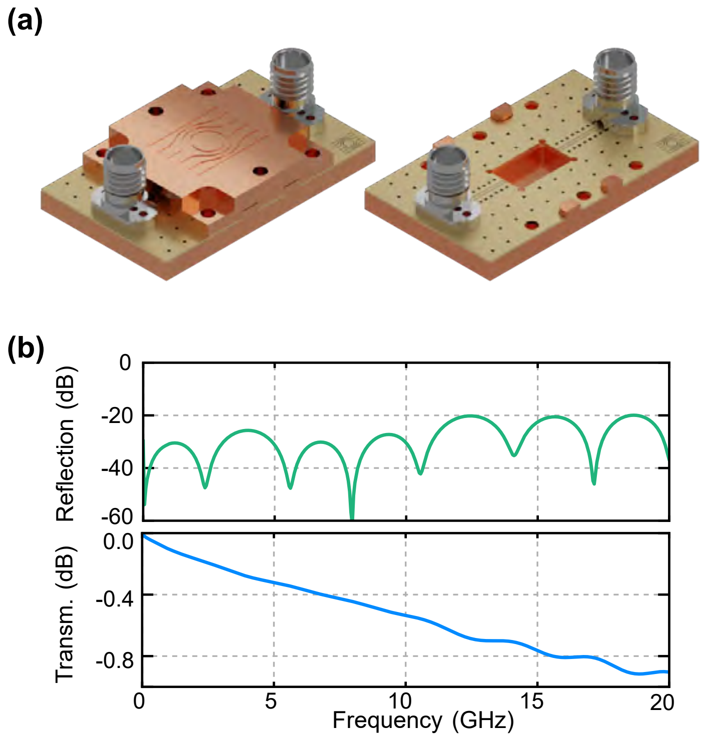

Figure 1: Overview of a QPU-packaging for two-port chips. (a) 3D model of the package with and without the top lid. The chip is placed inside a cutout of the PCB and connected to with wire-bonds. (b) Signal transmission and reflection characteristics of the PCB traces as a function of frequency.

For multiqubit processors, a package with denser wiring for a larger chip size is needed. A 3D graphic of such a packaging is shown in Fig. 2 (a). To scale up this approach for larger devices, we use multicoaxial Ardent Concepts connectors increasing the number of ports to 48. The connectors provide a small pitch of 2.54 mm and thus allow for denser routing compared to

[1]This project has received support by the BMBF program No. 13N15680 (GeCQoS) and the Munich Quantum Valley Quantum Computer Demonstrators - Superconducting Qubits (MUNIQC-SC; project number: 13N16188), and is part of the Munich Quantum Valley, which is supported by the Bavarian state government with funds from the Hightech Agenda Bayern Plus.

SMA or SMP connectors as well as being a reusable, solderless solution. We also increase the number of PCB layers to 6, allowing for signal routing using striplines on inner PCB layers.

This allows for high density routing while keeping crosstalk between adjacent traces minimal. To reduce signal crosstalk between adjacent traces even further, traces are routed on two separate layers and are shielded with dense via fences. To approve the design choice, we again use finite element simulations focusing on crosstalk between adjacent signal lines. As shown in Fig. 2 (b), crosstalk levels remain below -40 dB and attenuation increases above 1 dB at 12 GHz which is already above the cavity frequency of 10.4 GHz.
Scaling to larger chip sizes is limited by the enclosing cavity's fundamental mode which can cause Purcell decay of the individual qubits. A possible solution would be flip-integration of the chip that isolates the qubits from the cavity. Flip-chip architecture can also be used to increase the density of microwave connections from the PCB to the chip, allowing our approach to be scaled to potentially hundreds of ports.

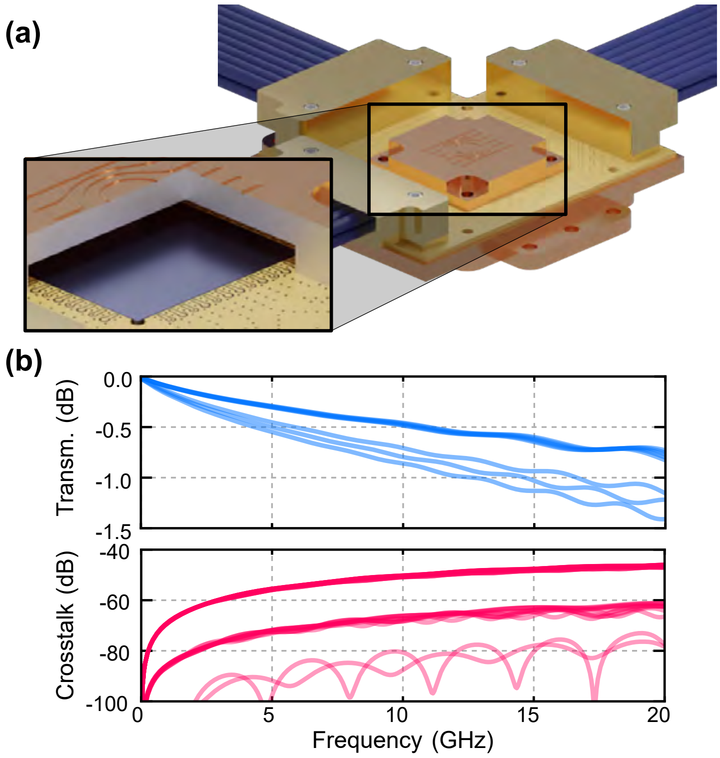

Figure 2: Overview of a QPU-packaging for 48 port chips. (a) 3D model of the package including three multi-coax connectors, the copper base-plate and lid as well as a multilayer PCB. (inset) Section view of the package. The chip is mounted in a dedicated slot of the PCB and is connected through wirebonds. (b) Signal transmission and crosstalk characteristics of the PCB traces.

References

[1] S. Huang, B. Lienhard, G. Calusine, A. Vepsäläinen, J. Braumüller, D. K. Kim, A. J. Melville, B. M. Niedzielski, J. L. Yoder, B. Kannan, T. P. Orlando, S. Gustavsson, and W. D. Oliver, PRX Quantum **2**, 020306 (2021).

[2] A. A. Houck, J. A. Schreier, B. R. Johnson, J. M. Chow, J. Koch, J. M. Gambetta, D. I. Schuster, L. Frunzio, M. H. Devoret, S. M. Girvin, and R. J. Schoelkopf, Physical Review Letters **101**, 080502 (2008).

Experimental Facilities

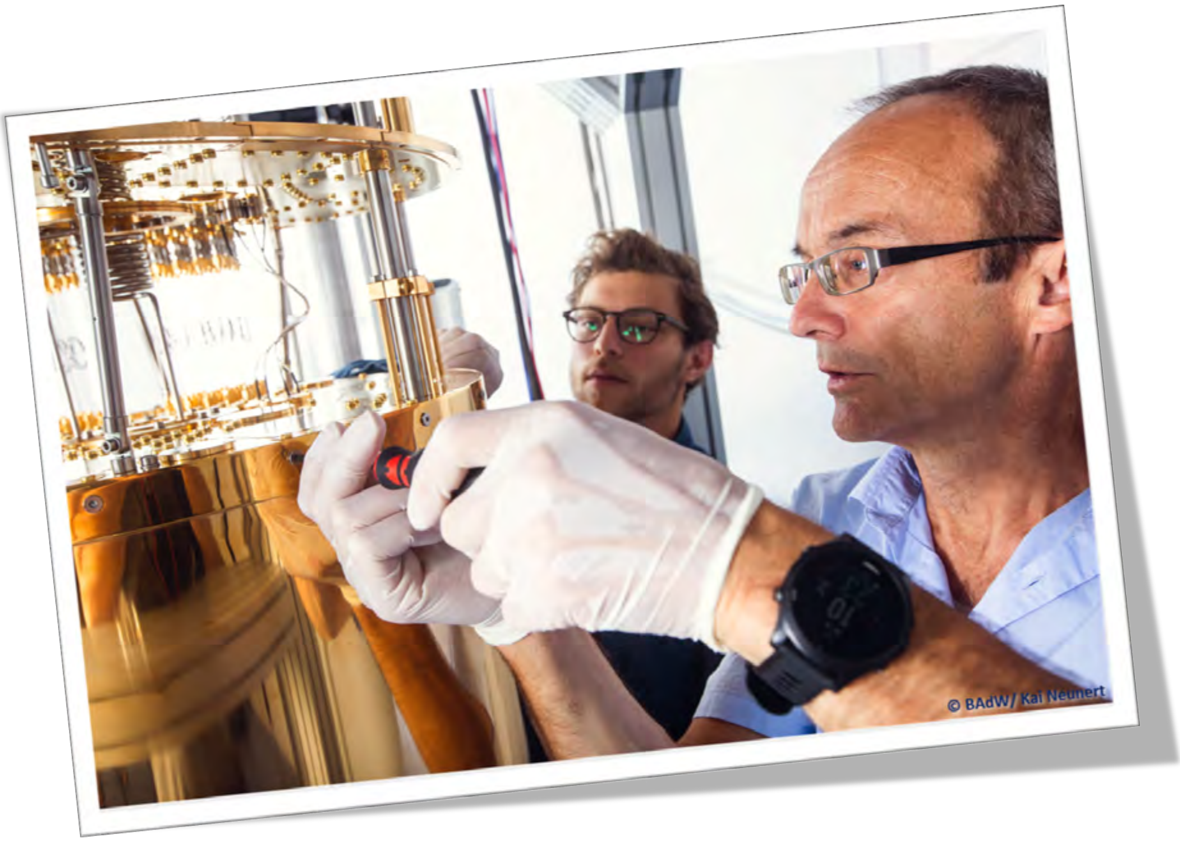

DISCO DAD3221 Automatic Dicing Saw

N. Bruckmoser, L. Koch, K. E. Honasoge, A. Marx and S. Filipp

Going from a single chip fabrication process towards wafer-scale fabrication is essential for scaling up superconducting quantum hardware. A key tool for enabling this fabrication technique is a dicing saw to cut the fully processed wafer into single dies. For this reason a new DISCO DAD3221 automatic dicing saw has been installed. The machine is capable of dicing wafer sizes up to 150 mm and is thus fully compatible with the newly established fabrication process for 100 mm silicon wafers. A built-in microscope allows for an alignment precision of 3 µm and direct analysis of the die street, which has a width of less than 50 µm for silicon wafers. Furthermore, the machine can be equipped with different blades for dicing specific materials such as sapphire.

Figure 1: Photograph of the DISCO DAD3221 wafer dicer.

While the dicing saw has great applications for wafers, we can furthermore realize unconventional sample sizes by processing chips on larger substrates and dicing them in the end. With that procedure, we were able to fabricate Josephson parametric amplifiers with a footprint of 5 mm $\times$ 2.5 mm.

New Dilution Refrigerators and Microwave Electronics for Scaling Quantum Processing Units and Exploring Alternative Qubits

F.X. Haslbeck, I. Tsitsilin, F. Wallner, J. Schirk, C. Schweizer, G. Krylov, M. Werninghaus, F. Roy, G. Huber, A. Marx, S. Filipp [1]

A key effort in the rapidly advancing field of quantum computing is scaling the systems from a few to hundreds of quantum bits (qubits). One of the most promising platforms are superconducting qubits which allow fast gate and readout times and are controlled by microwave pulses. Generating, coordinating, and routing microwave pulses to control the quantum computing chip with tens or hundreds of superconducting qubits requires dedicated microwave electronics integrated in multi-channel devices. In addition, more powerful and larger dilution refrigerators are needed which are able to cool hundreds of cables that transfer the signals generated at room temperature to the chip at its millikelvin environment and offer sufficient space for microwave components at various temperature stages. In our efforts to increase the number of qubits on quantum processing units (QPU) we set up a new large dilution refrigerator from Bluefors for QPUs up to 24 qubits and installed multiple microwave control setups. Furthermore, a second dilution refrigerator was installed dedicated to investigate new superconducting qubit designs beyond current standard transmon designs.

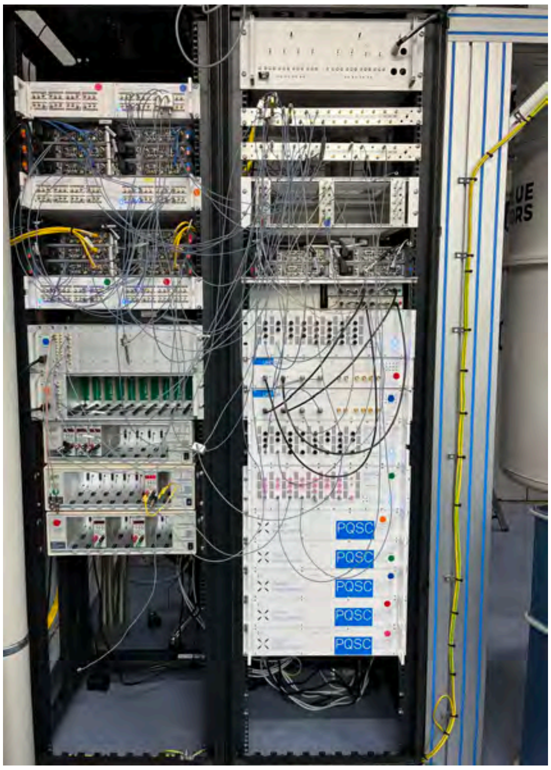

Figure 1: Qubit control electronics. Five experimental setups to control and readout superconducting qubits each controlled by a programmable quantum system controller (PQSC) (bottom right) from Zurich Instruments (ZI). Signals from AWGs and local oscillators are combined (top left) to perform single- and two-qubit gates or generated in integrated systems such as the ZI SHFQC (centre right). The base qubit frequency is adjusted by flux biasing a Josephson junction using current and voltage sources (bottom left). Quantum analyzers measure the frequency shift of readout resonators to measure the qubit state (centre right).

Single qubit gates on superconducting qubits are driven by microwave pulses at the qubit frequency which ranges for typical transmon qubits between about $4 - 6\,\mathrm{GHz}$. To create arbitrary pulse shapes at this frequency, the signal from an arbitrary waveform generator is upconverted by mixing it with a local oscillator signal. As we scale up the number of qubits on a QPU, the number of control channels increases and, in addition, the complexity of coordinating pulse sequences which are optimized for each individual qubit and gate. Therefore, SHFQC signal generators by Zurich Instruments as shown in Fig. 1 were installed which provide output channels to control up to six qubits and operate from DC to $8.5\,\mathrm{GHz}$ eliminating the task of mixer calibration. In addition, the system can perform frequency-multiplexed readout of several readout resonators connected to the same line. Moreover, dedicated SHFQA systems for readout were installed that can each be connected to

[1]This project is part of the Munich Quantum Valley, which is supported by the Bavarian state government with funds from the Hightech Agenda Bayern Plus and has received support by the Munich Quantum Valley Quantum Computer Demonstrators - Superconducting Qubits (MUNIQC-SC; project number: 13N16188) and by the BMBF program No. 13N15680 (GeCQoS).

four readout lines. Pulse sequences for gates and readout among several devices are coordinated by the PQSC systems.

As the microwave electronics operate at room temperature, the control signals are routed by coaxial microwave cables to the millikelvin stage. To control the qubit frequency, perform single- and two-qubit gates, and readout the qubit state on average about three to four microwave lines are required per qubit on typical QPU architectures. With the limited cooling power of dilution refrigerators, the thermal conductivity of cables needs to be optimized and the density of wires in the system increased to enable scaling to hundreds of qubits. We installed a Bluefors XLD 1000sl dilution refrigerator as shown at the top of Fig. 2 with 72 high-density wires to increase the number of control lines. The system is able to be upgraded to 1008 control lines sufficient for QPUs comprising more than 100 qubits.

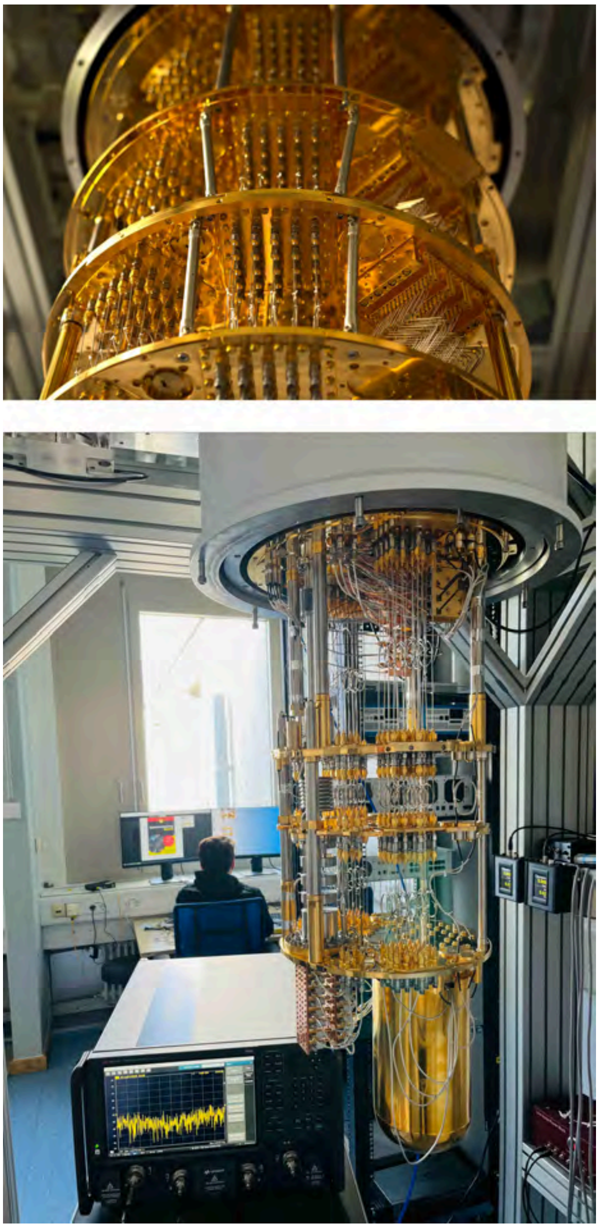

Figure 2: Open dilution refrigerators. Top: Bluefors XLD1000sl dilution refrigerator. The system is equipped with 122 input lines and eight output lines including high-frequency lines (center) which allow to measure up to 40 GHz and high-density wiring (right) which increases the number of cables that can be routed to the sample from room temperature. Bottom: Bluefors LD400 dilution refrigerator. Microwave lines are thermalized from top to bottom on each of the four temperature stages at 4 K, 900 mK, 100 mK and 7 mK (50 K stage not visible). Attenuators are place at each temperature stage to thermalize the inner conductor of the coaxial cables and reduce electronic noise. The QPU is placed inside the gold-plated cryophy shield. High-electron-mobility transistor amplifiers are placed on the 4 K-stage.

One key feature of superconducting circuits with Josephson Junctions is the ability to modify the inductances, capacitances, and critical currents and, hence, change the properties of the qubits, their transition frequencies, anharmonicities and interactions with the environment and other qubits. Over the past decade the transmon design was optimized and is used in many QPU architectures due to e.g. its robustness to charge noise. However, there are many more alternative designs such as the fluxonium qubit that offer higher anharmonicities for faster gate operation or better protection from decoherence. To develop, investigate and optimize the properties of QPUs with alternative qubits, a Bluefors LD400 dilution refrigerator was installed shown at the bottom of Fig. 2. It is equipped with 8 readout lines, 42 input lines and a double-layer cryophy shield to protect the qubits from magnetic stray fields. Attenuators on each temperature stage in the dilution refrigerator are optimized to reduce the Johnson-Nyquist noise propagating from higher temperatures through the microwave cables down to the sample. Isolators protect the QPU from electronic noise from the high-electron-mobility transistor amplifier at the 4 Kelvin-stage that amplify the readout signal with minimal noise.

JEOL JSM-IT800 Schottky Field Emission Scanning Electron Microscope

L. Koch, N. Bruckmoser, D. Bazulin, K. Honasoge, T. Luschmann, Y. Nojiri, C. Schneider, N. Fernandez, A. Marx, S. Filipp[1]

The increasing demand for precise feature size targeting in modern nano-fabrication requires advanced metrology and inspection methods. Therefore, a new JEOL JSM-IT800 Schottky Field Emission Scanning Electron Microscope (Fig. 1) has been set up. A key use case is the geometrical characterisation of Josephson junctions. Frequencies of transmon type quantum bits (qubits) are proportional to the square root of the critical current (I_c) of the Josephson junctions they are comprised of [?]. Therefore, any spread in Josephson junction area transfers into a spread in qubit frequencies, which leads to frequency crowding. This is an unsolved challenge for scaling up superconducting quantum processors and can be characterized using a scanning electron microscope.

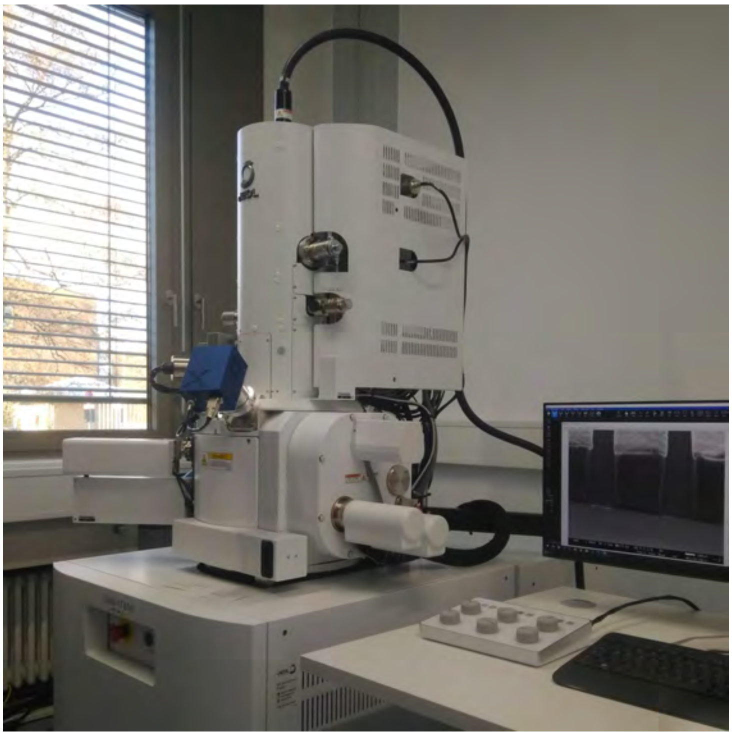

Figure 1: Photograph of the installed Scanning Electron Microscope.

The microscope has a magnification varying from 10 to 2.000.000 and a resolution down to 0.5 nm. The accelerating voltage can be tuned from 10 V to 30 kV and the probe-current from 10 pA to 500 nA. The low voltage and current capabilities allow imaging of sensitive structures like optical and electron beam resist as shown in Fig. 2. Additionally depending on the application one can choose between an Everhart-Thornley detector, in-lens detectors for backscattered and secondary electrons as well as a retractable backscattered electron detector.

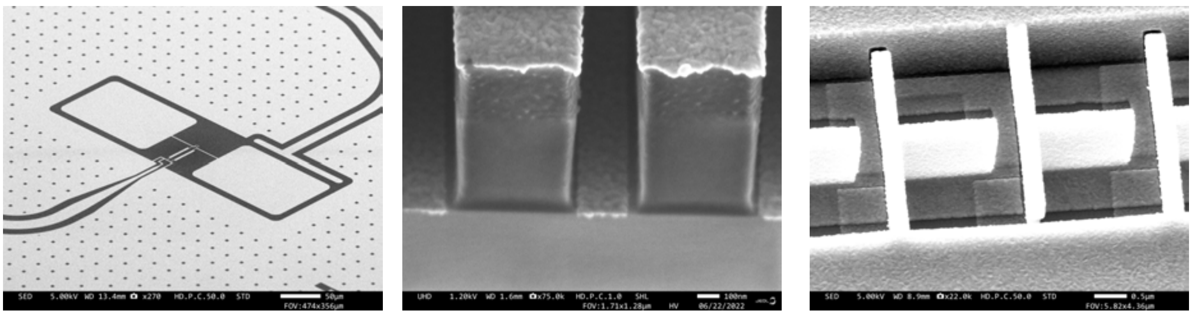

Figure 2: Exemplary SEM images of metal and resist structures. On the left side a fluxonium qubit is depicted. In the center and on the right electron beam resist structures with aluminum on top are shown.

[1]This project has received support by the BMBF program No. 13N15680 (GeCQoS), and by the German Research Foundation under Germany's Excellence Strategy - EXC-2111-390814868.

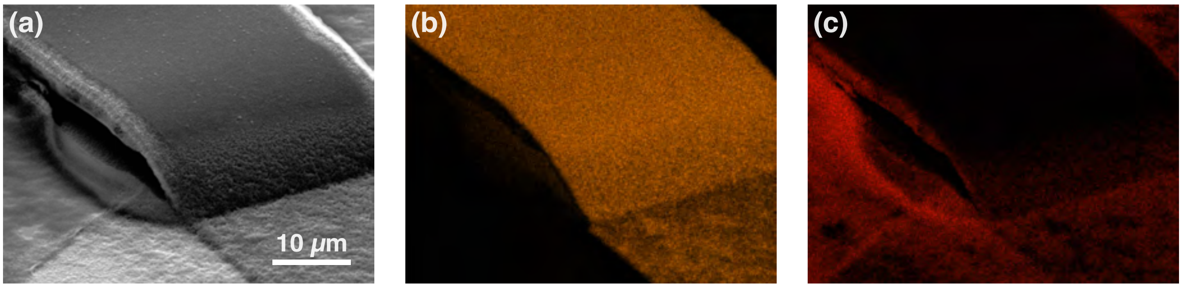

Figure 3: Example pictures of EDS analysis of an aluminum air-bridge. **(a)** SEM picture of the analysed area. **(b)** EDS response of aluminum atoms (coloured in orange). **(c)** EDS response of carbon atoms (coloured in red).

Furthermore the system is equipped with an fully eucentric goniometer sample stage for taking images of tilted samples, a plasma cleaner to remove carbon contamination, as well as energy-dispersive X-ray spectroscopy (EDS) for elemental analysis and chemical characterization of our samples. An example for the EDS response is shown in Fig. 3.

Statistics

Publications

1. **Direct implementation of a perceptron in superconducting circuit quantum hardware**
Marek Pechal, Federico Roy, Samuel A. Wilkinson, Gian Salis, Max Werninghaus, Michael J. Hartmann, Stefan Filipp
Physical Review Research **4**, 033190 (2022).

2. **Effective nonlocal parity-dependent couplings in qubit chains**
Maximilian Nägele, Christian Schweizer, Federico Roy, Stefan Filipp Physical Review Research **4**, 033166 (2022).

3. **Quantum optimal control in quantum technologies. Strategic report on current status, visions and goals for research in Europe**
Christiane P. Koch, Ugo Boscain, Tommaso Calarco, Gunther Dirr, Stefan Filipp, Steffen J. Glaser, Ronnie Kosloff, Simone Montangero, Thomas Schulte-Herbrüggen, Dominique Sugny, Frank K. Wilhelm
EPJ Quantum Technology **9**, 19 (2022).

4. **Single Shot i-Toffoli Gate in Dispersively Coupled Superconducting Qubits**
Aneirin J. Baker, Gerhard B. P. Huber, Niklas J. Glaser, Federico Roy, Ivan Tsitsilin, Stefan Filipp and Michael J. Hartmann
Applied Physics Letters **120**, 054002 (2022).

5. **Tuning and Amplifying the Interactions in Superconducting Quantum Circuits with Subradiant Qubits**
Qi-Ming Chen, Florian Fesquet, Kedar E. Honasoge, Fabian Kronowetter, Yuki Nojiri, Michael Renger, Kirill G. Fedorov, Achim Marx, Frank Deppe, Rudolf Gross
Physical Review A **105**, 012405 (2022).

6. **Mechanical frequency control in inductively coupled electromechanical systems**
Thomas Luschmann, Philip Schmidt, Frank Deppe, Achim Marx, Alvaro Sanchez, Rudolf Gross, Hans Huebl
Scientific Reports **12**, 1608 (2022).

7. **Magnetic field robust high quality factor NbTiN superconducting microwave resonators**
Manuel Müller, Thomas Luschmann, Andreas Faltermeier, Stefan Weichselbaumer, Leon Koch, Gerhard B. P. Huber, Hans Werner Schumacher, Niels Ubbelohde, David Reifert, Thomas Scheller, Frank Deppe, Achim Marx, Stefan Filipp, Matthias Althammer, Rudolf Gross, Hans Huebl
Materials for Quantum Technology **2**, 015002 (2022).

8. **Aluminum nitride integration on silicon nitride photonic circuits: a new hybrid approach towards on-chip nonlinear optics**
Giulio Terrasanta, Timo Sommer, Manuel Müller, Matthias Althammer, Rudolf Gross, Menno Poot
Optics Express **30**, 8537-8549 (2022).

9. **Influence of low-energy magnons on magnon Hanle experiments in easy-plane antiferromagnets**
Janine Gückelhorn, Akashdeep Kamra, Tobias Wimmer, Matthias Opel, Stephan Geprägs, Rudolf Gross, Hans Huebl, Matthias Althammer
Structural Dynamics **9**, 045101 (2022).

10. **Low-Temperature Nanoscale Heat Transport in a Gadolinium Iron Garnet Heterostructure Probed by Ultrafast X-ray Diffraction**
Deepankar Sri Gyan, Danny Mannix, Dina Carbone, James L. Sumpter, Stephan Geprägs, Maxim Dietlein, Rudolf Gross, Andrius Jurgilaitis, Van-Thai Pham, Hélène Coudert-Alteirac, Jörgen Larsson, Daniel Haskel, Jörg Strempfer, Paul G. Evans
Physical Review B **105**, 094440 (2022).

11. **Flow of quantum correlations in noisy two-mode squeezed microwave states**
M. Renger, S. Pogorzalek, F. Fesquet, K. Honasoge, F. Kronowetter, Q. Chen, Y. Nojiri, K. Inomata, Y. Nakamura, A. Marx, F. Deppe, R. Gross, K. G. Fedorov
Physical Review A **106**, 052415 (2022).

12. **Festkörperphysik** (4^{th} revised and extended edition)
R. Gross, A. Marx
Walter de Gruyter GmbH, Berlin/Boston (2022), ISBN: 9783110782349 (hardcover), ISBN 9783110782394 (eBook).

13. **The scattering coefficients of superconducting microwave resonators. I. Transfer-matrix approach**
Qi-Ming Chen, Meike Pfeiffer, Matti Partanen, Florian Fesquet, Kedar E. Honasoge, Fabian Kronowetter, Yuki Nojiri, Michael Renger, Kirill G. Fedorov, Achim Marx, Frank Deppe, Rudolf Gross
Physical Review B **106**, 214505 (2022).

14. **The scattering coefficients of superconducting microwave resonators. II. System-bath approach**
Qi-Ming Chen, Matti Partanen, Florian Fesquet, Kedar E. Honasoge, Fabian Kronowetter, Yuki Nojiri, Michael Renger, Kirill G. Fedorov, Achim Marx, Frank Deppe, Rudolf Gross
Physical Review B **106**, 214506 (2022).

15. **Reduced effective magnetization and damping by slowly-relaxing impurities in strained γ-Fe_2O_3 thin films**
Manuel Müller, Monika Scheufele, Janine Gückelhorn, Luis Flacke, Mathias Weiler, Hans Huebl, Stephan Geprägs, Rudolf Gross, Matthias Althammer
Journal of Applied Physics **132**, 233905 (2022).

16. **Evolution of lattice, spin, and charge properties across the phase diagram of $FeSe_{1-x}S_x$**
N. Lazarević, A. Baum, A. Milosavljević, L. Peis , R. Stumberger, J. Bekaert , A. Šolajić, J. Pešić Aifeng Wang, M. Šćepanović, A. M. Milinda Abeykoon, M. V. Milošević, C. Petrovic, Z. V. Popović, R. Hackl
Physical Review B **106**, 094510 (2022).

17. **Suppression of Superconductivity and Nematic Order in $Fe_{1-y}Se_{1-x}S_x$ ($0 \leq x \leq 1, y \leq 0.1$) Crystals by the Anion Height Disorder**
Aifeng Wang, Ana Milosavljevic, A. M. Milinda Abeykoon, Valentin Ivanovski, Qianheng Du, Andreas Baum, Eli Stavitski, Yu Liu, Nenad Lazarevic, Klaus Attenkofer, Rudi Hackl, Zoran Popovic, and Cedomir Petrovic
Inorganic Chemistry **61**, 11036 (2022).

18. **Carboxymethyl-Dextran-Coated Superparamagnetic Iron Oxide Nanoparticles for Drug Delivery: Influence of the Coating Thickness on the Particle Properties**
Chiara Turrina, Davide Milani, Anna Klassen, Diana M. Rojas-González, Jennifer Cookman, Matthias Opel, Barbara Sartori, Petra Mela, Sonja Berensmeier, Sebastian P. Schwaminger
International Journal of Molecular Sciences **23**, 14743 (2022).

19. **Deviations from the extended London model at high magnetic fields in $YBa_2Cu_3O_7$**
E. Campillo, M. Bartkowiak, R. Riyat, E. Jellyman, A. S. Cameron, A. T. Holmes, O. Prokhnenko, W.-D. Stein, A. Erb, E. M. Forgan, and E. Blackburn
Physical Review B **105**, 184508 (2022).

20. **Advances in Magnetics Roadmap on Spin-Wave Computing: Chapter VIII "Toward Quantum Magnonics", Section C. "Nano-Mechanical Magnetic Resonators for Magnon–Phonon Quantum Hybrid Systems"**
Hans Huebl, Georg Schmidt,Olivier Klein, and Benjamin Pigeau
IEEE Transactions on Magnetics **58**, 0800172 (2022).

21. **In Situ Study of FePt Nanoparticles-Induced Morphology Development during Printing of Magnetic Hybrid Diblock Copolymer Films**
Wei Cao, Shanshan Yin, Martin Bitsch, Suzhe Liang, Martina Plank, Matthias Opel, Manuel A. Scheel, Markus Gallei, Oliver Janka, Matthias Schwartzkopf, Stephan V. Roth, Peter Müller-Buschbaum
Advanced Functional Materials **32**, 2107667 (2022).

22. **Magnetoelastic resonance as a probe for exchange springs at antiferromagnet-ferromagnet interfaces**
K. M. Seemann, O. Gomonay, Y. Mokrousov, A. Hörner, S. Valencia, P. Klamser, F. Kronast, A.

Erb, A. T. Hindmarch, A. Wixforth, C. H. Marrows, P. Fischer
Physical Review B **105**, 144432 (2022).

23. **Optimal broadband frequency conversion via magnetomechanical transducer**
Fabian Engelhardt, Victor A.S.V. Bittencourt, Hans Huebl, Oliver Klein, and Silvia Viola Kusminskiy
Physical Review Applied **18**, 044059 (2022).

24. **Magnetization dynamics affected by phonon pumping**
Richard Schlitz, Luise Siegl, Takuma Sato, Weichao Yu, Gerrit E. W. Bauer, Hans Huebl, and Sebastian T. B. Goennenwein
Physical Review B **106**, 014407 (2022).

25. **Probing spin-dependent dark matter interactions with ^{6}Li**
G. Angloher, G. Benato, A. Bento, E. Bertoldo, A. Bertolini, R. Breier, C. Bucci, L. Canonica, A. D'Addabbo, S. Di Lorenzo, L. Einfalt, A. Erb, F. v. Feilitzsch, N. Ferreiro Iachellini, S. Fichtinger, D. Fuchs, A. Fuss, A. Garai, V. M. Ghete, P. Gorla, S. Gupta, D. Hauff, M. Ješkovský, J. Jochum, M. Kaznacheeva, A. Kinast, H. Kluck, H. Kraus, A. Langenkämper, M. Mancuso, L. Marini, V. Mokina, A. Nilima, M. Olmi, T. Ortmann, C. Pagliarone, V. Palušová, L. Pattavina, F. Petricca, W. Potzel, P. Povinec, F. Pröbst, F. Pucci, F. Reindl , J. Rothe, K. Schäffner, J. Schieck, D. Schmiedmayer, S. Schönert, C. Schwertner, M. Stahlberg, L. Stodolsky, C. Strandhagen, R. Strauss, I. Usherov, F. Wagner, M. Willers, V. Zema
The European Physical Journal C **82**, 207 (2022).

26. **Quantum critical fluctuations in an Fe-based superconductor**
Daniel Jost, Leander Peis, Ge He, Andreas Baum, Stephan Geprägs, Johanna C. Palmstrom, Matthias S. Ikeda, Ian R. Fisher, Thomas Wolf, Samuel Lederer, Rudi Hackl
Communication Physics **5**, 201 (2022).

27. **Revealing the effect of interstitial oxygen on the low-energy crystal electric field excitations of Pr^{3+} in 214-nickelates**
Rajesh Dutta, Avishek Maity, Anna Marsicano, J. Ross Stewart, Matthias Opel, Werner Paulus
Physical Review B **105**, 195147 (2022).

28. **Spin-wave frequency combs**
Tobias Hula, Katrin Schultheiss, Francisco José Trindade Goncalves, Lukas Körber, Mauricio Bejarano, Matthew Copus, Luis Flacke, Lukas Liensberger, Aleksandr Buzdakov, Attila Kákay, Mathias Weiler, Robert Camley, Jürgen Fassbender, Helmut Schultheiß
Applied Physics Letters **121**, 112404 (2022).

29. **Quantencomputer – Präzise Kontrolle über die Welt der Quanten.**
S. Filipp
in Chancen und Risiken von Quantentechnologien (Eds. A. Wilms & F. Neukart), Springer-Verlag, ISSN 978-3-658-37533-1 (2022).

30. **Hybrid magnetization dynamics in Cu_2OSeO_3/NiFe heterostructures**
Carolina Lüthi, Luis Flacke, Aisha Aqeel, Akashdeep Kamra, Rudolf Gross, Christian Back, Mathias Weiler
Appl. Phys. Lett. **122**, 012401 (2023).

31. **Geometric and holonomic quantum computation**
J. Zhang, T. H. Kyaw, S. Filipp, L.-C. Kwek, E. Sjöqvist, D. Tong.
arXiv:2110.03602, submitted for publication (2021)

32. **Perspectives of microwave quantum key distribution in open-air**
Florian Fesquet, Fabian Kronowetter, Michael Renger, Qiming Chen, Kedar Honasoge, Oscar Gargiulo, Yuki Nojiri, Achim Marx, Frank Deppe, Rudolf Gross, Kirill G. Fedorov
arXiv:2203.05530, submitted for publication (2022).

33. **Quantum behavior of a superconducting Duffing oscillator at the dissipative phase transition**
Qi-Ming Chen, Michael Fischer, Yuki Nojiri, Michael Renger, Edwar Xie, Matti Partanen, Stefan Pogorzalek, Kirill G. Fedorov, Achim Marx, Frank Deppe, Rudolf Gross
arXiv:2206.06338, submitted for publication (2022).

34. **Coherent heavy charge carriers in an organic conductor near the bandwidth-controlled Mott**

transition
Sebastian Oberbauer, Shamil Erkenov, Werner Biberacher, Natalia D. Kushch, Rudolf Gross, Mark V. Kartsovnik
arXiv:2208.03230, submitted for publication (2022).

35. **Observation of nonreciprocal magnon Hanle effect**
Janine Gückelhorn, Sebastián de-la-Peña, Matthias Grammer, Monika Scheufele, Matthias Opel, Stephan Geprägs, Juan Carlos Cuevas, Rudolf Gross, Hans Huebl, Akashdeep Kamra, Matthias Althammer
arXiv:2209.09040, submitted for publication (2022).

36. **Dia- and Adiabatic Dynamics in a Phononic Network**
Daniel Schwienbacher, Thomas Luschmann, Rudolf Gross, Hans Huebl
arXiv:2011.08080, submitted for publication (2020).

37. **Controlled-controlled-phase gates for superconducting qubits mediated by a shared tunable coupler**
Niklas J. Glaser, Federico Roy, Stefan Filipp
arXiv:2206.12392, submitted for publication (2022).

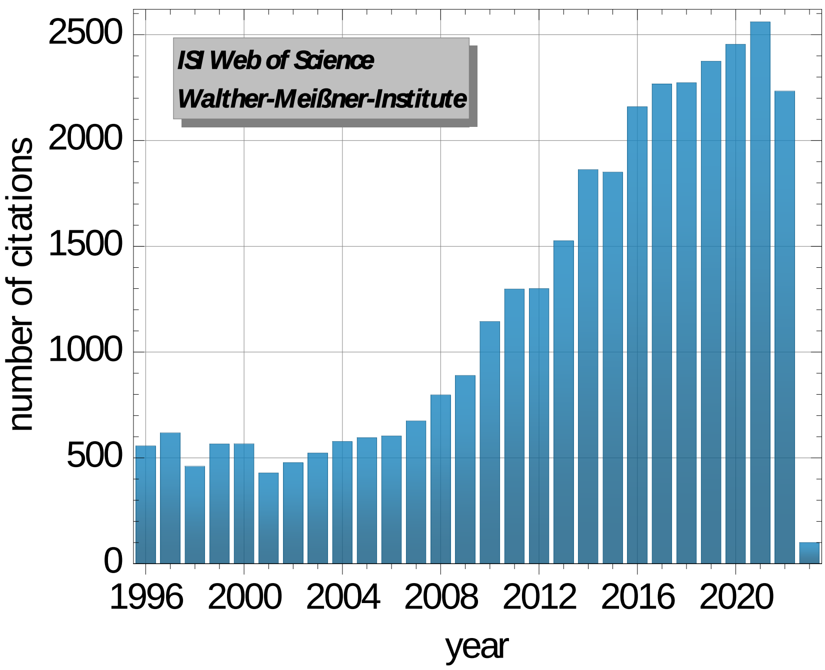

The total number of citations per year of papers published by members of WMI since 1996. This number has about quadrupled within the last twenty years and presently approaches 2 500.

Books

Festkörperphysik (4. überarbeitete und erweiterte Auflage)

The textbook on *«Festkörperphysik»* by Rudolf Gross and Achim Marx has been revised and enhanced over many years and meanwhile represents a standard textbook for students. The textbook as well as the related book with exercises and solutions are well received by university teachers and highly esteemed by the students. The authors present the full breadth of modern solid-state physics in an understandable and structured fashion, while at the same time conveying deeper insights into the historical development of the discipline.

The first, second and third edition of the textbook appeared in 2012, 2014 and 2018. Since the third edition was going to be sold out early in 2022, a fourth revised and expanded edition has been prepared during 2022 and has become available in November 2022 from De Gruyter Oldenbourg (ISBN: 9783110782349). It is also available as an ebook (ISBN: 9783110782394).

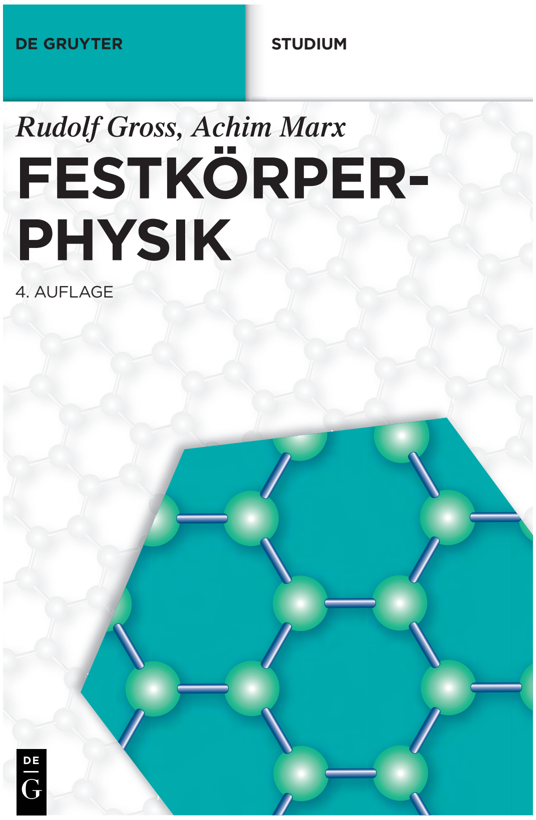

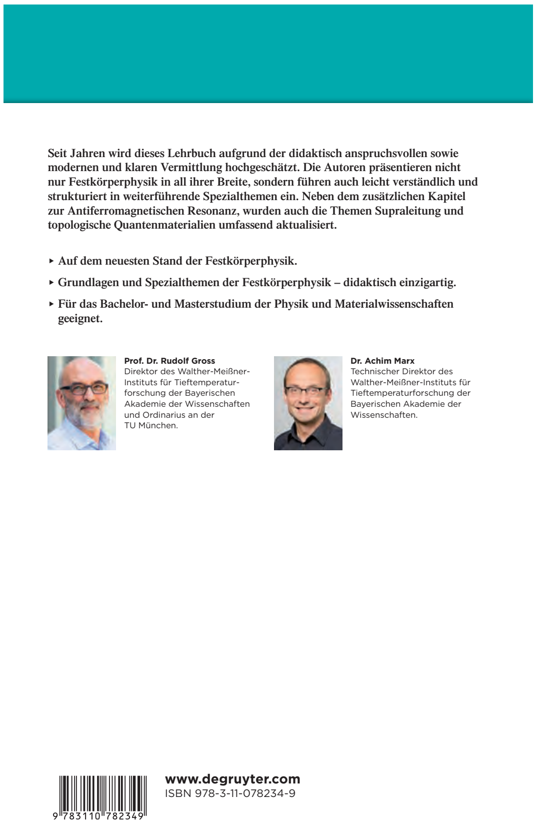

Since quantum matter and the concept of topology became important topics in solid-state physics over the past years, the chapter 14 on topological quantum matter has been extended again in the fourth edition of the textbook. Furthermore, all the other chapters have been updated and slightly revised to further improve readability of the book.

The supplementary book entitled *«Festkörperphysik. Aufgaben und Lösungen»* by Rudolf Gross, Achim Marx, Dietrich Einzel and Stephan Geprägs also has been revised and updated. The third edition of this book will appear in 2023. It contains more than 100 problems related to the solid-state physics textbook *«Festköperphysik»* together with detailed model solutions. In particular, the third edition contains seven new exercises to the topic quantum materials that has not been covered yet in the previous editions. The exercises & solutions book is ideal for preparing for exams and for learning on one's own.

Bachelor, Master, Doctoral, and Habilitation Theses

A. Completed and Ongoing Habilitation Theses

At present, two postdoctoral researchers – Kirill Fedorov and Nadezhda Kukharchyk – pass through the habilitation procedure of the Technical University of Munich. The habilitation serves as the formal assessment tool ascertaining whether or not a candidate is suitable, from an academic and a pedagogical point of view, to be a professor in a particular field at the university level. The WMI strongly supports habilitation candidates, as the fostering of young scholars is one of its key concerns.

Dr. Kirill Fedorov

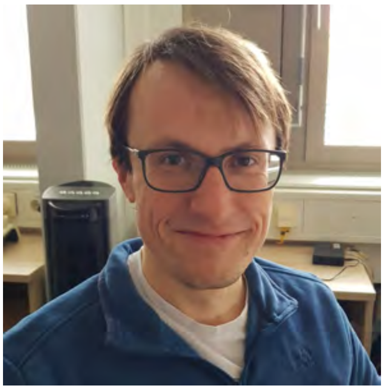

In 2022, Kirill Fedorov has submitted his habilitation thesis entitled ***Microwave Quantum Communication with Superconducting Circuits*** early in 2022. After the very positive reports of five international experts have been received, the *Fachmentorat* consisting of Rudolf Gross (WMI/BAdW and TUM), Jonathan Finley (TU Munich/Walter Schottky Institute) and Enrique Solano (Universidad del País Vasco and Ikerbasque Foundation, Bilbao, Spain) recommended his appointment as a docent in experimental physics in October 2022. Only the final decision of the TUM School of Natural Sciences and the TUM Board of Management is still missing and expected early in 2023.

Kirill Fedorov studied physics in Russia (Institute for Physics of Microstructures, Russian Academy of Sciences, Nizhny Novgorod), where he received his master degree in 2008. He then joined the group of Prof. Alexey Ustinov at the Karlsruhe Institute of Technology as a Ph.D. student. He finished his Ph.D. thesis entitled *Fluxon readout for superconducting flux qubits* in 2013 and then joined the group of Rudolf Gross at the Walther-Meißner-Institute as a postdoctoral researcher in December 2013. He was accepted as a *"Habilitand"* by the Physics Department of TUM in 2016.

The key research topic of Kirill Fedorov is the realization of seminal quantum experiments based on propagating quantum microwaves. With the realization of quantum teleportation using propagating quantum microwaves he recently added a further important milestone experiment (see K.G. Fedorov *et al.*, Science Advances **7**, eabk0891 (2021)). He is principal investigator in several projects of the European Union (e.g. EU Flagship project QMiCS, grant No. 820505), the Federal Ministry of Education and Research (e.g. QUARATE, grant No. 13 N 15380, and QuaMToMe, grant No. 16 KISQ 036), and the Munich Quantum Valley (e.g. Lighthouse Projects IQSense and NeQuS).

Dr. Nadezhda Kukharchyk

Nadezhda Kukharchyk received one of the prestigious ***START Fellowships*** of the Excellence Clusters MCQST in 2020. Supported by this fellowship, she joined the group of Rudolf Gross at WMI in November 2020 and built up a new research group at WMI focusing on the spectroscopy and application of spin-based quantum systems. On 25$^{\mathrm{th}}$ November 2021, she presented her research field and recent achievements to the teaching body of the Faculty of Physics within the Solid-State Colloquium. After this informal step, she submitted the required documents to the dean's office and was formally accepted as a habilitation candidate by the Faculty of Physics of TUM early in 2022. Her *Fachmentorat* consists of Rudolf Gross (WMI/BAdW and TUM, chairman), Jonathan Finley (TU Munich/Walter Schottky Institute, member) and Klaus Mølmer (Niels Bohr Institute, University of Copenhagen, Denmark, member).

Nadezhda Kukharchyk studied physics at the Belarussian State University in Minsk, Belarus, and then joined the University of Bochum (group of Prof. Andreas Wieck) as a Ph.D. student in 2011. She finished her thesis entitled *Focused Ion-Beam Implantation of Rare-Earth Ions for Realisation of Spin-Ensemble Systems* in 2015. She then joined the Saarland University, where she was setting up a newly established experimental laboratory for optical and microwave spectroscopy of rare-earth doped single crystals at mK-temperatures before accepting the MCQST offer and joining the group of Rudolf Gross at WMI. The WMI is very happy to be able to support the scientific career of an ambitious female researcher. Meanwhile, Nadezhda Kukharchyk already acquired a new BMBF-project on the ***Storage of Microwave Quantum Tokens in Electron and Nuclear Spin Ensembles (QuaMToMe, grant No. 16 KISQ 036)***. She is the coordinator of this new project, which started in November 2021.

B. Completed and Ongoing Ph.D. Theses

Completed Ph.D. Theses:

1. **Propagating Quantum Microwave Photonics: Transmon Qubit in a Broadband On-Chip Environment**
   Peter Eder, Technical University of Munich, Januar 2022.
2. **In-situ Tunable Nonlinearity and Competing Signal Paths in Coupled Superconducting Resonators**
   Michael Christian Fischer, Technical University of Munich, Januar 2022.
3. **Spin Wave Transport and Skyrmion Formation in CoFe-Based Thin Film Heterostructures**
   Luis Antonio Flacke, Technical University of Munich, Juli 2022.
4. **Quantum Statistical Properties of a Superconducting Duffing Oscillator**
   Qiming Chen, Technical University of Munich, November 2022.
5. **Experimental Optimal Control of Superconducting Qubits**
   Max Werninghaus, Technical University of Munich, November 2022.
6. **Industrielle Herstellungsverfahren für Hochtemperatur-Supraleiter basierte Bandleiter der 2. Generation**
   Alexei Troshyn, Technical University of Munich, December 2022.

The Ph.D. students of the Walther-Meißner-Institute finishing their Ph.D. theses in 2022.

Ongoing Ph.D. Theses:

1. **Quantum Microwave Communication**
   Michael Renger, Technical University of Munich, since November 2018.
2. **Pure Spin Currents in Epitaxial All Oxide Heterostructures**
   Janine Gückelhorn, Technical University of Munich, since March 2019.
3. **Hybride Solid State Quantum Systems**
   Thomas Luschmann, Technical University of Munich, since September 2019.
4. **Coherent Adiabatic Quantum Annealer Based on Superconducting Quantum Circuits**
   Yuki Nojiri, Technical University of Munich, since September 2019.
5. **Spin Phenomena in Superconductor/Ferromagnet Heterostructures**
   Manuel Müller, Technical University of Munich, starting from March 2020.
6. **Fabrication and Investigation of Superconducting Quantum Processors with Novel Architectures**
   Leon Koch, Technical University of Munich, since July 2020.
7. **Tailoring the Control of Superconducting Qubits to Efficiently Solve Molecular Chemistry Problems**
   Malay Singh, Technical University of Munich, since October 2020.
8. **Multi-Qubit Gates for the Efficient Exploration of Hilbert Space with Superconducting Circuits**
   Ivan Tsitsilin, Technical University of Munich, since October 2020.
9. **Microwave Photo Detection for a Quantum Radar Receiver**
   Kedar Honasoge, Technical University of Munich, since February 2021.
10. **Receiver for Quantum Microwave Radar**
    Fabian Kronowetter, Technical University of Munich, since February 2021.
11. **Remote Entanglement of Superconducting Qubits with Two-Mode Squeezing**
    Florian Fesquet, Technical University of Munich, since February 2021.
12. **Implementation of Optical Approaches in Microwave Quantum Memory Systems**
    Ana Strinic, Technical University of Munich, since April 2021.
13. **Development of Quantum Devices for Travelling Wave Parametric Amplifiers**
    Nicolas Arlt, Technical University of Munich, since July 2021.
14. **Josephson Travelling Wave Parametric Amplifier for Multi-qubit Readout**
    Daniil Bazulin, Technical University of Munich, since August 2021.
15. **Hardware-tailored Quantumalgorithms with Superconducting Qubits**
    Frederik Pfeiffer, Technical University of Munich, since November 2021.
16. **Scalable Multi-Qubit Architectures Based on Superconducting Qubits**
    Niklas Glaser, Technical University of Munich, since December 2021.
17. **Design and Application of Multi-Qubit Couplers**
    Gerhard Huber, Technical University of Munich, since December 2021.
18. **Scaling of Superconducting Qubit Systems for Quantum Information Processing**
    Florian Wallner, Technical University of Munich, since January 2022.
19. **Experimental Realization of Quantum Memory Based on Phosphorous Donors in Silicon Including Storage and Retrieval of Q-Tokens**
    Patrizia Oehrl, Technical University of Munich, since February 2022.
20. **Fabrication and Characterization of Superconducting Single Photon Detectors**

Maria-Teresa Handschuh, Technical University of Munich, since April 2022.

21. **Fabrication and Characterization of Thin Films and Heterostructures of Quantum Materials**
Monika Scheufele, Technical University of Munich, since April 2022.
22. **Investigating the Origin of Decoherence in Superconducting Quantum Circuits**
Niklas Bruckmoser, Technical University of Munich, since April 2022.
23. **Integration and Scaling of Quantum Processors**
Lea Richard Romeiro, Technical University of Munich, since June 2022.
24. **Benchmarking and Calibration of Superconducting Qubit Quantum Processors**
Joao Romeiro, Technical University of Munich, since July 2022.
25. **Quantum Information Processing based on Alternative Superconducting Qubits.**
Johannes Schirk, Technical University of Munich, since July 2022.
26. **Realization of a Multimode Quantum Memory Based on Rare-Earth Spin Ensembles**
Jianpeng Chen, Technical University of Munich, since August 2022.
27. **Microwave Quantum Communication over Thermal Channels**
Wun Kwan Yam, Technical University of Munich, since October 2022.
28. **Quantum Gravity – Levitated Superconductors and their Position Measurement**
Korbinian Rubenbauer, Technical University of Munich, since October 2022.
29. **Entanglement of Remote Superconducting Qubits via a Microwave Quantum Link**
Simon Gandorfer, Technical University of Munich, since January 2023.

C. Completed and Ongoing Bachelor and Master Theses

Completed Master Theses:

1. **Optimization of Aluminum Thin Films and Fabrication of Superconducting Qubit Systems**
   Leonhard Hölscher, Master Thesis, Technical University of Munich, since November 2020.
2. **Single-Shot Microwave Quantum Key Distribution**
   Philipp Krüger, Master Thesis, Technical University of Munich, April 2022.
3. **Controlling the environment of superconducting qubits**
   Johannes Schirk, Master Thesis, Technical University of Munich, March 2022.
4. **Controlling Magnon Transport in the Antiferromagnetic Insulator Hematite**
   Matthias Grammer, Technical University of Munich, July 2022.
5. **Pulse Optimization for Qutritts and a Function Approximator using Quantum Machine Learning**
   Shawn Storm, Master Thesis, Technical University of Munich, since August 2021.
6. **Microwave Quantum Teleportation Over a Thermal Channel**
   Wun Kwan Yam, Technical University of Munich, October 2022.
7. **Development of Surface Acoustic Wave Resonators Based on Thin-Film Lithium Niobate for Circuit Quantum Acoustics Platforms**
   Alexander Jung, Technical University of Munich, November 2022.
8. **Distribution of Quantum States in a Microwave Local Area Network**
   Simon Gandorfer, Technical University of Munich, December 2022.
9. **Frequency Control and Sensing of Mechanical Properties in Nanostring-Based Electromechanics**
   Lukas Niekamp, Technical University of Munich, December 2022.
10. **Improving Multiplexed Readout of Superconducting Qubits**
    Michal Chercynski, Master Thesis, Technical University of Munich, December 2022.
11. **Minimizing Losses in Superconducting Coplanar Waveguide Resonators**
    David Cole Bunch, Master Thesis, Technical University of Munich, December 2022.
12. **Wafer-scale Josephson Junction Fabrication for Superconducting Qubits**
    Tammo Sievers, Master Thesis, Technical University of Munich, December 2022.

Completed Bachelor Theses:

1. **Simulation of Lossy Through-Silicon Vias in a Coplanar Waveguide Resonator**
   Niklas Zischke, Technical University of Munich (2022).
2. **A Signals and Systems Approach to Characterizing the Superconducting Qubit and Tunable Coupler Platform**
   Aaron Anhalt, Technical University of Munich (2022).
3. **Investigating Interfaces for Quantum Circuits by Goniometer Measurements**
   Ruben Wernsdorfer, Technical University of Munich (2021).

Ongoing Master Theses:

1. **3D integration of Superconducting Qubits**
   Franziska Wilfinger, Technical University of Munich, since December 2021.
2. **Advanced Calibration of Superconducting Qubits**
   Catharina Broocks, Technical University of Munich, since December 2021.
3. **Elektrischer Spin-Transport in Supraleiter/Ferromagnetischer Isolator Heterostrukturen / All-electrical spin transport in Superconductor/Ferromagnetic insulator heterstructures**
   Yuhao Sun, Technical University of Munich, since December 2021.
4. **Fabrication of a Superconducting Transmission Line in a Planar Design on a Spin-Doped Crystalline Membrane**
   Georg Mair, Technical University of Munich, since March 2022.
5. **Generating Small Magnetic Fields Inside an open-End Magnetic Shielding with a Superconducting Solenoid Magnet**
   Lukas Vogl, Technical University of Munich, since April 2022.
6. **Non-reciprocal Devices**
   Christian Mang, Technical University of Munich, since April 2022.
7. **Microwave Manipulation of Magnon Transport**
   Franz Weidenhiller, Technical University of Munich, since May 2022.
8. **Growth Optimization of Ferromagnetic Gadolinium Nitride (GdN) Thin Films for Spintronics with Magnetic Isolators**
   Raphael Höpfl, Technical University of Munich, since June 2022.
9. **Superconducting Microwave Resonators for Spin Based Quantum Memories**
   Julian Franz, Technical University of Munich, since May 2022.
10. **Nano-scale NMR of PT Thin Films Using Quantum Sensors in Diamond**
    Joachim Leibold, Technical University of Munich, since June 2022.
11. **Thermal History Dependent Electronic Properties of κ-(BEDT-TTF)$_2$-X Near the Mott-Metal-Insulator Transition**
    Florian Kollmannsberger, Technical University of Munich, since August 2022.
12. **Observation of Quantum Switching in Driven-Dissipative Superconducting Oscillators**
    Sebastiano Davide Covone, Technical University of Munich, since October 2022.
13. **Fabrication of Low-Loss Josephson Parametric Devices**
    Nicolò Salerno, Technical University of Munich, since October 2022.
14. **Magnetoelastic Coupling in CoFe-Heterostructures**
    Johannes Weber, Technical University of Munich, since November 2022.
15. **Magnon Transport in Antiferromagnetic Insulators**
    Maria Sigl, Technical University of Munich, since November 2022.
16. **Study of Energy Exchange between Spatially Separated Rare-Earth Electronic Spin Ensembles at Cryogenic Temperatures**
    Owen Thomas Huisman, Technical University of Munich, since October 2022.
17. **Microwave Cryptography with Propagating Quantum Tokens**
    Valentin Weidemann, Technical University of Munich, since November 2022.
18. **Unconventional Superconducting Materials**

Herman Muzychko, Technical University of Munich, since November 2022.

Research Projects

A large number of our research projects are benefiting from the collaboration with other research institutions and industry in coordinated research projects, as well as from individual collaborations, exchange programs and visitors. Most collaborations are based on joint projects, which are funded by different funding agencies (see list below). A considerable number of collaborations also exists with universities, other research institutions and industry without direct financial support.

A. German Research Foundation: Excellence Initiative & Strategy

Cluster of Excellence *«Munich Center for Quantum Science and Technology» (MCQST)*

The new Cluster of Excellence has been granted in September 2018 within Germany's Excellence Strategy and started in January 2019. Together with Immanuel Bloch of LMU Munich and Ignacio Cirac of Max Planck Institute of Quantum Optics, Rudolf Gross of Walther-Meißner-Institute is one of the three spokespersons of MCQST and coordinator of the Research Unit C on Quantum Computing.

1. Research Unit C: *Quantum Computing*
   Principal Investigators: F. Deppe, S. Filipp, R. Gross
   Contributing Researchers: K. Fedorov, A. Marx
2. Research Unit D: *Quantum Communication*
   Principal Investigators: F. Deppe, S. Filipp, R. Gross
   Contributing Researchers: K. Fedorov, A. Marx, N. Kukharchyk
3. Research Unit E: *Quantum Sensing*
   Principal Investigators: F. Deppe, H. Hübl, R. Gross
   Contributing Researchers: K. Fedorov, A. Marx, N. Kukharchyk
4. Research Unit F: *Quantum Matter*
   Principal Investigators: H. Hübl, R. Gross
   Contributing Researchers: M. Althammer, S. Geprägs, M. Opel

B. German Research Foundation: Collaborative Research Centers

Transregional Collaborative Research Center TRR 80: *«From Electronic Correlations to Functionality»*

1. Project A2: *Spatially and Momentum Resolved Raman Studies of Correlated Systems*
   Principal Investigator: R. Hackl

D. German Research Foundation: Research Projects

1. Project: *Shortcuts to Adiabaticity for Quantum Computation and Simulation (STAQS)*, within the QuantERA II ERA-NET Cofund in Quantum Technologies.
   A. Marx, with F. Deppe, K. Fedorov, R. Gross, (Az. DE 3444/1-1)
2. Project: *Evolution of the Charge Carrier Properties and Electronic Correlations in Layered Organic Metals near the Mott Metal-Insulator Transition*, joint German-Russian project proposal within the RFBR-DFG Cooperation.
   M. Kartsovnik, R. Gross (Az. KA 1652/5-1 and GR 1132/19-1)

3. Project: *Multi-qubit Gates for the Efficient Exploration of Hilbert Space with Superconducting Qubit Systems*
   S. Filipp (Az. FI 2549/1-1)
4. Project: *Pure Spin Currents in Oxide-Based Epitaxial Heterostructures*
   M. Althammer, R. Gross (Az. AL 2110/12-1)

E. European Union

1. EU Collaborative Project (call identifier HORIZON-CL4-2021-Digital-Emerging-02), project title: *Exploring Non-classical States of Center-of-Mass Mechanical Motion with Superconducting Magneto- and Levitomechanics – SuperMeQ*
   H. Hübl, A. Marx, Grant Agreement No. 101080143
   project coordination: Chalmers University of Technology, partners: WMI/BAdW, OeAW, KIT, UAB.
2. EU Flagship Specific Grant Agreement (SGA) Project (call identifier HORIZON-CL4-2022-QUANTUM-01-SGA), project title: *Open Superconducting Quantum Computers - OpenSuperQPlus100*
   S. Filipp, H. Hübl, Grant Agreement No. 101113946.
   partners: several European Universities and research facilities.
   project period: (planned) 03/2023 – 09/2026
3. EU Flagship Framework Partnership Agreement (FPA) Project (call identifier HORIZON-CL4-2021-DIGITAL-EMERGING-02-15), project title: *Open Superconducting Quantum Computers - OpenSuperQPlus*
   S. Filipp, H. Hübl, Grant Agreement No. 101080139.
   partners: several European Universities and research facilities.
   project period: 03/2023 – 02/2027
4. EU Collaborative Project (call identifier H2020-FETOPEN-FET H2020-FETOPEN-2018-2020), project title: *Neuromorphic Quantum Computing - Quromorphic*
   S. Filipp, Grant Agreement No. 828826
   partners: several European Universities and research facilities.
   project period: 06/2019 – 02/2023
5. EU Innovative Training Network (call identifier H2020-MSCA-ITN-2020), project title: *MOlecular Quantum Simulations - MOQS*
   S. Filipp, Grant Agreement No. 955479
   partners: several European Universities and research facilities.
   project period: 11/2020 – 10/2024
6. EU MSCA Cofund Action (call identifier H2020-MSCA-COFUND-2018), project title: *Quantum Science and Technologies at the European Campus (QUSTEC)*
   S. Filipp, Grant Agreement 847471
   partners: several European Universities and research facilities.
   project period: 03/2019 – 07/2025
7. EU Collaborative Project (call identifier H2020-FETFLAG-2018-2020), project title: *Quantum Microwave Communication and Sensing – QMiCS*
   F. Deppe, K. Fedorov, A. Marx, R. Gross, Grant Agreement No. 820505
   project coordination: Walther-Meißner-Institute, partners: several European Universities, research facilities and companies.
   project period: 10/2018 – 04/2022

F. Bundesminister für Bildung, Wissenschaft, Forschung und Technologie

1. Project: *Skalierbare Einzelphotonendetektoren für Quantentechnologien (SEQT)*, project number: 13N16188
project part: *Aufstockungsantrag*
project coordinator: K. Müller (TUM)
principal investigators of WMI/TUM: S. Filipp
project partners: TUM
project period: 09/2022 – 08/2023
2. Coordinated Project: *Munich Quantum Valley Quantum Computer Demonstrators - Superconducting Qubits (MUNIQC-SC)*, project number: 13N16188
project part: *Systemoptimierung und -integration*
project coordinator: S. Filipp (TUM/WMI)
project partners: TUM, Fraunhofer-Gesellschaft, FAU Erlangen-Nürnberg, Infineon Technologies AG, IHP GmbH - Innovations for High Performance Microelectronics/Leibniz-Institut für innovative Mikroelektronik, IQM Germany GmbH, kiutra GmbH, Parity Quantum Computing Germany GmbH, Forschungszentrum Jülich GmbH, Zurich Instruments Germany GmbH.
project period: 01/2022 – 12/2026
3. Coordinated Project: *Storage of Microwave Quantum Tokens in Electron and Nuclear Spin Ensembles (QuaMToMe)*, project number: 16KISQ036
project coordinator: N. Kukharchyk (WMI)
principal investigators of WMI: K. Fedorov, R. Gross, H. Huebl, N. Kukharchyk.
project period: 11/2021 – 10/2024
4. Coordinated Project: *QUAntenRAdarTEam (QUARATE)*, project number: 13N15380,
project part: *Superconducting Circuits and Quantum Microwaves for Quantum Radar*,
project coordinator: Rohde & Schwarz GmbH & Co. KG,
principal investigators of WMI: F. Deppe, K. Fedorov, S. Filipp, R. Gross, A. Marx),
project partners: German Aerospace Center (DLR), Technical University of Munich
project period: 02/2021 – 01/2024
5. Coordinated Project: *German Quantum Computer based on Superconducting Qubits (GeQCoS)*, project number: 13N15680
project part: *Scaling and Demonstrator*,
project coordinator: S. Filipp (WMI)
principal investigators of WMI: F. Deppe, K. Fedorov, R. Gross, A. Marx
project partners: Forschungszentrum Jülich GmbH, Karlsruher Institut für Technologie, Friedrich-Alexander-Universität Erlangen-Nürnberg, Fraunhofer Gesellschaft zur Forderung der angewandten Forschung e.V, Infineon Technologies AG.
project period: 02/2021 – 01/2025

G. Free State of Bavaria

1. Munich Quantum Valley e.V. (MQV)
program: Grundlagenorientierte Leuchtturmprojekte für Forschung, Entwicklung und Anwendungen im Bereich der Quantenwissenschaften und Quantentechnologien
project part: Networked Quantum Systems (NeQuS)
Principal Investigators at WMI: R. Gross, S. Filipp, K. Fedorov, A. Marx
Jointly with research groups at the Technical University of Munich, the LMU Munich, and the Max Planck Institute of Quantum Optics.
project period: 01/2023–12/2025

2. Grundlagenorientierte Leuchtturmprojekte für Forschung, Entwicklung und Anwendungen im Bereich der Quantenwissenschaften und Quantentechnologien
project part: Integrated Spin Systems for Quantum Sensors (IQSense)
Principal Investigators at WMI: R. Gross, H. Hübl
Jointly with research groups at the University of Würzburg and the Technical University of Munich.
project period: 01/2023–12/2025
3. Munich Quantum Valley e.V. (MQV)
project part: Quantum Technology Park and Entrepreneurship (QTPE)
Principal Investigators at WMI: R. Gross (coordination), S. Filipp, K. Fedorov, A. Marx, H. Hübl, Ch. Trummer
Jointly with research groups at the Technical University of Munich, the LMU Munich, the FAU Erlangen, the Max Planck Institute of Quantum Optics, and the Fraunhofer-Gesellschaft zur Förderung der angewandten Forschung e.V.
project period: 10/2021–09/2026
4. Munich Quantum Valley e.V. (MQV)
project part: Superconducting Qubit Quantum Computing (SQQC)
Principal Investigators at WMI: S. Filipp (coordination), K. Fedorov, R. Gross, A. Marx, H. Hübl
Jointly with research groups at the Technical University of Munich, the LMU Munich, the FAU Erlangen, the Max Planck Institute of Quantum Optics, and the Fraunhofer-Gesellschaft zur Förderung der angewandten Forschung e.V.
project period: 10/2021–09/2026
5. International PhD Programme of Excellence *Exploring Quantum Matter (ExQM)* within the Elite Network of Bavaria, Project No. K-NW-2013-231,
R. Gross, A. Marx, F. Deppe, K. Fedorov,
jointly with 12 quantum physics research groups at the TU Munich, the LMU Munich, and the Max Planck Institute of Quantum Optics.
project period: 06/2014–05/2022

H. Max Planck Society

1. International Max Plank Research School for *Quantum Science and Technology (IMPRS-QST)*, spokesperson: Prof. Dr. J. Ignacio Cirac,
R. Gross, A. Marx, F. Deppe, K. Fedorov,
with several partners from the Max Planck Institute of Quantum Optics, the Ludwig-Maximilians-Universität Munich and the Technical University of Munich.
project period: 03/2016– 02/2028

I. German Academic Exchange Service

1. Project-based Personnel Exchange Programme with India (DAAD-DST), project 57452943: *Spin Current Transport Across Antiferromagnetic/Metallic Oxide Interfaces*, collaboration with the IIT Madras, Chennai (Prof. Dr. M. S. Ramachandra Rao),
R. Gross, M. Opel

J. Alexander von Humboldt Foundation

1. Humboldt Research Fellowship "Di Candia"
R. Gross (project No. 1162824 - ESP - HFST-P)

K. Scientific Instrumentation

1. UHV PLD-MBE System, DCA Instruments,
(R. Gross, DFG, Excellence Strategy, EXC-2111-390814868)
2. Tieftemperatur-Mikrowellenmessapparatur für schnellen Probenaustausch
(S. Filipp, DFG-GZ: INST 95/1636-1 FUGG)
3. Heliumverflüssigungsanlage, Vorbuchner VL 100
(R. Gross, DFG-GZ: INST 95/1637-1 LAGG)
4. Cryogen-Free Dilution Refrigerator System with Microwave Measurement Systems, Bluefors Model BF-XLD 400,
(S. Filipp, DFG-GZ: INST 95/1623-1 FUGG)

Conferences, Workshops, Public Engagement

Every year the Walther-Meißner-Institute organizes/co-organizes conferences, workshops, symposia, seminars and other events. It also participates in several public outreach events aiming at making science accessible to the public.

In previous years we were reporting in more depth on events, outreach activities, press releases, highlight publications and other events in our Annual Report. However, meanwhile these topics are well covered by our new web pages and social media accounts. Therefore, we are no longer covering these topics here in depth and refer the interested reader to the news section of our web pages: https://www.wmi.badw.de/news.

In the following we list relevant outreach activities and public engagement of WMI in the year 2022:

27.01.2022: Munich Quantum Valley e.V. is established. Only one year after the declaration of intent by the Bavarian State Government, the ***Munich Quantum Valley e.V.*** was formally established as a registered society with the ceremonial signing of the foundation charter on the premises of the Bavarian Academy of Sciences and Humanities in the Munich Residence. Complementing the funding from the High-Tech Agenda Bavaria amounting to 300 Mio. €, the members of the initiative have already raised federal funding of more than 80 Mio. €.

25.03.2022: The Bavarian Minister of State Markus Blume visits BAdW. The Bavarian Minister of State Markus Blume visited BAdW to get information on current research projects related to digitalization and quantum science. In addition to projects in earth sciences, glacier research, and art history (presented by Hans-Peter Bunge, Christoph Mayer, and Matteo Burioni) Rudolf Gross of WMI and Dieter Kranzlmüller of LRZ were reporting on the activities in the field of quantum science and technology. Rudolf Gross was particularly pointing out the high international level of fundamental research at WMI as well as the relevance of materials science and technological developments for new scientific discoveries and experimental techniques.

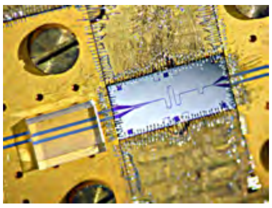

01.04.2022: Grand Challenge Quantum Communication. Within the BMBF program Grand Challenge Quantum Communication, which is part of the framework program of the German federal government on IT security, seven projects, including the WMI project QuaMToMe, receive funding for a 3-year period. In his welcome speech the Parliamentary Secretary of State Dr. h.c. Thomas Sattelberger said: *«We have to work on the future IT security already today. Therefore, by the competition "Grand Challenge in Quantum Communication" the Federal Ministry of Education and Research wants to speed up the development of quantum based techniques».* Three teams of the group of Rudolf Gross, led by Nadezhda Kukharchyk, Kirill Fedorov and Hans Huebl, participate in the program.

26.04. - 29.04.2022: World of Quantum fair premiers for the first time to industry and press. WMI presents its research with talks and posters.

06.05.2022: As part of the PLANCK 2022 contest, a group of young students from the jDPG visit WMI.

19.05.2022: The first Brazilian-German Quantum Symposium is hosted by MCQST with contributions from WMI.

30.05. - 03.06.2022: Canada-Germany Quantum Technolog Matchmaking Day. A delegation including representatives of 10 Canadian Quantum SMEs was visiting Germany to develop R&D partnerships. The meeting was jointly organized by the Embassy of Canada, the ***Munich Quantum Valley e.V.*** and the Excellence Cluster ***MCQST***. MCQST spokesperson Rudolf Gross was excited to meet and partner with Canadian quantum technology leaders and chat with stakeholders of both countries. *«It was a perfect opportunity to learn about Canadian quantum-technology capabilities and how they could complement our efforts in Munich»*, he said.

21.06.2022: Pupils get enthusiastic about physics. WMI regularly makes public outreach events for school pupils either at WMI or nearby high schools to increase their interest in natural sciences. On 21st June, Matthias Opel put his exciting low-temperature show on stage at the Gymnasium Vaterstetten, where Sebastian Bauer - a former WMI master student - is teaching physics. Besides showing the fascinating properties of liquid gases and having fun with low temperature physics, the experiments give the pupils insight into applications of low temperatures in research and technology.

04.07. - 06.07.2022: Munich Conference on Quantum Science and Technology 2022. The excellence cluster ***MCQST*** was organizing the Munich Conference on Quantum Science and Technology 2022, which brought together the Munich quantum community with international invited guests in academia and industry for three days of talks and poster sessions. The conference was taking place at Sonthofen in the Bavarian Alps and allowed participants to exchange ideas, learn about innovative research, and discuss the latest advancements in all fields of quantum science and technology.

08.07.2022: Dr. Harald Mahrer, president of the Austrian Federal Economic Chamber, visits WMI. The WMI was hosting Dr. Harald Mahrer to discuss the MQV and the future of quantum technology. State of the art in quantum technologies, the Bavarian quantum roadmap, and the role of WMI in the endeavor of building a full-stack quantum computer were among the topics discussed during the visit. Stefan Filipp particularly touched upon the future use cases of quantum computers in science and industry, the current challenges in their development and implementations, and the initiatives across Bavaria, Germany, and Europe that are striving to make quantum computers a reality.

21.07.2022: Matthias Opel and Matthias Althammer were taking care about pupils from the Michaeli high school Munich. They informed them about low temperature and quantum physics with a talks and live experiments.

21.07.2022: Lincoln Carr visits WMI. Lincoln Carr, an expert in quantum science and technology and a Jefferson Science Fellow with the U.S. State Department, was visiting WMI to inform himself on the Munich QST activities within the ***Munich Quantum Valley e.V. (MQV)*** and the excellence cluster ***Munich Center for Quantum Science and Technology (MCQST)***. He presently serves as a foreign affairs officer in the State Department's Office of Science and Technology Cooperation and discussed possible international collaborations in QST with WMI director Rudolf Gross.

24.07.2022: Stefan Filipp of WMI presents a talk about quantum computers during the Festival der Zukunft at Deutsches Museum Munich.

26.08.2022: Barbara Goldstein of NIST visits WMI. Rudolf Gross welcomed Barbara Goldstein, who is Associate Director at the Physical Measurement Laboratory of the US National Institute of Standards and Technology (NIST) and Program Manager of NIST on a Chip, at WMI to give her insight into the research program and visions of ***MQV e.V.***, ***MCQST*** and the TUM Venture Lab Quantum. The meeting with Barbara Goldstein was joined by representatives of Invest in Bavaria and the Munich Start-ups kiutra, Qlibri, and planqc. *«I am impressed by the high level of quantum research and efficient networking in the field of quantum science and technology in Munich»*, she said after lab tours at WMI, MPQ and LRZ.

14.09.2022: HTX delegation from Singapore visits WMI. Rudolf Gross welcomed a delegation of HTX Singapore headed by Mr. CHEW Hock Yong, chairman of HTX and Permanent Secretary at the Ministry of Home Affairs, and informed it about quantum-related research activities. HTX is a Science & Technology Agency, bringing together science and engineering capabilities across Singapore's Home Team Departments. As security issues are a key focus area of HTX, the delegation was particularly impressed by the WMI activities on quantum microwave communication.

24.11. - 25.11.2022: French-Bavarian Dialog on Quantum Technologies. A delegation from the French ministry of Science visits the ***Munich Quantum Valley e.V. (MQV)*** and the laboratories at WMI. During the meeting, Stefan Filipp was presenting the WMI plans on a full-stack quantum computer based on superconducting circuits. Rudolf Gross was discussing the strategy of the Munich Quantum Valley e.V. in building a deep-tech infrastructure for quantum technologies. Christopher Trummer was presenting the activities in quantum entrepreneurship.

03.12.2022: Lasst uns den Quantensprung wagen! In his ceremonial lecture at the Annual Meeting 2022 of the Bavarian Academy of Sciences and Humanities in the Herkules Hall of the Munich Residence, Rudolf Gross addresses the pioneering advances in quantum science and technology and their fascinating application potential. *«Quantum technologies and the associated quantum revolution will have a strong impact on society in the 21st century»*, he pointed out and asked the audience to dare the leap into the quantum age.

Cooperations

The Walther-Meißner-Institute is involved in many collaborations also without any direct project funding. In the following we list the most relevant collaboration partners:

- IBM Research - Zurich, Zurich, Switzerland (A. Fuhrer, D. Egger, G. Salis)
- Green Innovation Research Laboratories, NEC Corporation, Japan (J.S. Tsai, K. Inomata, T. Yamamoto)
- Forschungszentrum Jülich (P. Bushev, F.K. Wilhelm-Mauch, D. DiVincenzo)
- Fraunhofer Research Institution for Microsystems and Solid State Technologies EMFT (Ch. Kutter, K. Bauer)
- Fraunhofer Institute for Applied Solid State Physics IAF (L. John, S. Chartier, R. Quay)
- Fraunhofer Institute for Integrated Circuits IIS (T. Edelhäuser, T. Thönes, H. Adel)
- University of Tokyo, Tokyo, Japan (Y. Nakamura)
- ETH-Zurich, Switzerland (C. Eichler, A. Wallraff, L. Degiorgi, R. Monnier, Dr. M. Lavagnini)
- Chalmers University of Technology Gothenburg, Sweden (J. Bylander, P. Delsing, G. Wendin)
- Stanford University, Stanford, USA (T.P. Devereaux, I. Fisher, B. Moritz, H.N. Ruiz, S.A. Kivelson)
- Universidad del País Vasco and Ikerbasque Foundation, Bilbao, Spain (E. Solano, M. Sanz, L. Lamata)
- Instituto de Física Fundamental, CSIC, Madrid, Spain (J.J. Garcia-Ripoll)
- Instituto de Ciencia de Materials de Barcelona, CSIC, Spain (E. Canadell)
- University of Tohoku, Sendai, Japan (G.E.W. Bauer, E. Saitoh, J. Barker)
- Japan Science and Technology Agency, Sendai, Japan (H. Adachi, S. Maekawa)
- Osaka Prefecture University, Osaka, Japan (H. Fujiwara)
- University of Chinese Academy of Science, Beijing, China (D. Li, P.P. Shen, X.L. Dong, Z.X. Zhao)
- European Synchrotron Radiation Facility (ESRF), Grenoble (H. Müller, F. Wilhelm, K. Ollefs, A. Rogalev)
- Lund University, Lund, Sweden (D. Mannix)
- Materials Science Research Centre, IIT Madras, India (M.S. Ramachandra Rao, J. Mukherjee, T.S. Suraj)
- University of Geneva, Geneva, Switzerland (I. Maggio-Aprile)
- University of Alabama, MINT Center, Tuscaloosa, USA (A. Gupta)
- Helsinki University of Technology, Materials Physics Laboratory, Finland (T. Heikkilä)
- Delft University of Technology, Kavli Institute of NanoScience, Delft, The Netherlands (G.E.W. Bauer)
- B. Verkin Institute for Low Temperature Research and Engineering, Kharkov, Ukraine (V.G. Peschansky)
- Landau Institute for Theoretical Physics, Chernogolovka, Russia (P. Grigoriev)
- University of Oxford, Clarendon Laboratory, England (A. Karenowska)
- Institute of Solid State Physics, Chernogolovka, Russia (V. Zverev)
- Russian Academy of Sciences, Chernogolovka, Russia (N. Kushch, E. Yagubskii)

- High Magnetic Field Laboratory, Dresden (E. Kampert, J. Wosnitza, T. Helm)
- High-Magnetic-Field Laboratory, Grenoble, France (I. Sheikin, D. LeBoeuf)
- High Magnetic Field Laboratory, Toulouse, France (C. Proust, D. Vignolles)
- National High Magnetic Field Laboratory, Tallahassee, USA (J. Brooks)
- University of British Columbia, Vancouver, Canada (D. Bonn, A. Damascelli)
- Université de Toulouse, Laboratoire de Physique Théorique, Toulouse, France (R. Ramazashvili)
- University of Belgrade, Belgrade, Serbia (Z. Popovic, N. Lazarevic, D. U. Ralevic, R. Gajic)
- University of Aveiro, Portugal (N. A. Sobolev)
- Macquarie University, MQ Research Centre for Quantum Science and Technology, Australia (J. Twamley)
- University of Vienna, Austria (M. Aspelmeyer, S. Rotter)
- Technical University of Vienna, Austria (A. Pustogow)
- University of Innsbruck, Austria (G. Kirchmair)
- University of Florida, Gainesville, Florida, USA (P.J. Hirschfeld, S. Maiti)
- University of Manitoba, Winnipeg, Canada (C.-M. Hu)
- Kyoto University, Japan (M. Shiraishi)
- IFIMAC and Departamento de Física Teórica de la Materia Condensada, Universidad Autónoma de Madrid, Spain (A. Kamra)
- Universität Erlangen-Nürnberg (M. Hartmann)
- Universidad Nacional de Colombia, Colombia (O. Moran)
- Université Grenoble Alpes, CEA, CNRS, Grenoble INP, Grenoble, France (O. Klein)
- Karlsruhe Institute of Technology (I. Pop, A. Ustinov, A. Metelmann)
- IFW Dresden, Germany (B. Büchner, J. Fink, S.V. Borisenko, M. Knupfer, A. Thomas)
- Max-Planck-Institute for the Science of Light, Erlangen (S. Viola-Kusminskiy)
- University of Tübingen, Germany (R. Kleiner, D. Kölle)
- University of Augsburg, Germany (A. Wixforth, A. Kampf, J. Deisenhofer, V. Tsurkan)
- University of Leipzig, Germany (J. Haase)
- Ernst-Moritz-Arndt Universität Greifswald, Germany (M. Münzenberg)
- Martin-Luther-Universität Halle, Germany (G. Woltersdorf, G. Schmidt)
- Center for Spinelectronic Materials and Devices, Universität Bielefeld, Germany (G. Reiss, T. Kuschel M. Meinert)
- Aalto University, Aalto, Finland (M. Möttönnen, R. Di Candia)
- Technical University of Munich, Physics Department, Germany (Ch. Back, P. Böni, Ch. Pfleiderer, M. Poot, F.C. Simmel, P. Müller-Buschbaum)
- Technical University of Munich, Walter Schottky Institute, Germany (M. Stutzmann, J. Finley, M. Brandt, A. Holleitner)
- Technical University of Munich, Electrical Engineering (M. Becherer, W. Utschick, E. Weig)
- Technical University of Munich, Heinz Maier-Leibnitz Zentrum (J.M. Gomez, R. Dutta, A. Maity)
- LMU Munich, Physics Department, Germany (J. von Delft, E. Frey, J. Rädler, A. Högele)
- University of Konstanz (A. Leitenstorfer, S.T.B. Goennenwein, M. Müller, W. Belzig)

- Jülich Centre for Neutron Science JCNS, Garching, Germany (S. Pütter)
- Goethe University, Frankfurt, Germany (S. Winter, M. Lang)
- Technical University of Braunschweig, Germany (D. Menzel, S. Süllow)
- Fritz Haber Institut Berlin, Germany (T. Seifert, T. Kampfrath)
- Technical University of Dortmund, Germany (M. Müller)
- Johannes-Gutenberg University, Mainz, Germany (C. Cramer, M. Kläui, O. Gomomay)
- Infineon AG, Munich, Germany (F. Brandl, S. Luber)
- Rohde & Schwarz GmbH, Munich, Germany (B. Guezelarslan, C. Dille, K. Glas, G. Hechtfischer)
- Zurich Instruments, Zurich, Switzerland (C. Riek, C. Müller)
- BMW Group, Munich, Germany (J. Klepsch, A. Luckow, W. Stadlbauer, G. Steinhoff)
- Attocube, Munich, Germany (K. Karrai, D. Andres, E. Hoffmann)
- Kiutra, Munich, Germany (A. Regnat, F. Rucker)
- Parity Quantum Computing, Innsbruck, Austria (W. Lechner, M. Hauser)
- THEVA Dünnschichttechnik, Ismaning, Germany (W. Prusseit)
- Innovent Technologieentwicklung Jena, Germany (C. Dubs, O. Surzhenko)

Research Stays

Also in 2022, extended research stays of members of the Walther-Meißner-Institute at other national or international laboratories have been significantly reduced due to the Covid-19 pandemic.

1. **Stephan Geprägs**
   European Synchrotron Radiation Facility (ESRF), Grenoble, France
   20.09. - 26.09.2022
2. **Stephan Geprägs**
   Diamond Light Source, Didcot, England
   28.09. - 03.10.2022
3. **Mark Kartsovnik**
   Dresden High Magnetic Field Laboratory (HLD), Rossendorf, Germany
   08. 10. - 15. 10. 2022
   23. 10. - 05. 11. 2022
4. **Shamil Erkenov**
   Dresden High Magnetic Field Laboratory (HLD), Rossendorf, Germany
   08. 10. - 15. 10. 2022 and 23. 10. - 05. 11. 2022
5. **Florian Kollmannsberger**
   Dresden High Magnetic Field Laboratory (HLD), Rossendorf, Germany
   08. 10. - 15. 10. 2022 and 23. 10. - 05. 11. 2022

Conference Talks and Seminar Lectures

Matthias Althammer

1. **Antiferromagnetic Magnon Pseudospin Dynamics and the Magnon Hanle effect in Hematite thin films**
   Contributed talk, Joint Magnetism and Magnetic Materials and Intermag Conference, New Orleans, USA,
   10. 01. - 14. 01. 2022
2. **Observation of Magnon Pseudospin Dynamics and the Magnon Hanle Effect in Antiferromagnetic Insulators**
   Invited talk (Focus Session), APS March Meeting 2022, Chicago, IL, USA
   14. 03. - -18. 03. 2022
3. **Observation of the magnon Hanle effect in antiferromagnetic insulators**
   Invited talk, Spincaloritronics XI, Urbana-Champaign, USA
   22. 05. - 27. 05. 2022
4. **Observation of the magnon Hanle effect in antiferromagnetic insulators**
   Invited talk, Magnonics 2022, Oxnard, USA
   31. 07. - 04. 08. 2022
5. **Temperature-dependent spin-transport and current-induced torques in superconductor ferromagnet heterostructures**
   Invited talk, SPIE Spintronics XV, San Diego, USA
   21. 08. - 25. 08. 2022
6. **Observation of the magnon Hanle effect in antiferromagnetic insulators**
   Invited talk, Trends in Magnetism 2022, Venice, Italy
   04. 09. - 09. 09. 2022
7. **Revealing multidimensional spin textures and their dynamics via x-rays and electrons**
   Organization of a Focus Session (together with S. Geprägs) at Meeting of the Condensed Matter Section of the German Physical Society, Regensburg, Germany
   04. 09. - 09. 09. 2022

Kirill Fedorov

1. **Quantum teleportation of propagating microwave states**
   Invited talk, Workshop on Entanglement Assisted Communication Networks, Bad Honnef, Germany
   03. - 06. 02. 2022
2. **Quantum microwave communication**
   Seminar talk, University of Ulm, Ulm, Germany
   25. 07. 2022
3. **Microwave quantum communication with squeezed light**
   Invited talk, International Workshop on Superconducting Quantum Networks, Vienna, Austria
   12. - 15. 09. 2022

Florian Fesquet

1. **Perspectives of open-air microwave quantum key distribution**
   Contributed talk, APS March Meeting 2022, Chicago, IL, USA
   14 .03. - 18. 03. 2022
2. **Perspectives of open-air microwave quantum key distribution**
   Munich conference on Quantum Science and Technology 2022, Sonthofen, Germany
   04. 07. - 06. 07. 2022
3. **Perspectives of open-air microwave quantum key distribution**
   Meeting of the German Physical Society, Regensburg, Germany
   04. - 09. 09. 2022
4. **Perspectives of open-air microwave quantum key distribution**
   International Workshop on Superconducting Quantum Networks, Vienna, Austria
   12. - 15. 09. 2022

item **Microwave single-shot quantum key distribution**
Contributed talk, Kryoelektronische Bauelemente 2022, Villard De Lans, France
09. 10. - 11. 10. 2022

Stefan Filipp

1. **Quantumcomputing – How to solve difficult problems efficiently**
Guest Lecture, TUM Young Professionals – Master Management and Innovation (Munich, Germany).
13. 12. 2022.
2. **Nobel Prize 2022 in Physics: Quantum Entanglement – from scientific curiosity to quantum applications**
Invited Talk, TUM IAS Wednesday Coffee Talk
23. 11. 2022.
3. **Die Welt der Quantencomputer**
Invited Talk, TUM IL3 Energy Talk (Munich, Germany)
13. 12. 2022.
4. **Quantencomputer – effiziente Lösung von schwierigsten Rechenaufgaben**.
Invited Talk, attempto Innovations-Manufaktur (Munich, Germany)
29. 11. 2022.
5. **Full-Stack Quantum Computer based on Superconducting Qubits**.
Invited Talk, French-Bavarian Dialog on Quantum Technologies (Munich, Germany)
25. 11. 2022.
6. **Optimized Control of Superconducting Qubits**.
Invited Talk, 2022 Applied Superconductivity Conference (Honolulu, USA)
25. 10. 2022.
7. **Quanten Computing Hardware – Aktueller Stand der Technologie**.
Invited Online Talk, Wirtschaftsbeirat Bayern Konferenz
10. 10. 2022.
8. **Beyond standard qubit control**.
Invited Talk, Workshop on Superconducting Quantum Networks (Vienna, Austria)
14. 09. 2022.
9. **Scalable control of superconducting qubits**
Invited Talk, DPG Spring Meeting (Regensburg, Germany)
09. 09. 2022.
10. **Optimizing the control of superconducting qubits for quantum information processing**
Invited Talk, 3rd PSI Condensed Matter Summer Camp (Zuoz, Switzerland)
10. 08. 2022.
11. **Die Welt der Quantencomputer**
Invited Talk, Festival der Forschung (Munich, Germany)
22. 07. 2022.
12. **Control of superconducting qubits**
Invited Talk and Panel Discussion, Quantum Technology User Meeting by Zurich Instruments (Munich, Germany)
14. 06. 2022
13. **Quantum Hardware and Applications**
Invited Talk, Brazilian-German Quantum Symposium (Munich, Germany)
29. 05. 2022.
14. **Optimizing the control of superconducting qubits**
Invited Talk, WACQT Workshop 2022 (Gothenburg, Sweden)
12. 05. 2022.
15. **Challenges for superconducting QC**
Invited Talk, BMBF Networking Event 2022 (Munich, Germany)
28. 04. 2022.
16. **Quantum Computing Governance - where are we in Europe?**
Panel Discussion, World of Quantum 2022 (Munich, Germany)

27. 04. 2022.

17. **German Quantum Computer based on Superconducting Qubits (GEQCOS)**
Invited Talk, BMBF Networking Event 2022 (Munich, Germany)
27. 04. 2022.
18. **Munich Quantum Valley Superconducting Quantum Computing Demonstrator (MuniQC-SC)**
Invited Talk, BMBF Networking Event 2022 (Munich, Germany)
26. 04. 2022.

Niklas Glaser

1. **Analysis and Optimization of Tunable-Coupler-Based Controlled-Phase Gates**
Contributed Talk, APS March Meeting (Chicago, USA)
14. 03. 2022.
2. **Tunable-coupler mediated controlled-controlled-phase gate with superconducting qubits**
Contributed Talk, DPG Spring Meeting (Regensburg, Germany)
04. 09. 2022.

Franz Haslbeck

1. **Weak crystallization of fluctuating skyrmion textures in MnSi**
Contributed Talk, APS March Meeting (Chicago, USA)
14. 03. 2022.

Gerhard Huber

1. **Coupler-mediated unconditional reset of fixed-frequency superconducting qubits**
Contributed Talk, DPG Spring Meeting (Regensburg, Germany)
04. 09. 2022.

Hans Hübl

1. **Sensing Solid-State Excitations with Hybrid Quantum Systems**
Seminar talk, Universidad Autónoma de Madrid, Spain
19. 10. - 21. 10. 2022
2. **Connecting Quantum Systems**
Seminar talk, University of Konstanz, Germany
08. 04. 2022
3. **The Dynamics of Spin-Photon Hybrids**
Invited talk, International Symposia on Creation of Advanced Photonic and Electronic Devices 2022 and Advanced Quantum Technology for Future 2022, Kyoto Japan
08. 03. 2022
4. **High harmonic overtones in bulk acoustic resonators played by magneto-elastics**
Invited talk, Spin Cavitronics 4, Erlangen, Germany
07. 12. - 09. 12. 2022
5. **Multi-mode magnetoelastic coupling in bi- and multi-layer bulk acoustic resonators**
Invited talk, Spin Mechanics 7, Gerolfingen, Germany
22. 08. - 24. 08. 2022

Mark Kartsovnik

1. **Metallic ground state near the Mott transition in organic conductors probed by magnetic quantum oscillations**
Invited talk, International School and Workshop on Electronic Crystals, ECRYS 2022, Cargèse, Corsica, France
08. 08. - 20. 08. 2022
2. **Evolution of Charge Carriers near the Mott Transition: Theory vs. Experiment in κ-(BEDT-TTF)$_2$X**
Invited talk, 14th International Symposium on Crystalline Organic Metals, Superconductors and Ferromagnets, ISCOM 2022, Le Pouliguen, France
25. 09. - 30. 09. 2022

Leon Koch

1. **Characterization of fabrication methods to reach high coherence superconducting quantum circuits**
   Contributed Talk, APS March Meeting (Chicago, USA)
   16. 03. 2022
2. **Quantumprocessors and their fabrication**
   Invited Seminar Talk, TUM Electrical Engineering (Munich, Germany)
   12. 01. 2022.

Nadezhda Kukharchyk

1. **Cavity-free spectral hole burning below 1 K with propagating microwaves**
   Invited talk, Workshop on Rare Earth Ion Doped Crystals for Quantum Information, Edinburg, UK
   29. 06 - 01. 07. 2022
2. **Quantum thermodynamics of rare earth spin ensembles embedded into Y_2SiO_5**
   Contributed Talk, Spring Meeting of the German Physical Society, Condensed Matter Section, Regensburg, Germany
   06. 03 - 11. 03. 2022
3. **Cavity-free spectral hole burning below 1 K with propagating microwaves**
   Regular talk, Spring Meeting of the German Physical Society, Condensed Matter Section, Regensburg, Germany
   06. 03 - 11. 03. 2022

Thomas Luschmann

1. **Fabrication of Superconducting Quantum Circuits**
   Contributed talk, BEAMeeting Munich 2022, Taufkirchen, Germany
   28. 03. - 29. 03, 2022
2. **Optomechanical Systems Enabling Novel Quantum-Enhanced Technologies and Tests of Fundamental Physics**
   Gordon Research Seminar, Ventura Beach, CA, USA
   18. 06. - 19. 06. 2022
3. **Quantum Phononics for Fundamental Measurements and Quantum Technology**
   Contributed talk, Gordon Research Conference, Ventura Beach, CA, USA
   19 .06. - 24. 06. 2022

Manuel Müller

1. **Optical detection of magnon-phonon coupling using μFR-MOKE technique**
   Contributed talk, The Joint European Magnetic Symposia (JEMS 2022), Warsaw, Poland
   24. - 29. 07. 2022
2. **Optical detection of magnon-phonon coupling using μFR-MOKE technique**
   Contributed talk, Spring Meeting of the German Physical Society, Regensburg, Germany
   04. - 09. 09. 2022

Matthias Opel

1. **Tiefe Temperaturen, Supraleitung und Spinelektronik**
   Invited talk, MINT-Berufsinformationstag im Rahmen der "Humboldt Academy of Science and Engineering" (HASE), Humboldt-Gymnasium Vaterstetten, Germany
   21. 06. 2022)
2. **Magnonic Hanle Effect in Easy-Plane Antiferromagnets**
   Invited talk, The Joint European Magnetic Symposia (JEMS 2022), Warsaw, Poland
   24. - 29. 07. 2022
3. **Magnon Hanle Experiments in Antiferromagnetic α-Fe_2O_3** 28th International Workshop on Oxide Electronics (iWOE28), Portland (Maine), USA
   02. - 05. 10. 2022

4. **Diffusive Transport of Antiferromagnetic Magnons in α-Fe_2O_3**
   Seminar talk, Martin-Luther-Universität Halle-Wittenberg, Halle (Saale), Germany
   17. - 18. 11. 2022

Michael Renger

1. **Microwave quantum teleportation over a thermal noise channel**
   Contributed talk, APS March Meeting 2022, Chicago, IL, USA
   14 .03. - 18. 03. 2022
2. **Microwave quantum teleportation over a thermal channel**
   Contributed talk, Messe München, Munich, Germany
   27. 04. - 28. 04. 2022

Frederico Roy

1. **Implementation of controlled-controlled-phase gates by refocusing three-body interactions**
   Contributed Talk, APS March Meeting (Chicago, USA)
   14. 03. 2022.

Christian Schneider

1. **Superconducting Quantum Magnetomechanics**
   Invited Seminar Talk, Fraunhofer EMFT Seminar (Munich, Germany)
   07. 11. 2022.

Christian Schweizer

1. **Simultaneous parity-dependent XY entangling gates in superconducting qubit chains**
   Contributed Talk, APS March Meeting (Chicago, USA)
   15. 03. 2022.

Ivan Tsitsilin

1. **Tunable Multi-qubit couplers with low residual ZZ interactions**
   Contributed Talk, APS March Meeting (Chicago, USA)
   14. 03. 2022.

Max Werninghaus

1. **Control of Superconducting Qubits**
   Invited Talk, Quantum Technologies User Meeting (Munich, Germany)
   15. 03. 2022.
2. **Introduction to Superconducting Qubits**
   Invited Talk, Rohde & Schwarz Workshop (Munich, Germany)
   04. 05. 2022.

Honors and Awards

A. "Goldene Kreide" awarded to Rudolf Gross

During the annual celebration of the day of physics, the student body of the TUM faculty of physics regularly awards the so-called ***Golden Chalks*** to reward excellent teaching.

After already receiving several Golden Chalks in previous years for lectures in the bachelor and master courses, this year Rudolf Gross received the special ***Golden Chalk for Lifelong Excellence in Teaching***. This Golden Chalk is awarded to professors to acknowledge their outstanding and continuous engagement in teaching over their whole career.

B. Matthias Althammer receives Supervisory Award

Matthias Althammer received the ***Supervisory Award*** of the TUM Graduate Center Physics for excellence in mentoring PhD students. Mathias Althammer was proposed for this award by several Ph.D. students of WMI and the selection committee selected him among several candidates suggested for this award.

Figure 4: Supervisory Award handed over to Matthias Althammer (left) during the Graduation Ceremony of the TUM Physics Department in June 2022.

Beyond meeting the typical selection criteria like excellence in leadership, scientific support, education and career development for Ph.D. students, Matthias Althammer always succeeds to establish and maintain a friendly work atmosphere thereby stimulating the exchange and development of novel scientific ideas. We cordially congratulate Matthias Althammer on the recognition of his efforts in supporting Ph.D. students. Of course, the Scientific Directors of WMI are particular happy about the fact that WMI researcher regularly receive best teaching and mentoring awards, documenting the excellent quality of the teaching efforts of WMI scientists.

C. Other Awards

In 2022, Max Werninghaus of WMI has received one of three *Student Travel Grants* sponsored by *Zurich Instruments* for his Ph.D. thesis on *Leakage reduction in fast superconducting qubit gates via optimal control*. Congratulations!

Membership in Advisory Boards, Committees, etc.

1. **Frank Deppe** is Coordinator of the European Quantum Technology Flagship Project *Quantum Microwaves for Communication and Sensing (QMiCS)*.
2. **Frank Deppe** is member and principal investigator of the Cluster of Excellence *Munich Center for Quantum Science and Technology (MCQST)*.
3. **Andreas Erb** is spokesmen of the *Arbeitskreis Intermetallische und oxydische Systeme mit Spin- und Ladungskorrelationen* of the *Deutsche Gesellschaft für Kristallzüchtung und Kristallwachstum (DGKK)*.
4. **Stefan Filipp** is coordinator of the *Munich Quantum Valley (MQV)* consortium *K1 - Superconducting Qubit Quantum Computing*.
5. **Stefan Filipp** is coordinator of the *Munich Quantum Valley Quantumcomputer Demonstrators – Superconducting Qubits* (MUNIQC-SC) project funded by the Federal Ministry of Education and Research (BMBF).
6. **Stefan Filipp** is advisory board member of the *International AIQT Foundation*.
7. **Stefan Filipp** is member of the scientific advisory board of the EU FET Open project *AVAQUS - Annealing based Variational Quantum Processors*.
8. **Stefan Filipp** is member of the scientific advisory board of the *Wallenberg Center for Quantum Technology*.
9. **Stefan Filipp** is editorial board member of the IOP multidisciplinary journal *Materials for Quantum Technology*.
10. **Stefan Filipp** is member and principal investigator of the Cluster of Excellence *Munich Center for Quantum Science and Technology (MCQST)*.
11. **Stefan Filipp** is adjoint Member of the Special Research Fund (SFB) *BeyondC* funded by the Austrian Science Fund (FWF).
12. **Stefan Filipp** is member of the *Munich Quantum Center (MQC)*.
13. **Rudolf Gross** is spokesperson (together with Immanuel Bloch and Ignacio Cirac) of the Cluster of Excellence *Munich Center for Quantum Science and Technology (MCQST)* and coordinator of the Research Unit C on *Quantum Computing*.
14. **Rudolf Gross** is initiator and Principal Investigator of the *Munich Quantum Valley e.V. (MQV)*.
15. **Rudolf Gross** is member of the *Deutsche Akademie der Technikwissenschaften e.V. (acatech)*.
16. **Rudolf Gross** is member of the Advisory Board of the permanent exhibition on *Matter and Light* of the German Science Museum.
17. **Rudolf Gross** is member of the *Committee for the allocation of Alexander von Humboldt Foundation Research Awards*.
18. **Rudolf Gross** is member of the *Appointment and Tenure Board* of the Technical University of Munich.
19. **Rudolf Gross** is member of the *Munich Quantum Center (MQC)*.

20. **Rudolf Gross** is member of the *Scientific Advisory Board of the Bavarian Research Institute of Experimental Geochemistry and Geophysics (BGI)*, Bayreuth, Germany.

21. **Rudolf Gross** is member of the *Scientific Advisory Board of the Institut de Ciència de Materials de Barcelona*, Spain.

22. **Hans Hübl** is member and principal investigator of the Cluster of Excellence *Munich Center for Quantum Science and Technology (MCQST)*.

23. **Mark Kartsovnik** is member of the *Selection Committee of EMFL* (European Magnetic Field Laboratories).

24. **Mark Kartsovnik** is member of the *International Advisory Committee of the* 14^{th} *International Symposium on Crystalline Organic Metals Superconductors and Ferromagnets (ISCOM 2022)*.

25. **Matthias Opel** is one of the four elected members of the *Speaker Council* for the scientists of the Bavarian Academy of Sciences and Humanities.

Teaching

Lectures, Courses and other Teaching Activities

Several members of the Walther-Meißner-Institute give lectures and seminars at the Technical University of Munich.

Matthias Althammer

WS 2021/2022
- Magnetism
- Magnetism, Problem Sessions (with M. Müller)
- Seminar: Spin Currents and Skyrmionics (with M. Althammer, M. Opel, S. Geprägs)
- Seminar: Advances in Solid-State Physics (with R. Gross, S. Geprägs, H. Hübl, A. Marx, M. Opel)
- Seminar: Topical Issues in Magneto- and Spin Electronics (with M. S. Brandt, S. Geprägs, H. Hübl, M. Opel)

SS 2022
- Spin Electronics
- Spin Electronics, Problem Sessions (with M. Müller)
- Seminar: Spin Currents and Skyrmionics (with M. Althammer, M. Opel, S. Geprägs)
- Seminar: Advances in Solid-State Physics (with R. Gross, S. Geprägs, H. Hübl, A. Marx, M. Opel)
- Seminar: Topical Issues in Magneto- and Spin Electronics (with M. S. Brandt, S. Geprägs, H. Hübl, M. Opel)

WS 2022/2023
- Seminar: Spin Currents and Skyrmionics (with M. Althammer, M. Opel, S. Geprägs))
- Seminar: Advances in Solid-State Physics (with R. Gross, S. Geprägs, H. Hübl, A. Marx, M. Opel)
- Seminar: Topical Issues in Magneto- and Spin Electronics (with M. S. Brandt, S. Geprägs, H. Hübl, M. Opel)

Frank Deppe

WS 2021/2022
- Seminar: Superconducting Quantum Circuits (with K. Fedorov, S. Filipp, R. Gross, A. Marx)

SS 2022
- Seminar: Superconducting Quantum Circuits (with K. Fedorov, S. Filipp, R. Gross, A. Marx)

WS 2022/2023
- Seminar: Superconducting Quantum Circuits (with K. Fedorov, S. Filipp, R. Gross, A. Marx)

Dietrich Einzel

WS 2021/2022
- Mathematical Methods of Physics I
- Mathematical Methods of Physics I, Problem Sessions

SS 2022
- Mathematical Methods of Physics II
- Mathematical Methods of Physics II, Problem Sessions

Kirill Fedorov

WS 2021/2022
- Applied Superconductivity I: from Josephson Effects to RSFQ Logic
- Applied Superconductivity I: from Josephson Effects to RSFQ Logic, Problem Sessions

	• Seminar: Superconducting Quantum Circuits (with F. Deppe, S. Filipp, R. Gross, A. Marx)
SS 2022	• Applied Superconductivity II: from superconducting quantum circuits to microwave quantum optics • Applied Superconductivity II: from superconducting quantum circuits to microwave quantum optics, Problem Sessions • Seminar: Superconducting Quantum Circuits (with F. Deppe, S. Filipp, R. Gross, A. Marx)
WS 2022/2023	• Applied Superconductivity I: from Josephson Effects to RSFQ Logic • Applied Superconductivity I: from Josephson Effects to RSFQ Logic, Problem Sessions • Seminar: Superconducting Quantum Circuits (with F. Deppe, S. Filipp, R. Gross, A. Marx)

Stefan Filipp

WS 2021/2022	• Quantum Computing with Superconducting Qubits: Architecture and Algorithms • Quantum Computing with Superconducting Qubits: Architecture and Algorithms, Problem Sessions • Seminar: Superconducting Quantum Circuits (with F. Deppe, R. Gross, A. Marx, K. Fedorov) • WMI Seminar on Modern Topics of Low Temperature Solid-State Physics (with M. Althammer, F. Deppe, K. Fedorov, S. Geprägs, R. Gross, H. Hübl, N. Kukharchyk, A. Marx, M. Opel) • Seminar: Quantum Entrepreneurship Laboratory (with Ch. Mendl, F. Pollmann) • Journal Club on Quantum Systems
SS 2022	• Quantum Computing with Superconducting Qubits 2: Advanced Topics • Quantum Computing with Superconducting Qubits 2: Advanced Topics, Problem Sessions • Seminar: Superconducting Quantum Circuits (with F. Deppe, R. Gross, A. Marx, K. Fedorov) • WMI Seminar on Modern Topics of Low Temperature Solid-State Physics (with M. Althammer, F. Deppe, K. Fedorov, S. Geprägs, R. Gross, H. Hübl, N. Kukharchyk, A. Marx, M. Opel) • Journal Club on Quantum Systems
WS 2022/2023	• Quantum Science and Technology Experiment: Quantum Hardware • Quantum Science and Technology Experiment: Quantum Hardware, Problem Sessions (with F. Haslbeck) • Seminar: Superconducting Quantum Circuits (with F. Deppe, R. Gross, A. Marx, K. Fedorov) • WMI Seminar on Modern Topics of Low Temperature Solid-State Physics (with M. Althammer, F. Deppe, K. Fedorov, S. Geprägs, R. Gross, H. Hübl, N. Kukharchyk, A. Marx, M. Opel) • Seminar: Quantum Entrepreneurship Laboratory (with Ch. Mendl, F. Pollmann) • Journal Club on Quantum Systems

Rudolf Gross

WS 2021/2022

- Superconductivity and Low Temperature Physics I
- Superconductivity and Low Temperature Physics I, Problem Sessions
- WMI Seminar on Modern Topics of Low Temperature Solid-State Physics (with M. Althammer, F. Deppe, K. Fedorov, S. Filipp, S. Geprägs, H. Hübl, N. Kukharchyk, A. Marx, M. Opel)
- Seminar: Advances in Solid-State Physics (with M. Althammer, S. Geprägs, H. Hübl, A. Marx, M. Opel)
- Seminar: Superconducting Quantum Circuits (with F. Deppe, K. Fedorov, S. Filipp, A. Marx)
- Colloquium on Solid-State Physics, with D. Einzel

SS 2022

- Superconductivity and Low Temperature Physics II
- Superconductivity and Low Temperature Physics II, Problem Sessions
- Seminar: Advances in Solid-State Physics (with M. Althammer, S. Geprägs, H. Hübl, A. Marx, M. Opel)
- WMI Seminar on Modern Topics of Low Temperature Solid-State Physics (with M. Althammer, F. Deppe, K. Fedorov, S. Filipp, S. Geprägs, H. Hübl, N. Kukharchyk, A. Marx, M. Opel)
- Seminar: Superconducting Quantum Circuits (with F. Deppe, K. Fedorov, S. Filipp, A. Marx)
- Colloquium on Solid-State Physics, with D. Einzel

WS 2022/2023

- Superconductivity and Low Temperature Physics I
- Superconductivity and Low Temperature Physics I, Problem Sessions
- WMI Seminar on Modern Topics of Low Temperature Solid-State Physics (with M. Althammer, F. Deppe, K. Fedorov, S. Filipp, S. Geprägs, H. Hübl, N. Kukharchyk, A. Marx, M. Opel)
- Seminar: Advances in Solid-State Physics (with M. Althammer, S. Geprägs, H. Hübl, A. Marx, M. Opel)
- Seminar: Superconducting Quantum Circuits (with F. Deppe, K. Fedorov, S. Filipp, A. Marx)
- Colloquium on Solid-State Physics, with H. Huebl

Hans Hübl

WS 2021/2022

- Quantum Sensing (with M. Brandt, D. Bucher)
- Seminar: Spin Currents and Skyrmionics (with M. Althammer, M. Opel, S. Geprägs)
- Seminar: Advances in Solid-State Physics (with M. Althammer, S. Geprägs, H. Hübl, A. Marx, M. Opel)
- WMI Seminar on Current Topics of Low Temperature Solid State Physics (with M. Althammer, F. Deppe, K. Fedorov, S. Filipp, S. Geprägs, R. Gross, N. Kukharchyk, A. Marx, M. Opel)
- Seminar: Topical Issues in Magneto- and Spin Electronics (with M. S. Brandt, M. Althammer, S. Geprägs, M. Opel)

SS 2022

- Seminar: Spin Currents and Skyrmionics (with M. Althammer, M. Opel, S. Geprägs)
- Seminar: Advances in Solid-State Physics (with M. Althammer, S. Geprägs, H. Hübl, A. Marx, M. Opel)
- WMI Seminar on Current Topics of Low Temperature Solid State Physics (with M. Althammer, F. Deppe, K. Fedorov, S. Filipp, S. Geprägs, R. Gross, N. Kukharchyk, A. Marx, M. Opel)
- Seminar: Topical Issues in Magneto- and Spin Electronics (with M. S. Brandt, M. Althammer, S. Geprägs, M. Opel)

WS 2022/2023
- Quantum Sensing (with M. Brandt, D. Bucher)
- Seminar: Spin Currents and Skyrmionics (with M. Althammer, M. Opel, S. Geprägs)
- Seminar: Advances in Solid-State Physics (with M. Althammer, S. Geprägs, R. Gross, A. Marx, M. Opel)
- WMI Seminar on Current Topics of Low Temperature Solid State Physics (with M. Althammer, F. Deppe, K. Fedorov, S. Filipp, R. Gross, S. Geprägs, N. Kukharchyk, A. Marx, M. Opel)
- Seminar: Topical Issues in Magneto- and Spin Electronics (with M. S. Brandt, M. Althammer, S. Geprägs, M. Opel)

Nadezhda Kukharchyk

WS 2022/2023
- Magnetism
- Magnetism, Problem Sessions
- WMI Seminar on Current Topics of Low Temperature Solid State Physics (with M. Althammer, F. Deppe, K. Fedorov, S. Filipp, R. Gross, S. Geprägs, H. Huebl, A. Marx, M. Opel)

Seminars and Colloquia

A. Walther-Meißner-Seminar on Modern Topics in Low Temperature Physics WS 2021/2022, SS 2022 and WS 2022/2023

WS 2021/2022

1. **Fabrication of Superconducting-Ferromagnetic and Hybrid S-I-F Devices**
   Mihai Gabureac, Laboratorium für Festkörperphysik, ETH Zurich, Switzerland
   22. 10. 2021
2. **Mid-infrared Intersubband Polariton Devices**
   Ngoc Linh Tran, Université Paris-Saclay, Centre de Nanosciences et de Nanotechnologies(C2N), Palaiseau, France
   28. 10. 2021
3. **Optical heterostructures and multilayer stacks down to atomic scale grown by atomic layer deposition**
   Pallabi Paul, Friedrich-Schiller University Jena, Germany
   09. 11. 2021
4. **Investigation of proximity induced superconductivity in Al-based topological Josephson junctions**
   Wilhelm Wittl, Forschungszentrum Jülich and University of Regensburg, Germany
   26. 11. 2021
5. **Quantum Communication at LNT/Quantum Clustering for Nonlinear Noise Mitigation in Fibre Communication Systems/An information-theoretic perspective on quantum repeaters**
   Christian Deppe/Roberto Ferrara/Uzi Pereg, Department of Electrical Engineering, TU Munich, Germany
   03. 12. 2021
6. **Magnonics: unique opportunities for classical and quantum information sciences**
   Akashdeep Kamra, Universidad Autónoma de Madrid, Spain
   10.12.2021
7. **Pump-probe Femtosecond Spectroscopy and Photocurrent Spectroscopy on Semiconductor Nanowire Emitters**
   Boris Stanchev, University of Massachusetts Amherst, USA
   12.01.2022
8. **Superconducting MoGe and MoRe for Graphene Quantum Electronics**
   Maria-Teresa Handschuh, Institut für experimentelle und angewandte Physik, Universität Regensburg, Germany
   21.01.2022
9. **A variational quantum eigensolver on superconducting qubits**
   Arne Wulff, Department of Physics, ETH Zurich, Switzerland
   25.02.2022

SS 2022:

10. **Photonic and Phononic Bandgap Engineering for Quantum Electrodynamics and Quantum Transduction**
    Jash Banker, Fraunhofer EMFT, Munich, Germany
    01.04.2022
11. **Repeated Quantum Error Correction in a Surface Code Using Superconducting Circuits**
    Christopher Eichler, Department of Physics, ETH Zurich, Switzerland
    12.04.2022
12. **Electronic transport in free-standing rhombohedral graphene and Charge Density Waves in 1T-TaS_2**
    Noelia Fernández, University of Göttingen & LMU Munich, Germany
    05.05.2022

13. **Coherent Ising machines: from parametrons to cat qubits**
Oded Zilberberg, University of Konstanz, Germany
20.05.2022
14. **Controllable States of Superconducting Qubit Ensembles**
Elena Redchenko, IST Austria, Klosterneuburg, Austria
23.05.2022
15. **Coherent Control of Multi-Qubit Dark States in Waveguide QED**
Maximilian Zanner, University of Innsbruck, Austria
24.05.2022
16. **Magnetization Switching with Spin-Orbit Torques**
Prof. Dr. Markus Meinert, Fachgebiet Neue Materialien Elektronik (FB 18), Technische Universität Darmstadt, Germany
15.07.2022
17. **How Resonant Inelastic Scattering (RIXS) changes our understanding of quantum materials**
Dr. Daniel Jost, Stanford Institute for Materials and Energy Sciences, SLAC National Accelerator Laboratory, Menlo Park, CA, USA
16.09.2022

WS 2022/2023:

18. **InGaAs Nanowire and Quantum Well Devices**
Lasse Södergren, Lund University, Department of Electrical and Information Technology, Lund, Sweden InGaAs Nanowire and Quantum Well Device
14.11.2022
19. **Boring phases with interesting features: Helitronic pumps and transport by fluctuations**
Dr. Jan Masell, Institute of Theoretical Solid State Physics (TFP), Karlsruhe Institute of Technology (KIT), Germany
25.11.2022
20. **Tailored High Temperature Superconductors for Power- and Magnet Applications**
Prof. Dr. Bernhard Holzapfel, Karlsruher Institut für Technologie, Institut für Technische Physik (ITEP), Germany
02.12.2022
21. **Two-qubit gates on fluxoniums and transmons**
Ilya Moskalenko, Russian Quantum Center, 143025 Skolkovo, Moscow, Russia
05.12.2022
22. **Dynamics of Transmon Ionization**
Prof. Alexandru Petrescu, Centre Automatique et Systèmes, Ecole des Mines de Paris, France
09.12.2022
23. **THz time-domain spectroscopy of Dirac- and topological materials as well as corresponding circulator geometries**
Johannes Gröbmeyer, Sergey Lavrentyev, and Alexander, Walter Schottky Institute and Physics Department, TU Munich, Germany
16.12.2022
24. **Evaluating the performance of sigmoid quantum perceptrons in quantum neural networks**
Samuel Wilkinson, Friedrich-Alexander-Universität Erlangen-Nürnberg, Institute for Theoretical Physics II, Erlangen, Germany
13.01.2023

B. Topical Seminar on Advances in Solid State Physics WS 2021/2022, SS 2022 and WS 2022/2023

WS 2021/2022:

1. **Preliminary discussion and assignment of topics**
R. Gross, Walther-Meißner-Institute (E23), Technical University of Munich and BAdW

19. 11. 2021 and 26. 11. 2021

2. **Observation of first and second sound in a BKT superfluid**
   Meike Pfeiffer, Technical University of Munich
   07. 12. 2021
3. **Cascaded superconducting junction refrigerators: Optimization and performance limits**
   Julian Franz, Technical University of Munich
   14. 12. 2021
4. **Quantum-enhanced nonlinear microscopy**
   Michael Schmidlechner, Technical University of Munich
   21. 12. 2021
5. **All-electric magnetization switching and Dzyaloshinskii-Moriya interaction in WTe_2/ferromagnet heterostructures**
   Ferdinand Menzel, Technical University of Munich
   18. 01. 2022
6. **Observation of Unconventional Charge Density Wave without Acoustic Phonon Anomaly in Kagome Superconductors AV_33Sb_5 (A=Rb,Cs)**
   Ramona Stumberger, Technical University of Munich and WMI
   25. 01. 2022

SS 2022:

7. **Layer-by-Layer Growth of Complex-Shaped Three-Dimensional Nanostructures with Focused Electron Beams**
   Sebastian Loy, Technical University of Munich
   17.05.2022
8. **Quantum anomalous Hall octet driven by orbital magnetism in bilayer graphene**
   Björn Sinz, Technical University of Munich
   31.05.2022
9. **Antiferromagnetic half-skyrmions and bimerons at room temperature**
   Markus Kügle, Technical University of Munich
   14.06.2022
10. **Pauli-limit violation and re-entrant superconductivity in moiré graphene**
   Herman Muzychko, Technical University of Munich
   21.06.2022

WS 2022/2023:

11. **Mott-Driven BEC-BCS Crossover in a Doped Spin Liquid Candidate**
   Aeneas Leingärtner-Goth, Technical University of Munich
   13.12.2022
12. **Josephson diode effect from Cooper pair momentum in a topological semimetal**
   Tim Bohnen, Technical University of Munich
   20.12.2022
13. **Emission of Photon Multiplets by a dc-Biased Superconducting Circuit**
   Rubek Poudel, Technical University of Munich
   10.01.2023
14. **Titanium Nitride Film on Sapphire Substrate with Low Dielectric Loss for Superconducting Qubits**
   Tobias Waldmann, Technical University of Munich
   17.01.2023

C. Topical Seminar: Spin current and Skyrmionics WS 2021/2022, SS 2022 and WS 2022/2023

WS 2021/2022:

1. **CoFe hybrids for complex magnetic order**
   Luis Flacke, Technical University of Munich and WMI
   11. 11. 2021
2. **Vertical Pt/YIG/Pt heterostructures**
   Phillip Schwenke, Technical University of Munich and WMI
   18. 11. 2021
3. **Magnetic insulator/superconductor thin film heterostructures**
   Vincent Haueise, Technical University of Munich
   25.11.2021
4. **Ultrafast spin current generated from an antiferromagnet**
   Annarita Ricci, Technical University of Munich
   09. 12. 2021
5. **Magnon transport in magnetic insulators**
   Matthias Grammer, Technical University of Munich and WMI
   13. 01. 2022
6. **Manipulating magnon transport in YIG films with different crystalline orientations**
   Janine Gückelhorn, Technical University of Munich and WMI
   20. 01. 2022
7. **Spin transport effects in yttrium iron garnet films interfaced with a superconductor**
   Yunhao Sun, Technical University of Munich
   10. 02. 2022

SS 2022:

8. **Non-reciprocal Magnon Transport in Hematite**
   Janine Gückelhorn, Technical University of Munich and WMI
   19.05.2022
9. **Diffusive Spin Transport in Superconductor-Ferrimagnet Heterostructures**
   Yuhao Sun, Technical University of Munich and WMI
   02.06.2022
10. **Unidirectional Spin Wave Propagation**
    Christian Mang, Technical University of Munich and WMI
    23.06.2022
11. **Diffusive Magnon Transport in Orthoferrites**
    Monika Scheufele, Technical University of Munich and WMI
    30.06.2022
12. **Magnon Transport Phenomena in Antiferromagnetic Thin Films** Matthias Grammer, Technical University of Munich and WMI
    07.07.2022
13. **Excitation of Phonons by Ferromagnetic Resonance** Manuel Müller, Technical University of Munich and WMI
    14.07.2022
14. **Growth Optimization and Magnetic Properties of GdN** Raphael Hoepfl, Technical University of Munich and WMI
    21.07.2022
15. **Control of Magnon Transport by Microwave Excitation**
    Franz X. Weidenhiller, Technical University of Munich and WMI

28.07.2022

WS 2022/2023:

16. **Magnon-Phonon Coupling**
Manuel Müller, Technical University of Munich and WMI
24.11.22
17. **Nonreciprocal Magnon Hanle Effect**
Monika Scheufele, Technical University of Munich and WMI
08.12.2022
18. **Microwave Control of Magnon Transport in Yttrium Iron Garnet**
Franz Weidenhiller, Technical University of Munich and WMI
15.12.2022
19. **Superconducting Spintronics with Magnetic Insulators**
Yuhao Sun, Technical University of Munich and WMI
12.01.2023
20. **All-Electrical Magnon Transport in Magnetic Insulators**
Maria Sigl, Technical University of Munich and WMI
19.01.2023
21. **Unidirectional Magnetoresistance in Antiferromagnet/Heavy-Metal Bilayers**
Stefan Wein, Technical University of Munich
26.01.2023
22. **GdN Growth Optimization and Magnetotransport Properties**
Raphael Höpfl, Technical University of Munich and WMI
02.02.2023
23. **Magnon-Phonon-Coupling with Metallic CoFe**
Johannes Weber, Technical University of Munich and WMI
09.02.2023

D. Topical Seminar on Superconducting Quantum Circuits WS 2021/2022, SS 2022 and WS 2022/2023

WS 2021/2022:

1. **Preliminary discussion and assignment of topics**
F. Deppe, A. Marx, S. Filipp, R. Gross, Walther-Meissner-Institute (E23), Technical University of Munich and BAdW
19. 10. 2021 and 26. 10. 2021
2. **Improving qubit coherence using closed-loop feedback**
Federico Roy, Technical University of Munich and WMI
09. 11. 2021
3. **Optimal Control of Entangling Gates in Superconducting Tunable-Coupler Architectures**
Niklas Glaser, Technical University of Munich and WMI
16. 11. 2021
4. **Direct observation of deterministic macroscopic entanglement**
Wun Kwan Yam, Technical University of Munich and WMI
23. 11. 2021
5. **Microwave Package Design for Superconducting Quantum Processors**
Johannes Schirk, Technical University of Munich and WMI
30. 11. 2021
6. **Parity Dependent XY Rotations in Qubit Chains**
Maximilian Nägele, Technical University of Munich
07. 12. 2021
7. **Enhancing quantum annealing performance by a degenerate twolevel system**

Yuki Nojiri, Technical University of Munich and WMI
14.12.2021

8. **A reversed Kerr traveling wave parametric amplifier**
Daniil Bazulin, Technical University of Munich and WMI
21. 12. 2021
9. **Superconducting qubit to optical photon transduction**
Nicoló Salerno, Technical University of Munich
11. 01. 2022
10. **Implementation of a canonical phase measurement with quantum feedback**
Thomas Narr, Technical University of Munich
18. 01. 2022
11. **Spin-Resonance Linewidths of Bismuth Donors in Silicon Coupled to Planar Microresonators**
Georg Mair, Technical University of Munich
25.01.2022
12. **Experimental demonstration of entanglement-enabled universal quantum cloning in a circuit**
Lion Frangoulis, Technical University of Munich
13. **Digital-analog quantum computation**
Malay Singh, Technical University of Munich and WMI
08. 02. 2022

WS 2022/23:

merged with **Topical Seminar on Advances in Solid State Physics**.

E. Solid State Colloquium

The WMI has organized the Solid-State Colloquium of the Faculty of Physics in WS 2021/2022, SS 2022, and WS 2022/2023. The detailed program can be found on the WMI webpage: www.wmi.badw.de/teaching/colloquium-on-solid-state-physics.

Staff

Staff of the Walther-Meißner-Institute

Scientific Directors
Prof. Dr. Stefan Filipp (managing director)
Prof. Dr. Rudolf Gross

Deputy Director
Priv.-Doz. Dr. habil. Hans Hübl

Technical Director
Dr. Achim Marx

The deputy director, the technical director and the elected representative of the scientific staff (Dr. Matthias Opel) are members of the WMI Executive Committee and support the scientific directors in the management of WMI.

Administration/Secretary's Office
Andrea Person
Carola Siegmayer
Emel Dönertas
Martina Meven

Scientific Staff
Dr. Matthias Althammer
Priv.-Doz. Dr. habil. Frank Deppe
Prof. Dr. Andreas Erb
Dr. Kirill Fedorov
Dr. Noelia Fernandez
Dr. Stephan Geprägs
Dr. Franz Haslbeck
Dr. Mark Kartsovnik
Dr. Gleb Krylov
Dr. Nadezhda Kukharchyk
Dr. Klaus Liegner
Dr. Matthias Opel
Dr. Christian Schneider (TUM)
Dr. Christian Schweizer (LMU)
Dr. Christopher Trummer (TUM)
M. Sc. Joao Romeiro Alves (TUM)
M. Sc. Agustí Bruzón
M. Sc. Daniil Bazulin
M. Sc. Niklas Bruckmoser
M. Sc. Qiming Chen
M. Sc. Jianpeng Chen
M. Sc. Shamil Erkenov
M. Sc. Florian Fesquet
M. Sc. Niklas Glaser
M. Sc. Janine Gückelhorn
M. Sc. Maria-Teresa Handschuh
M. Sc. Kedar Honasoge
M. Sc. Gerhard Huber
M. Sc. Martin Knudsen
M. Sc. Leon Koch
M. Sc. Thomas Luschmann
M. Sc. Manuel Müller
M. Sc. Yuki Nojiri
M. Sc. Patricia Oehrl
M. Sc. Frederik Pfeiffer (TUM)
M. Sc. Michael Renger
M. Sc. Lea Richard (TUM)
M. Sc. Federico Roy
M. Sc. Korbinian Rubenbauer
M. Sc. Monika Scheufele
M. Sc. Johannes Schirk
M. Sc. Malay Singh
M. Sc. Ana Strinic
M. Sc. Ivan Tsitsilin
M. Sc. Florian Wallner
M. Sc. Max Werninghaus
M. Sc. Wun Kwan Yam

Technical Staff

Peter Binkert
Thomas Brenninger, M.Sc.
Dieter Guratzsch
Astrid Habel
Dipl.-Ing. (FH) Josef Höß
Sebastian Kammerer
Jan Naundorf
Georg Nitschke
Mario Nodes
Christian Reichlmeier
Alexander Rössl
Andreas Russo
Harald Schwaiger

Assistants

Sybilla Plöderl
Maria Botta

Guest Researchers

The Walther-Meißner-Institute welcomes a significant number of guest every year for strengthening international collaborations and intensifying scientific exchange with internationally leading places. Unfortunately, also in 2022 the number of guests was disappointingly small due to the Covid-19 pandemic.

1. Dr. Werner Biberacher
   permanent guest
2. Prof. Dr. Dietrich Einzel
   permanent guest
3. Dr. Kurt Uhlig
   permanent guest
4. Dr. Roberto Di Candia, Aalto University, Aalto, Finland
   01. 09. 2021 - 28. 02. 2022
5. Dr. Mikael Afzelius, Department of Applied Physics, Université de Genève, Genève, Switzerland
   05. - 06. 05. 2022
6. Dr. Markus Meinert, Fachgebiet Neue Materialien Elektronik (FB 18), Technische Universität Darmstadt, Germany
   14.07. - 15. 07. 2022
7. Prof. Dr. Akashdeep Kamra, Universidad Autónoma de Madrid, Spain
   31. 08. - 02. 09. 2022
8. Dr. Jan Masell, Institute of Theoretical Solid State Physics (TFP), Karlsruhe Institute of Technology (KIT), Karlsruhe, Germany
   25. 11. - 26. 11. 2022
9. Prof. Dr. Sebastian Goennenwein, Univerity of Konstanz, Germany
   15. 09. - 16. 09. 2022
10. Shugo Yoshii, University of Kyoto, Japan
    16. 09. - 15. 12. 2022

Scientific Advisory Board & Executive Committee

Scientific Advisory Board

According to the statutes of the Bavarian Academy of Sciences and Humanities (BAdW) the Scientific Advisory Board evaluates the quality of the scientific work of Walther-Meißner-Institute (WMI) and gives advice to its Executive Committee to provide scientific quality assurance. The Scientific Advisory Board regularly reports to the Research Committee of BAdW.

The members of the Scientific Advisory Board include members of BAdW with appropriate scientific background, representatives of the two Munich universities (TUM and LMU), as well as leading national and international scientists. They are appointed by the Section III "Naturwissenschaften, Mathematik, Technikwissenschaften" of BAdW for five years. The scientific directors of WMI are consultive members of the WMI Scientific Advisory Board. The Scientific Advisory Board is headed by a chairperson and deputy chairperson. They are elected by the Section III "Naturwissenschaften, Mathematik, Technikwissenschaften" of BAdW for five years at the suggestion of the members of the WMI Scientific Advisory Board. The chairperson of the Scientific Advisory Board must be a member of BAdW.

The present members of the WMI Scientific Advisory Board are:

- **Vollhardt, Dieter**, chairman (BAdW, University of Augsburg)
- **Bloch, Immanuel**, deputy chairman (BAdW, LMU Munich and Max-Planck-Institute of Quantum Optics)

- **Abstreiter, Gerhard** (BAdW, Technical University of Munich)
- **Bühler-Paschen, Silke** (Technical University of Vienna)
- **Filipp, Stefan**, consultive member (Technical University of Munich)
- **Finley, Jonathan** (Technical University of Munich)
- **Gross, Rudolf**, consultive member (BAdW and Technical University of Munich)
- **Hänsch, Theodor** (BAdW, LMU Munich and Max-Planck-Institute of Quantum Optics)
- **Michael Hartmann** (FAU Erlangen-Nuremberg)
- **Laurens Molenkamp** (BAdW and University of Würzburg)
- **Wallraff, Andreas** (ETH Zurich)
- **Weiss, Dieter** (University of Regensburg)

In 2022, the annual meeting of the scientific advisory board was taking place on 18$^{\text{th}}$ February 2022 as an online meeting.

Executive Committee

The Walther-Meißner-Institute is headed by the board of scientific directors which is responsible for the development and implementation of the research program. The scientific directors hold a full professor position at one of the Munich universities (TUM or LMU). They are appointed in a joint process of the respective university and BAdW. The scientific directors are supported by the deputy director, the technical director and an elected representative of the scientific staff. They are appointed by the Section III "Naturwissenschaften, Mathematik, Technikwissenschaften" of BAdW for five years at the suggestion of the members of the WMI Scientific Advisory Board.

The present members of the WMI Executive Committee are:

- **Filipp, Stefan**, scientific director (managing director)
- **Gross, Rudolf**, scientific director
- **Hübl, Hans**, deputy director
- **Marx, Achim**, technical director
- **Opel, Matthias**, representative of the scientific staff

Stefan Filipp was taking over the task of the managing director on 1st January 2022 from Rudolf Gross who has been the managing director of WMI for more than 20 years starting from July 2000. The number of scientific directors in the WMI Executive Committee is presently two and will further increase to three staring from January 2023, when Peter Rabl will start his new theory group at WMI. Therefore, the position of the managing director can now be switched every second year to allocate the workload among the scientific directors.

Contact:

Walther–Meißner–Institut
Bayerische Akademie der Wissenschaften
Walther–Meißner–Str. 8
D - 85748 Garching
GERMANY

Phone: +49 – (0)89 289 14202
Fax: +49 – (0)89 289 14206
E–mail: Sekretariat@wmi.badw.de

www.wmi.badw.de

Published by:

Walther–Meißner–Institut
Walther–Meißner–Str. 8, D - 85748 Garching
December 2021

Walther-Meißner-Institut
DER BAYERISCHEN AKADEMIE DER WISSENSCHAFTEN